MODELLING OF DEBONDING MECHANISMS IN EXTERNALLY BONDED FRP SHEETS IN RC SHEAR WALLS FOR EARTHQUAKE RESISTANCE

A thesis submitted to

The Faculty of Graduate and Postdoctoral Affairs

In Partial Fulfillment of the requirements for the degree

Master of Applied Science

By

Ahmed Hassan

Department of Civil and Environmental Engineering

Carleton University

Ottawa-Carleton Institute of Civil and Environmental Engineering

September

ABSTRACT

Compared to other rehabilitation techniques, the use of externally bonded Fibre Reinforced Polymers (FRP) sheets for repair of damaged and strengthening of deficient reinforced concrete (RC) structures has gained increasing acceptance as a viable alternative especially in rapid repair application or as a less disruptive rehabilitation strategy. In previous studies of FRP retrofit applications, the focus has been directed mainly on the retrofit of one-dimensional structural elements of beams and columns. In the present study, seismic retrofit of two-dimensional structural element of shear wall using FRP sheets is investigated. An important component in the failure mechanism of RC shear wall retrofitted with FRP sheets is the separation or debonding of the FRP sheets from the concrete wall surface during seismic responses. After the occurrence of concrete cracking in a shear wall under the reversed loading actions of an earthquake, it is observed that debonding of the FRP sheet from the concrete substrate spreads quickly reducing its lateral load resisting capacity. The interaction behaviour between the performance of the FRP and the concrete cracking behaviour is known as Intermediate Crack (IC) debonding mechanism. Although previously developed models are able to account for the debonding of FRP in one-dimensional beam members, they are unable to predict the behaviour of two-dimensional shear dominated shear wall components. This thesis presents a new computer simulation model that can accurately capture the hysteresis response behaviour of reinforced concrete shear walls repaired or strengthened with externally boned FRP sheets

under the reversed cyclic loading of earthquakes. The proposed computer model can accurately simulate the IC debonding mechanism under the two-dimensional stress state of the wall panel and the subsequent ductile flexural or brittle shear failure modes of walls with different aspect ratios. Computer simulation results correlate well with experimental test results. The proposed computer model can accurately predict the hysteresis response behaviour, lateral load resisting strength, energy dissipation capacity and ductility performance of FRP repaired or strengthened shear walls in seismic applications.

ACKNOWLEDGEMENTS

First and foremost I would like to thank God the most Merciful, the most Gracious, and the only Cherisher and Sustainer. I would then like to thank Professor David T. Lau, for his support and guidance over the past few years. Without him, the work would not have been possible. I would also like to acknowledge Professor Carlos A. Cruz-Noguez for his contributions in the early stages of this project, as well as his unwavering support, guidance, and friendship during his time at Carleton University.

I would also like to thank the contributions from his family and friends during this work. Specifically, my always supportive parents Alaa El-Din and Enas, brothers Amr and Khaled, the always supportive, inspiring friends and family outside home in the CUMSA as well as fellow graduate students Joshua Woods, Moneer Al-Tamimi and Eytan Fiszman. Finally, I would like to thank my students throughout the past years for their respect, support, inspiration and pushing me to further my knowledge.

TABLE OF CONTENTS

LIST OF TABLES

LIST OF FIGURES

1.0 INTRODUCTION

Reinforced-concrete (RC) shear walls are a common type of lateral load resisting system found in structures located in seismically active regions. Although the current practices of shear wall design have been significantly improved in recent decades (ACI 2005; CSA 1994), many older shear wall buildings are at risk of suffering severe damage during moderate or large earthquakes due to their structural deficiencies (Lombard et al. 2000). The common structural deficiencies associated with old shear wall structures include insufficient in-plane stiffness, flexural strength, shear strength and/or ductility (Lombard et. al. 2000). Replacing the old vulnerable RC shear walls with shear walls meeting current more stringent code provisions is both prohibitively expensive and disruptive to the structure functionality; therefore, research has been conducted recently to develop retrofit techniques to mitigate the vulnerabilities and risks of old deficient structures so that they can achieve a minimum life safety performance in the event of an earthquake. Commonly used retrofitting techniques include the application of shotcrete, filling of openings with masonry infills, or the addition of new shear walls or steel bracing elements (FEMA, 1997). However, these techniques add significant weight to a structure, which can change its dynamic properties and result in additional dynamic earthquake loads not accounted for in the original foundation design of the structure. An attractive, minimally disruptive option for the repair and strengthening of shear walls in existing RC structures is the use of fibre-reinforced polymers (FRP) sheets (Triantafillou, 1998).

The use of externally bonded FRP sheets has gained increasing interest in the past decade and a number of experimental studies have been conducted to examine its efficiency in retrofitting RC shear walls. The experimental studies that examine the use of FRP for strengthening RC shear walls can be divided into two main categories. The first category includes tests which examine the effect of FRP on shear strength and energy dissipation capacity of the walls (Antoniades et al. 2003; Paterson and Mitchell 2003; Khalil and Ghobarah 2005; Elnady 2008, Shaheen 2013). The second category includes tests that focus on enhancing the flexural capacity and stiffness of shear walls (Lombard et al. 2000; Hiotakis 2004). Although the use of FRP had been proven to enhance shear strength, flexural strength, ductility and energy dissipation capacities in a number of experimental studies; in comparison very few studies have focused on developing numerical models for modelling FRP retrofit applications in RC shear walls. Developing a numerical model capable of accurately predicting the response of walls strengthened using externally bonded FRP under earthquake loads is crucial for determining the enhancement effects of the FRP on both the flexural and shear strength of the strengthened walls. Such a model can be used to assess the failure mechanism of a structural wall whether it will suffer a brittle shear failure or a ductile flexural failure. A quick overview of some of the existing numerical models for predicting the seismic response of the RC structures strengthened using FRP is presented in the following section.

1.1 Literature Review

Smith and Teng (2002) have presented an extensive literature review of experimental studies on the use of FRP plate for strengthening simply supported RC beams. They identified 6 different failure mechanisms as shown in Figure 1-1. Among the six failure modes shown in Figure 1-1, the first three are common modes of failure in conventional RC beams; however, the failure modes (d) to (f) are modes unique to beams bonded with a soffit plate. These failure modes are identified as premature debonding failures since they occur before the flexural failure of the section in mode (a) or (b) or the shear failure in mode (c) occurs. They have classified the premature debonding failure mechanisms into two main categories: (a) Debonding that initiates at or near one of the plate ends (which they referred to as plate end debonding); and (b) Debonding that initiates at an intermediate flexural or flexural-shear crack and then propagates towards the plate end. They have decided to focus on the plate end debonding in their studies since it was the more common debonding mechanism in the simply supported beams strengthened with FRP plates. They have completed an assessment of 12 different debonding strength models' strengths and weaknesses through comparing their predictions with a database which includes the results of 59 beams failed due to plate end debonding. The interesting conclusion from their study is that they found that the most reliable models are originally developed for steel plated beams rather than FRP plated beams.

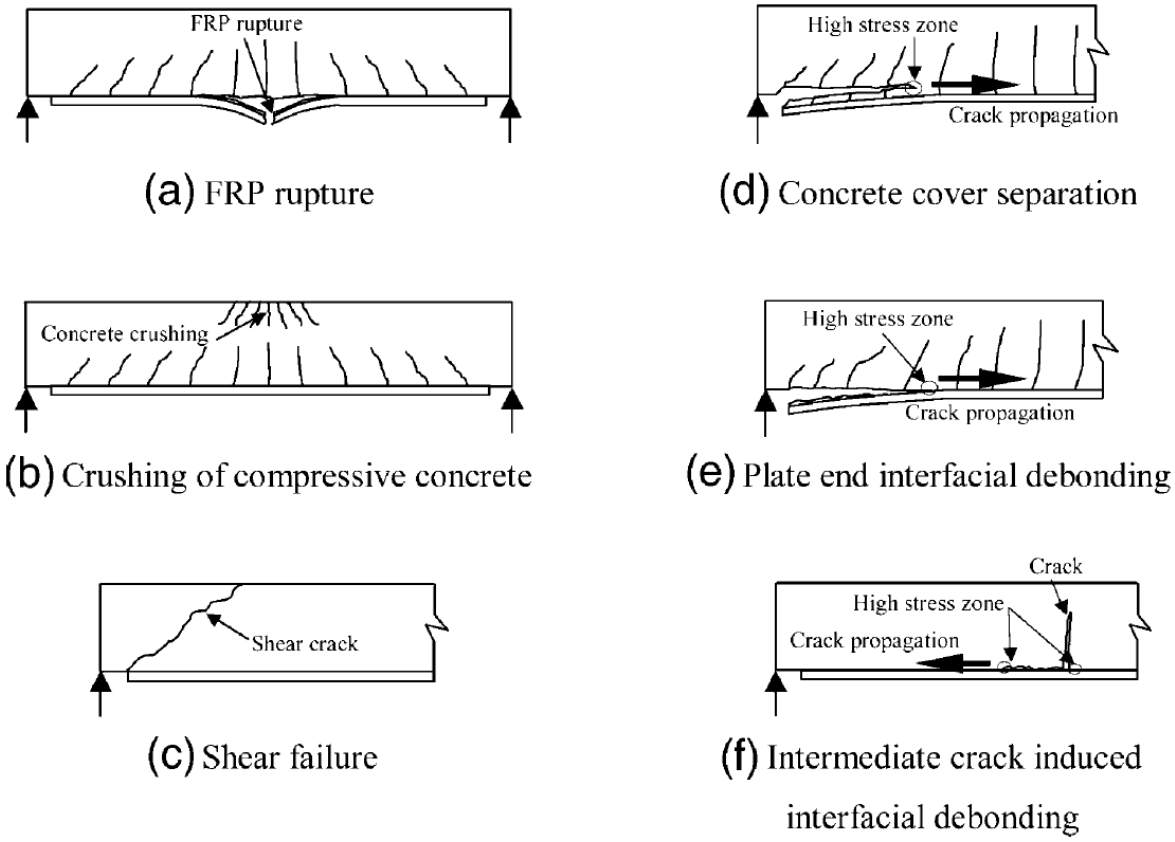

Figure 1-1: Failure modes of FRP-strengthened RC beams (Smith &Teng, 2002)

Oehler et al. (2003) performed a close examination of the three debonding mechanisms briefly introduced by Smith and Teng (2002). In the study, three debonding types are identified: Intermediate Crack (IC) Debonding, Plate End (PE) Debonding and Critical Diagonal Crack (CDC) Debonding. CDC and IC debonding are grouped together in the classification by Smith and Teng (2002), however; Oehler suggests that they should be classified differently since the primary cause of debonding differs between both types. In CDC the primary cause for debonding is the shear displacement across the diagonal crack, on the other hand, in IC debonding axial strains are the main cause for debonding. Table

1-1 summarizes the different debonding mechanisms. After studying the debonding mechanisms carefully, Oehler provides recommendations to prevent both CDC and PE debonding by carefully placing the FRP plates. Nevertheless, IC debonding could not be prevented by judicious placement of the plate.

Table 1-1: Summary of Debonding mechanisms (Oehler, 2003)

Debonding types	Primary Cause	Debonding crack propagation
IC: Intermediate crack	Axial strains in a plate bridging a crack induced by flexure or flexure/shear	Debonding cracks initiate at the intercept of the plate with a flexural, flexural/shear or diagonal crack. Generally propagates towards the plate end.
CDC: Critical diagonal crack	Rigid body shear displacement across a critical diagonal crack	Debonding cracks initiate at the intercept of the plate with the critical diagonal crack. Propagates towards the plate end.
PE: plate end	Curvature in the beam adjacent to plate end	Debonding cracks initiate at the plate end. Propagates inwards.

The strength models reviewed and assessed by Teng et al. (2003) and others focus on the use of FRP for the flexural strengthening of RC beams. Wong and Vecchio's (2003) study investigates the application of FRP composites for shear strengthening. Their study is composed of an experimental program as well as modifying previous numerical finite element (FE) models to account for debonding of the FRP. Modelling the bond at the concrete-FRP interface was given recognition due to its importance in providing a load transfer mechanism between the two components. The bond model accounts for the relative displacement between FRP and Concrete combined with using local stress-slip relationships. A proposal was made for the use of two possible bond elements to model the concrete-FRP interface, namely link elements and contact elements. The bond elements follow one of two constitutive relationships for the bond interface, either elastic-plastic or

linear elastic (Figure 1-2). The parameters in these models include the maximum shear stress that can be sustained by the bond interface U_{max}, the slip at the first occurrence of maximum bond stress S_{max}, and the ultimate slip when the bond fails S_{ult}. The slope of the linear relationship is termed the slip modulus E_b and is based on the shear stiffness of the epoxy G_a used, as defined by Equation 1-1:

$$E_b = \frac{G_a}{t_a} \quad where \quad G_a = \frac{E_a}{2(1+v_a)} \qquad (Equation\ 1-1)$$

After incorporating these bond elements into the FE analyses it was determined that accounting for bond-slip is viable and that it is necessary to model the interface behavior to accurately predict the Response of FRP-Strengthened RC members. However, they suggest that more clearly defined constitutive relationship must be developed to improve modelling capability.

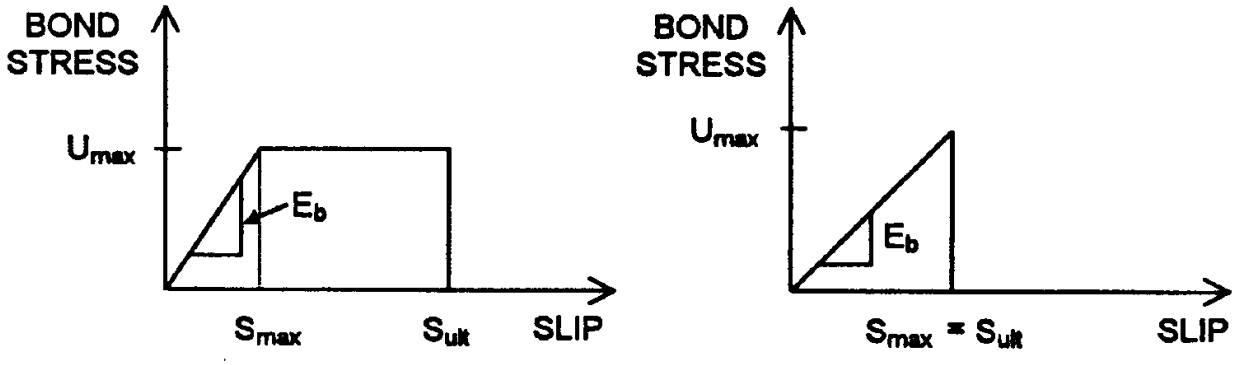

Figure 1-2: Constitutive relationship for bond interface: Elastic Plastic (left) and Linear Elastic (right) (Wong & Vecchio, 2003)

In their study, Teng et al. (2003) recognize the lack of strength models which account for IC debonding, an issue previously noted by Wong and Vecchio. Chen and Teng (2001) had already developed a bond strength model capable of predicting bond strength and effective bond length for FRP and steel plates bonded to concrete members based on a series of single and double shear tests (Figure 1-3). To predict the strength of beams and slabs that fail by IC debonding, a modification to the original model was developed using a simple section analysis. The modified model is defined as follows:

$$\sigma_p = \alpha\beta_p\beta_L\sqrt{\frac{E_p\sqrt{f'_c}}{t_p}} \qquad (Equation\ 1-2a)$$

where

$$\beta_p = \sqrt{\frac{2 - {b_p}/{b_c}}{1 + {b_p}/{b_c}}} \qquad (Equation\ 1-2b)$$

$$\beta_L = \begin{cases} 1 & if\ L \geq L_e \\ \sin\dfrac{\pi L}{2L_e} & if\ L < L_e \end{cases} \qquad (Equation\ 1-2c)$$

$$L_e = \sqrt{\frac{E_p t_p}{\sqrt{f'_c}}} \qquad (Equation\ 1-2d)$$

in which E_p, t_p and b_p are the elastic modulus (MPa), thickness (mm) and width (mm) of the bonded plate; while f'_c and b_c correspond to concrete compressive strength (MPa) and width (mm) of the concrete block respectively. The variables L and L_e correspond to the

bond length (mm) and effective bonded length (mm). The parameter of α = 0.48 is determined to provide the best fit with the experimental data in which the debonding occurrs due to intermediate cracks.

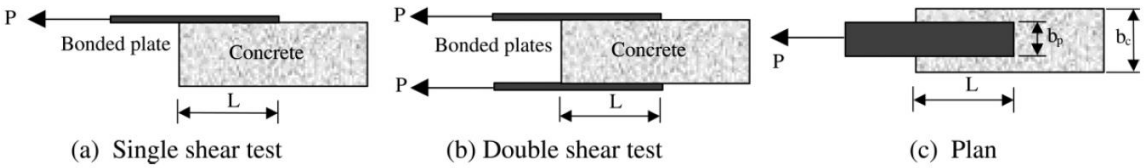

Figure 1-3: Single and double shear tests (Teng, 2003)

Lu et al. (2004) develops a more sound understanding of the FRP-to-Concrete interface rather than solely base the relationship on experimental results and a sectional analysis. Therefore, to be able to study the bond-slip relation of the FRP-Concrete interface a finite element (FE) model of FRP-to-Concrete bonded joints was developed. Debonding was directly simulated by modelling the cracking and failure of concrete elements adjacent to the adhesive layer. The advantage of this approach is that the model can predict the debonding behaviour using an appropriate constitutive model for concrete, without the need of adopting an interfacial bond–slip model for modelling the interfacial interaction behaviour between the FRP and concrete substrate. In general, the debonding of FRP from concrete is observed to occur within a thin layer of concrete adjacent to the adhesive layer for adhesives of typical strength. The thickness of this concrete layer is about 2–5 mm. In order to capture accurately the cracking and debonding behaviour within the thin layer of concrete at the interface with the FRP sheet, a very fine finite element mesh with element sizes one order of magnitude smaller than the thickness of the facture layer of concrete is

necessary in the model (0.25-0.5 mm) in order to capture the development and propagation of cracks in the concrete. This modelling technique is referred to as a meso-scale finite element modelling. The computer simulation results from the model correlates well with the ultimate load, effective bond length and strain distributions from experimental test results.

After demonstrating the reliability of the meso-scale modelling technique, Teng et al. (2004) use the model to closely examine the bond-slip relationship between the external FRP reinforcement sheet and the underlying concrete. They develop a constitutive relationship used for the interface elements between the FRP materials and concrete. A finite element parametric study was conducted using three different proposed bond-slip models of different levels of sophistication; namely precise model, simplified model and bilinear model. All Three models have shown to be more accurate than previously proposed bond-slip models (Figure 1-4). The bilinear model, which is the simplest model of the three models considered, correlates between the local bond stress (τ) and the local slip (s) follows:

$$\tau = \begin{cases} \tau_{max}\, {}^{s}/_{s_o} & if\ s \le s_o \\ \tau_{max}\ (s_f - s)/(s_f - s_o) & if\ s_o < s \le s_f \end{cases} \qquad (Equation\ 1-3a)$$

where,

$$s_f = \frac{2G_f}{\tau_{max}} \qquad (Equation\ 1-3b)$$

$$s_o = 0.0195\ \beta_w f_t \qquad (Equation\ 1-3c)$$

$$\tau_{max} = 1.5\beta_w f_t \qquad (Equation\ 1-3d)$$

$$\beta_w = \sqrt{\left(2.25 - {}^{b_f}/_{b_c}\right)/\left(1.25 + {}^{b_f}/_{b_c}\right)} \qquad (Equation\ 1-3e)$$

with f_t being the tensile strength of concrete while b_f and b_c refer to the width of the concrete prism and the FRP plate respectively.

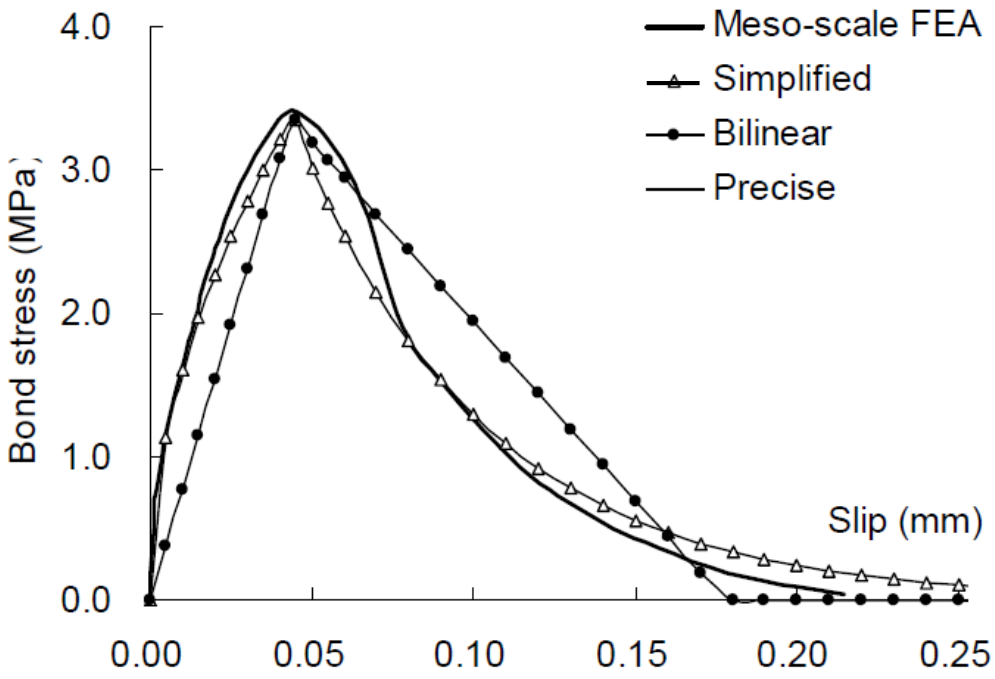

Figure 1-4: Bond-slip curves (Lu et al., 2004)

In the study by Lu et al. (2007), they attempt to model the IC debonding mechanism by using the stress-slip model proposed earlier. Since the meso-scale modelling is very computationally demanding especially in large structures, it is attractive to develop a simple model that can give reasonably accurate results on the prediction of the debonding of FRP sheets from the concrete substrate in large-scale structures. First, a number of

previously tested strengthened beams were modeled using the meso-scale modelling technique. To be able to define the bond between concrete and FRP more accurately, the beams were divided into two main zones and depending on the location of the FRP, the bond-slip model adopted for the modelling will be different. If the wall lies outside the zone with major flexural cracking then the FRP-Concrete bond can be defined using any of the three models described earlier in Equation 3. For FRP located within zones of major flexural cracking, the average bond-slip response from the numerical results over a certain length was obtained and averaged since it is difficult to obtain a stable bond-slip curve for a single point along the interface. Two averaging lengths that correspond to interface element widths were used. The result of averaging the bond-slip responses for these two averaging lengths was used to determine the bond-slip relationship for FRP within major flexural cracking zone. As shown in Figure 1-5, both curves are composed of a curved ascending branch, which is very similar to the ascending branch in bond-slip relationship for FRP outside flexural cracking zone, and a highly brittle descending branch. Therefore, to account for this difference, bond-slip responses can be closely described by the use of the original bond-slip model of Lu et al. (2005) with a brittle post peak branch, as shown in Figure 1-5. This modified model is referred to as Bond-Slip model II and is derived using the bilinear model:

$$\tau = \begin{cases} \tau_{max}\, {}^{s}/_{s_o} & if\ s \le s_o \\ 0 & if\ s > s_o \end{cases} \qquad (Equation\ 1-4)$$

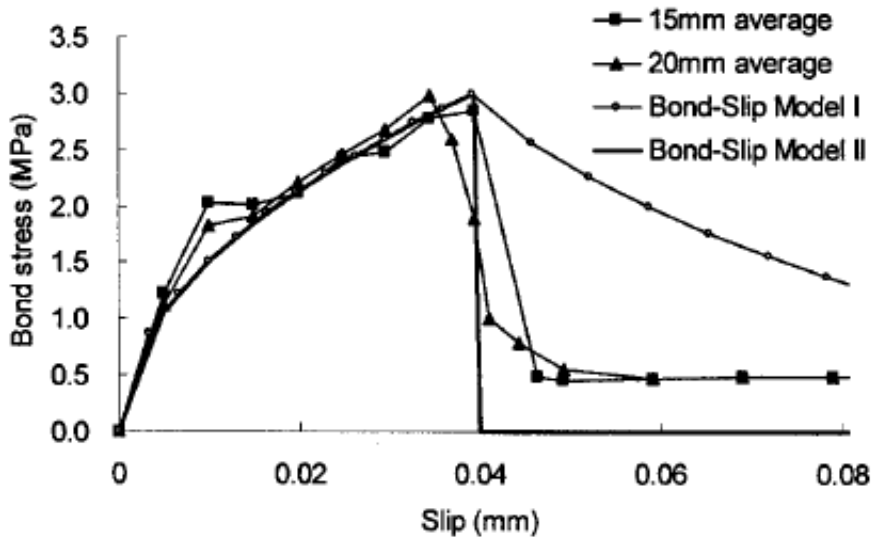

Figure 1-5: Bond-Slip model within major flexural crack zone (Lu et al., 2007)

Once a Bond-slip interface model was clearly defined, it was possible to model larger beams using the conventional FE approach, in which the elements of normal size are used. Link elements can then be used to link the concrete mesh to the FRP which is usually modeled as truss elements since the FRP sheets are applied in a single direction parallel to the longitudinal reinforcements. All the link elements originally follow the bond-Slip model associated with FRP outside flexural cracking zone, i.e. Bond-Slip model I. Once concrete element to which the link element is connected to undergoes extensive cracking that causes debonding, the link element follows the bond-slip model corresponding to FRP within major flexural cracking zone, i.e. Bond-Slip model II. Figure 1-6 shows that in any given concrete element with a flexural crack of width w, the interfacial FRP-concrete slips s that- appear at both sides of the flexural crack can be approximated as $w/2$. Since IC debonding is considered to take place if the slip , s, is greater than slip at ultimate, s_o, the

crack width in a concrete element that causes FRP-concrete debonding should be therefore equal or larger than $2s_o$; In which case Bond-Slip model II is used. However, if the crack width in a concrete element is smaller than $2s_o$, the bond-slip model I still apply.

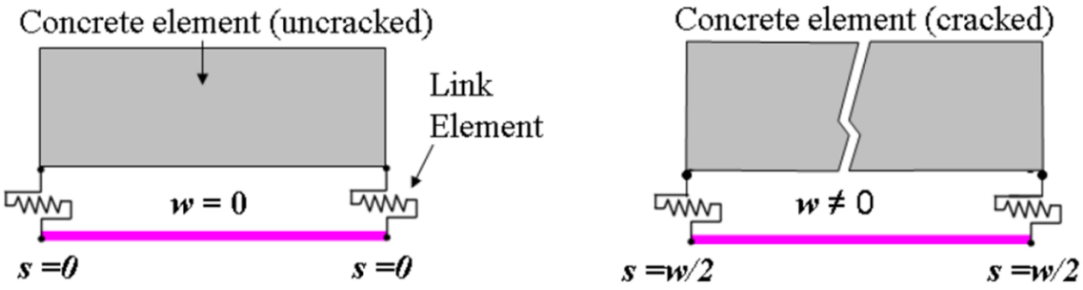

Figure 1-6: Slips at interface elements (Cruz-Noguez et al., 2012)

1.2 Objective and scope

As apparent in the previous section, a number of researchers have developed numerical models for RC beams and slabs repaired/strengthened in flexure with FRP (Smith and Teng 2002; Wong and Vecchio 2003; Oehler et al. 2003; Lu et al. 2007), however there is relatively scant information on the analytical modelling of RC shear walls flexurally-reinforced with FRP sheets. Previously a numerical model to predict the nonlinear response for the flexurally reinforced walls was developed by Cruz-Noguez et al. (2012); which will be discussed in details later in this thesis. The major problem with that model was its inaccuracy when analyzing walls which are shear deficient and strengthened in shear rather than in flexure. In this study, a numerical model capable of predicting the response of both shear deficient and flexural dominant walls is developed. Using this new model, this thesis presents a numerical study on the simulation of the nonlinear hysteretic response behaviour

of two shear deficient shear wall specimens strengthened with FRP which have been tested to failure at Carleton University (Woods, 2014). The novel aspect in this study is the implementation of a computationally efficient computer procedure that can capture the entire debonding process between the concrete substrate and the FRP material from initial debonding failure of the FRP sheets to post peak ultimate collapse of shear deficient walls. The computer simulation results are compared with measured experimental data to validate the accuracy of the numerical model.

2.0 EXPERIMENTAL PROGRAM

The analytical study presented in this study is verified through an experimental program that is ongoing at Carleton University. In order to fully understand the methodology of the modelling techniques and relate to the analytical results a thorough understanding of the experimental program is required. Although the experimental program is done on three phases, the first and second phase are almost identical when it comes to analytical modelling, as will be discussed in the following sections. Therefore, it is appropriate to divide the experimental study overview in this section into two categories based on their design approach and failure mechanism, hence whether it is a flexural dominant wall or a shear dominant wall.

2.1 Overview

In research literature, shear walls are often classified based on the aspect ratio and failure mechanism of the walls. Walls with aspect ratios (h_w/l_w) less than or equal to 2 are typically referred to as short or squat walls, whereas walls with aspect ratios greater than or equal to 3 are referred to as flexural or slender walls. Typical failure mechanisms in shear walls include: a) Flexural failure consisting of crushing of concrete in compression together with yielding of vertical steel reinforcement; b) Sliding shear failure typically along the construction joint at the base; and c) Brittle diagonal tension or compression shear failure, as shown in Figure 2-1.

Design objectives of current design standards aim to achieve flexural failure mode in shear walls since flexural failure is more ductile which gives prior warning signs of imminent failure. Shear failure modes on the other hand are brittle which occur suddenly without prior warning signs. Shear walls designed according to older design standard requirements typically have insufficient shear reinforcements and lack of ductile detailing. These old shear walls have lower shear strength than their flexural strength and thus are more susceptible to shear failure dominating the response of these walls.

All the walls tested in the experimental program in this study have aspect ratio less than 2 (1.2, 0.85 and 0.65). Thus they would all be classified as squat walls in research literature. However, for the sake of easier identification, the walls with the highest aspect ratio of 1.2 are referred to as slender walls. Whereas walls with aspect ratios of 0.85 and 0.65 are referred to in this study as intermediate and squat walls respectively. Also, walls identified as flexural dominant walls have flexural failure mode. Walls identified as shear dominant have shear failure mode.

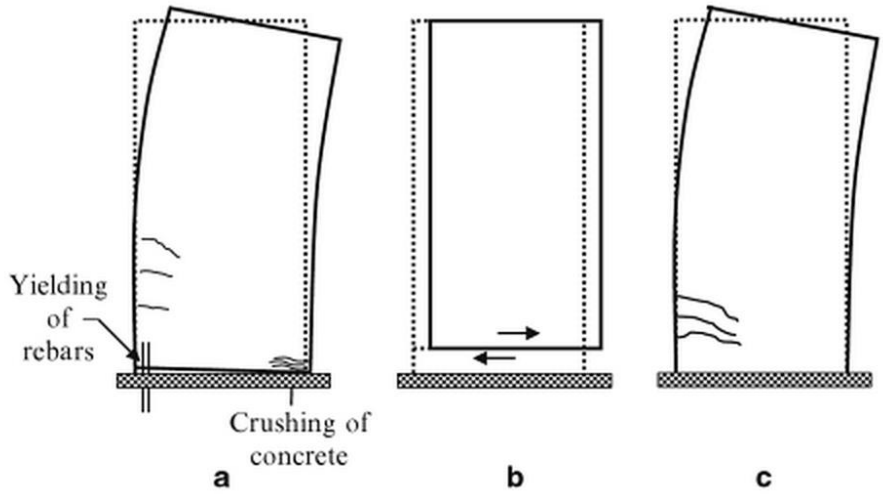

Figure 2-1: Typical failure modes of shear walls (a) Flexural failure, (b) Sliding failure, (c) Shear failure (Moehle, 2014)

2.2 Flexural dominant walls

The objective of the first phase of the experimental program is to evaluate the feasibility and effectiveness of using externally bonded FRP tow sheets for strengthening and repair of RC shear walls as well as developing an analytical model suitable for designing repair and strengthening schemes (Lombard, 1999). Although the use of externally bonded FRP sheets for strengthening and repairing RC beams and columns has been studied extensively; very scarce information was available on the use of the material on RC shear wall.

This phase of the experimental study consisted of three large scale shear wall specimens, two of which were to be strengthened while the other was to be repaired. One of the walls is tested in its as built condition up to a certain predetermined ductility. This wall is then repaired and loaded up to failure to determine the effectiveness of the repair technique. The results from the wall tested in the as-built condition are used as the results for the control

wall. The control wall results are used as a baseline to determine the effectiveness of the repair and strengthening techniques. The other two walls are strengthened in their as-built conditions then tested to failure. All the three specimens had the same size and detailing. The walls are designed to simulate a wall that would exhibit a flexural failure, the wall is also designed to have sufficient shear strength so that it could be repaired to its original state without the need to repair or add additional shear reinforcement. The design resulted in walls with longitudinal and transverse reinforcement ratios of 0.8 and 0.5% respectively. Additional concrete confinement at the edges of the walls was provided by steel stirrups. The height-to-length aspect ratio h_w/l_w for all walls was 1.20, and the thickness of the walls t_w was 0.10 m (Figure 2-2 & Figure 2-3). The strengthening scheme for the repaired wall aims to recover the initial stiffness and if possible increase the strength. Similarly, both the strengthened walls are designed to prompt a ductile flexural failure at its ultimate capacity. Strengthened wall 1 (Referred to hereafter as SW1-1), is designed to have a higher in-plane flexural strength and stiffness. Strengthened wall 2 (referred to hereafter as SW2-1) is designed to have even higher flexural strength and stiffness than SW1-1. This resulted in using different numbers of FRP layers as described in Table 2-1. The anchoring system used to anchor the FRP sheets to the wall surface consists of L150x100x10, 400 MPa structural steel angles epoxy bonded to vertical CFP layers then bolted to the foundation (Figure 2-4).The load was applied using a hydraulic actuator to the top beam in the wall specimens. The loading sequence consisted of quasi-static cycles predetermined to aim for critical load points such as yielding of the vertical steel reinforcement. The loading was

force controlled up to yield and then it was displacement controlled up to failure, as shown in Figure 2-5. Each load cycle was repeated twice to simulate the effect of damage caused by an earthquake. The wall was fixed to the laboratory strong floor using a rigid foundation block at the bottom of the wall panel which acted as the footing of the wall. Six 60 mm diameter high strength bolts were used to anchor the footing of the wall to the laboratory strong floor as shown in Figure 2-6.

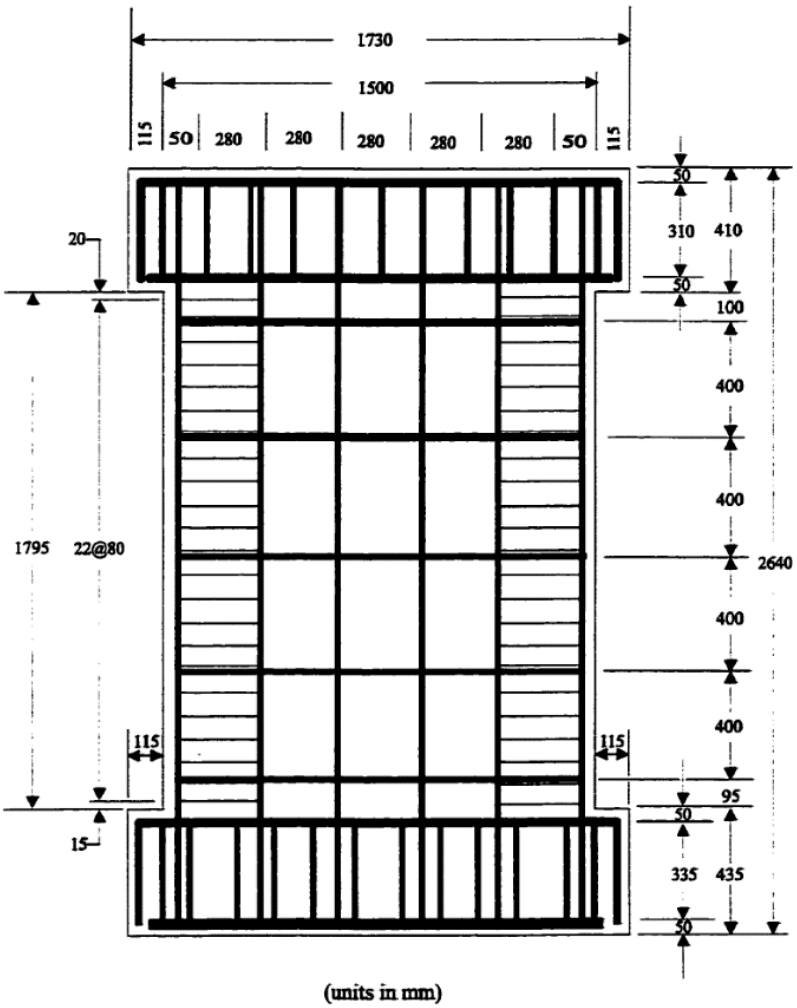

Figure 2-2: Reinforcement details of a shear wall test specimen in phase 1 of the experimental program (Lombard, 1999)

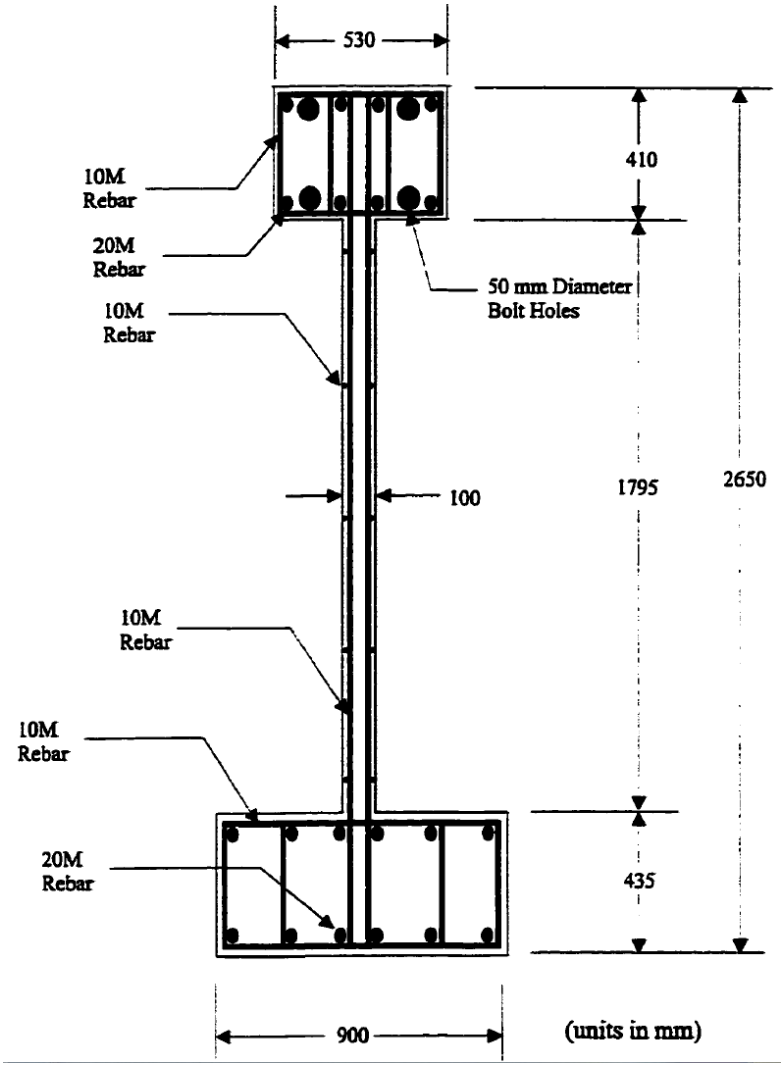

Figure 2-3: End view of the reinforcement layout for wall specimens in phase 1 of the experimental program (Lombard, 1999)

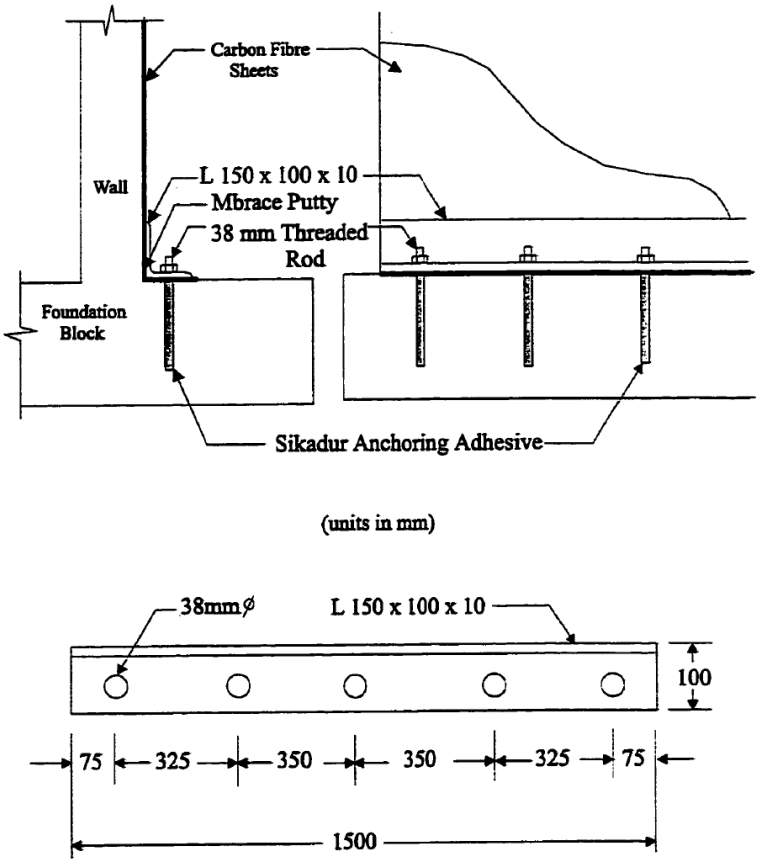

Figure 2-4: Schematic diagram of the anchoring system for the CFRP sheets in phase 1 of the experimental program (Lombard, 1999)

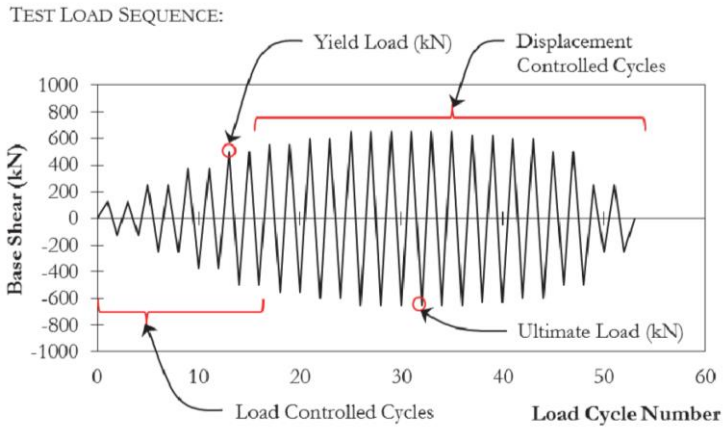

Figure 2-5: A typical loading sequence used for the testing of the RC shear walls (Woods, 2014)

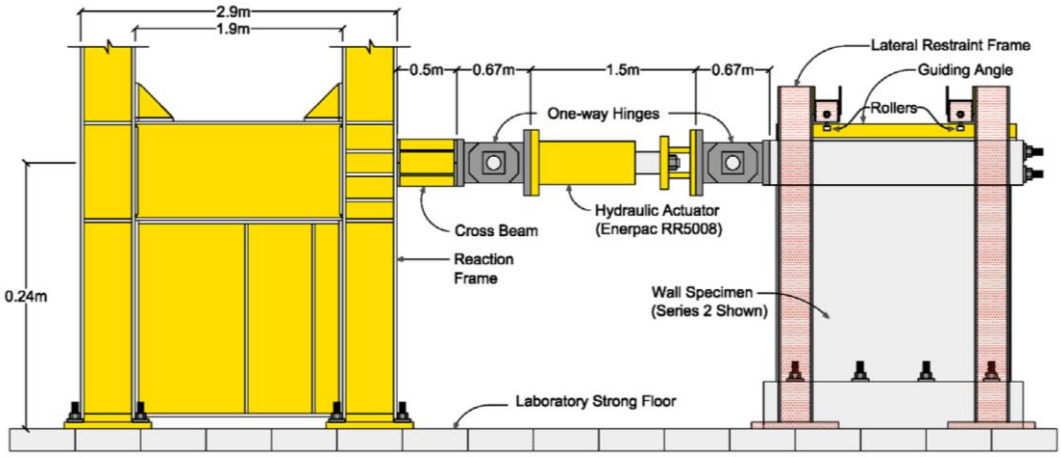

Figure 2-6: Experimental setup used for the testing of the walls in different phases (Woods, 2014)

Table 2-1: Strengthening and repair schemes used in phase 1 of the experimental program

Phase	Anchor type	Type of Specimen	Repair/Strengthening Scheme*	Code
1	Angle	Control	---	CW-1
		Repaired	1V	RW-1
		Strengthened	1V	SW1-1
		Strengthened	2V + 1H	SW2-1

*V-Vertically oriented FRP sheets and H-Horizontally oriented FRP sheets

The experimental investigation proved the ability of the FRP strengthening technique to increase (Figure 2-7), or at least recover in the case of repair applications (Figure 2-8), the initial stiffness of the shear walls. The techniques are also capable of increasing the ultimate flexural capacity, however this increase is limited by the ability of the anchor to transfer the loads efficiently. This is apparent when looking at the failure mechanism in strengthened wall SW1-1 where the anchor prematurely fails and leads to tear in the FRP sheets (Figure 2-9). Lombard (1999) suggested testing more walls with different aspect ratios and determining the efficiency of using the FRP to enhance the shear strength of RC shear walls. Another suggestion was the improvement of the anchorage system for the

vertical FRP so that it would reduce prying action, optimize bolt spacing and investigate different types of anchors.

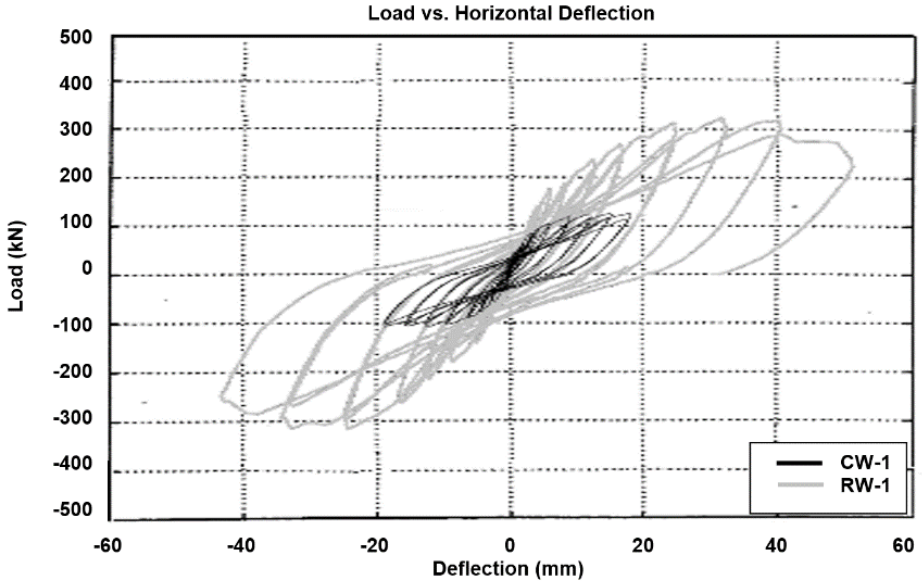

Figure 2-7: Load vs Displacement response of walls repaired with FRP in phase 1 (Lombard, 1999)

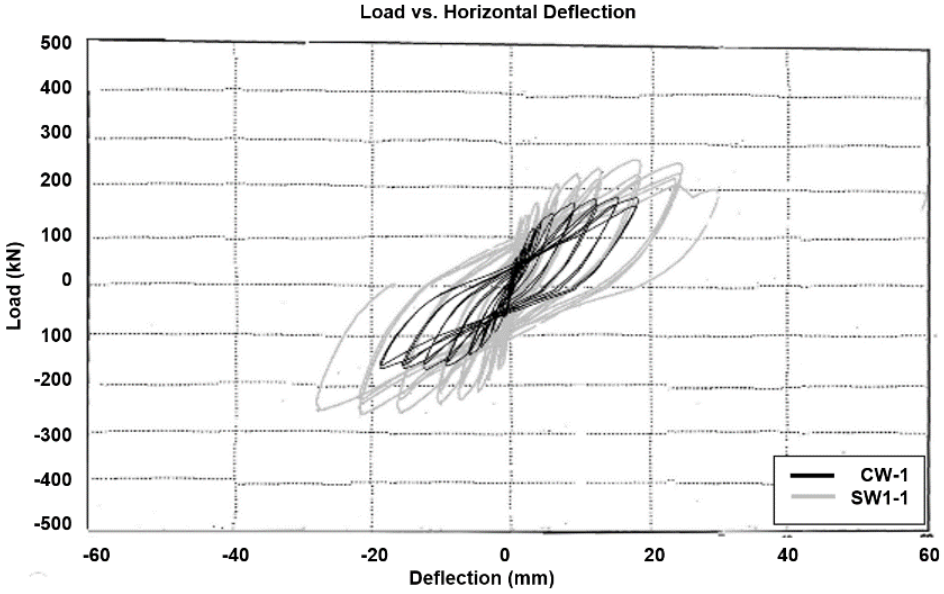

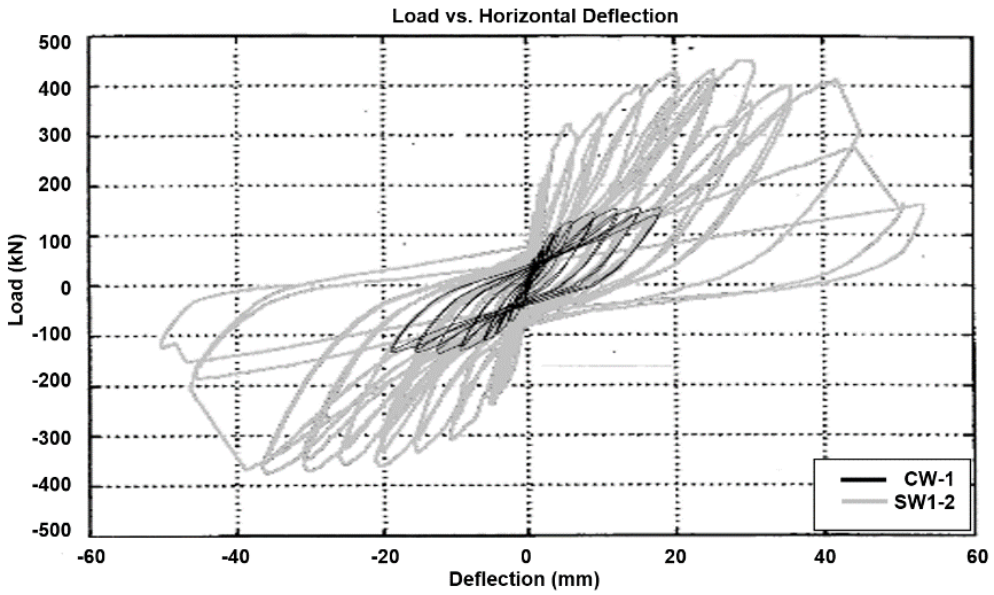

Figure 2-8: Load vs Displacement response of walls strengthened with FRP in phase 1(Lombard, 1999)

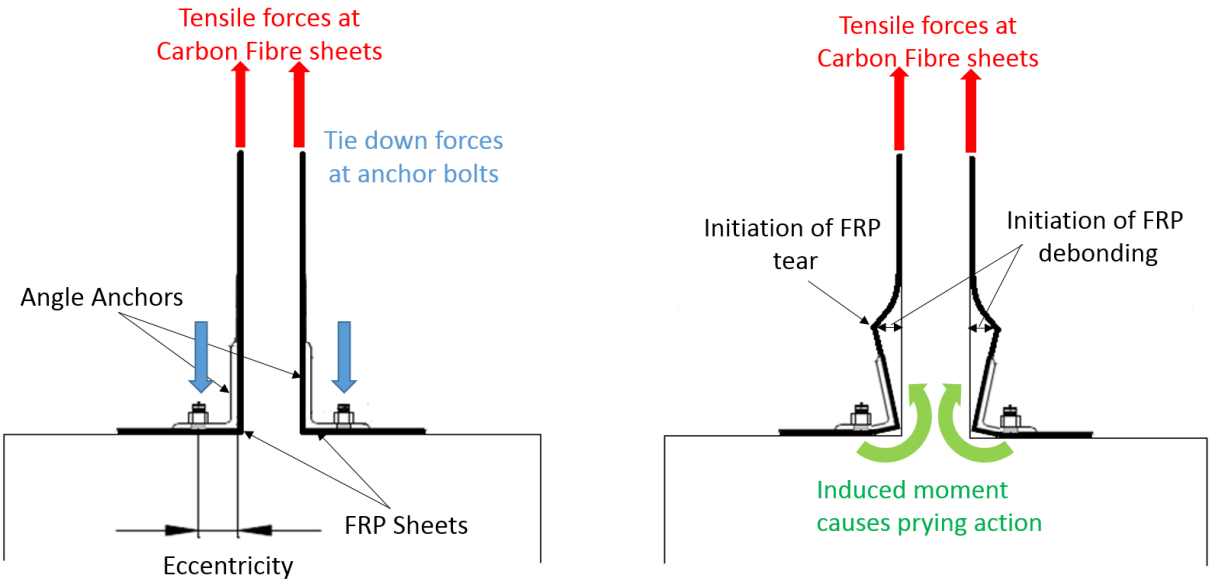

Figure 2-9: The load transfer mechanism in the angle anchor and initiation of debonding

The second phase of the experimental program aims to solve the problems encountered during phase one of the experimental tests (Hiotakis, 2004). That meant that the study has to focus on the design and testing of a new load transfer mechanism/anchor in an attempt to utilize the Carbon Fibre Sheet material to its maximum capacity. In order to validate the effectiveness of the newly designed anchor systems, the walls tested, repaired and strengthening using FRP sheets in this phase of the experimental study had to have the same dimensions and design as those tested in the first phase of the experimental study (Figure 2-2 & Figure 2-3).

This phase of the experimental study consisted of four shear wall specimens, three of which were to be strengthened while the other was to be repaired. Similar to phase 1 of the study, one wall is tested in its as built condition up to a certain predetermined ductility then repaired and loaded up to failure. The other three walls are strengthened in their as-built conditions then tested to failure. The strengthening and repair schemes utilized in this phase are described in Table 2-2. As for the new anchor system, the main objective is to eliminate the prying action effect of the L-shaped angle anchor by eliminating the moment arm between the lines of action of FRP resistance forces and the anchor tie-down forces. Based on this consideration a new anchor is designed based on the pulley mechanisms in which a cylindrical hollow section (CHS) is used. In this new anchor system the line of action for all the FRP tension forces as well as the anchor tie-down reaction is centralized at one point in turn eliminating any eccentricity and hence preventing prying action (Figure 2-10).

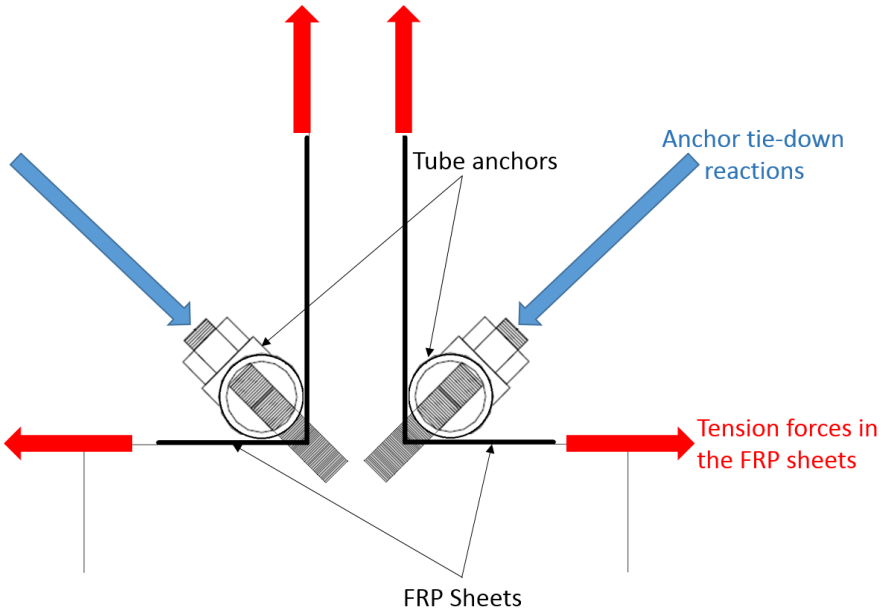

Figure 2-10: The load transfer mechanism in the tube anchor preventing debonding

The new anchoring system performed very well and eliminated any deficiencies associated with using the L-shaped steel angle anchor used in the first phase. The use of FRP sheets was capable of enhancing the strength, ductility and initial stiffness for both the repair and the strengthening applications (Figure 2-11 & Figure 2-12).

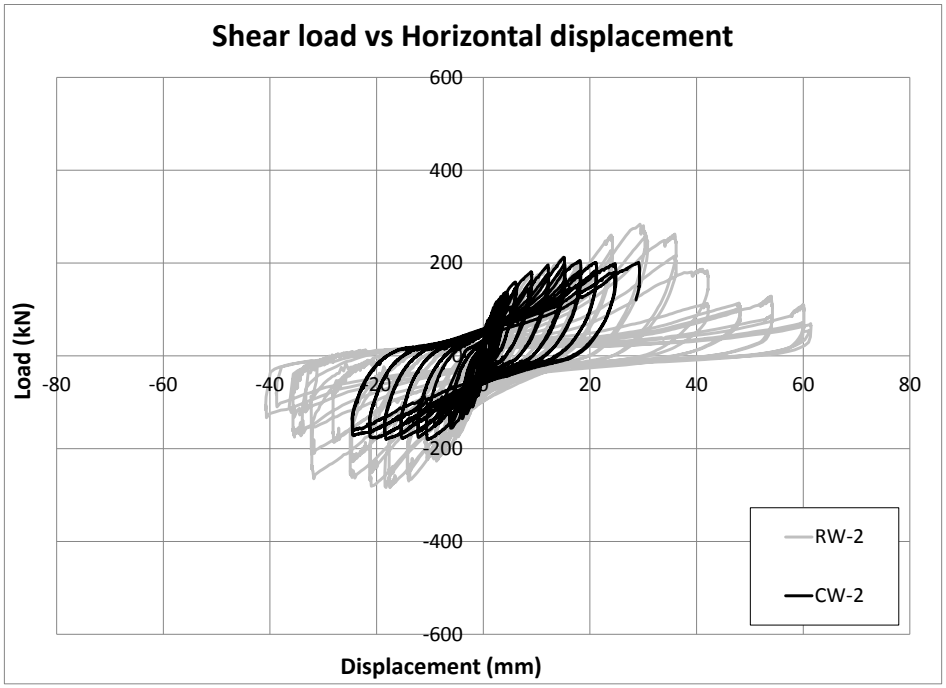

Figure 2-11: Load vs Displacement response of walls repaired with FRP in phase 2 (Hiotakis, 2004)

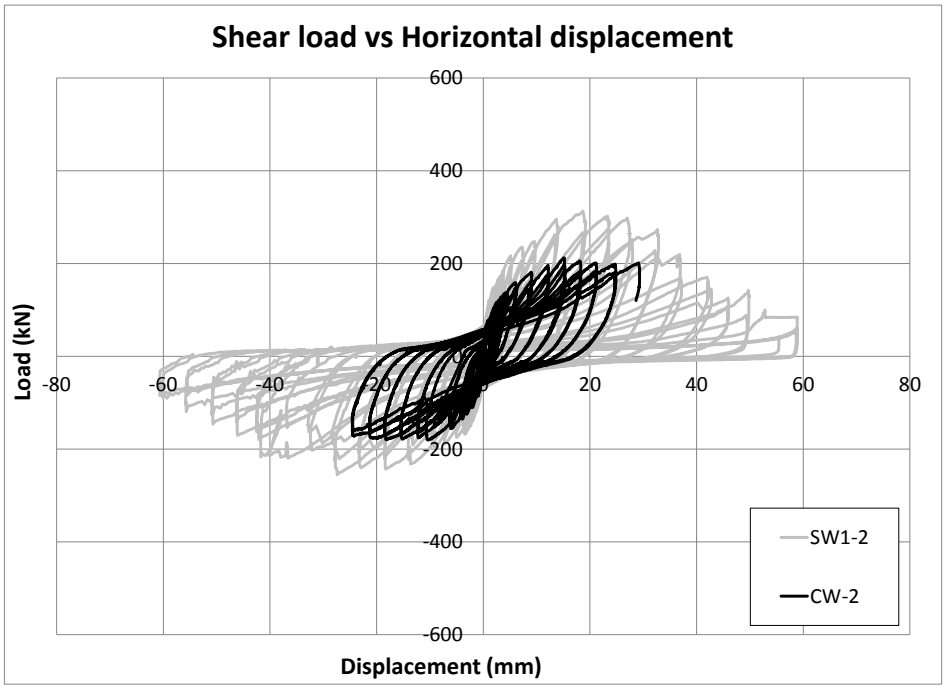

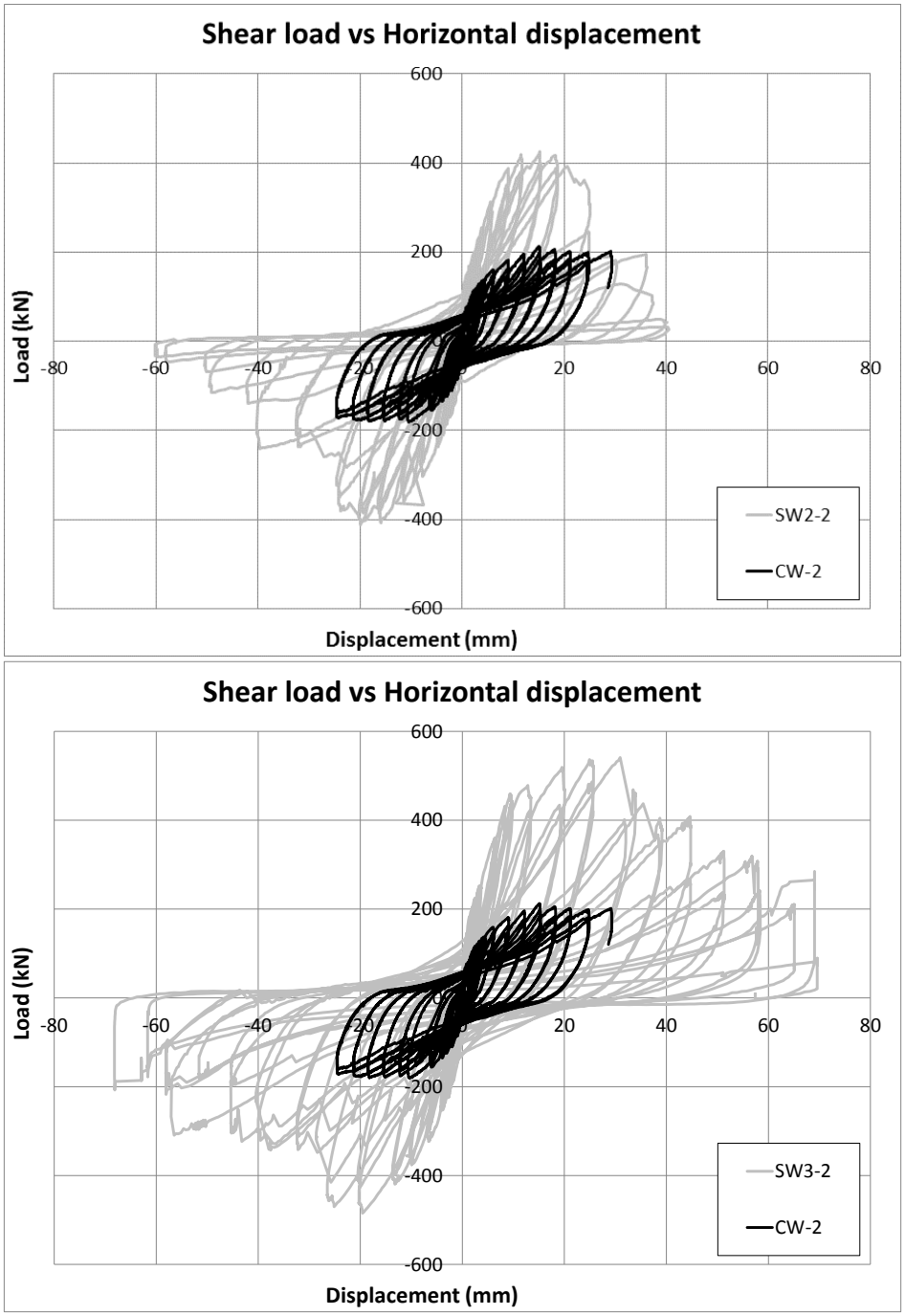

Figure 2-12: Load vs Displacement response of walls strengthened with FRP in phase 2 (Hiotakis, 2004)

Table 2-2: Strengthening and repair schemes used in phase 2 of the experimental program

Phase	Anchor type	Type of Specimen	Repair/Strengthening Scheme*	Code
2	Tube	Control	---	CW-2
		Repaired	1V	RW-2
		Strengthened	1V	SW1-2
		Strengthened	2V	SW2-2
		Strengthened	3V+1H	SW3-2

*V-Vertically oriented FRP sheets and H-Horizontally oriented FRP sheets

2.3 Shear dominant walls

The third phase of the experimental study investigates the effectiveness of externally bonded FRP sheets to strengthen shear walls designed according to older design standards (ACI 318-68; CSA A23.3-77). Unlike the previously tested walls, the walls in this phase of study are designed with poor detailing such as insufficient shear reinforcement, poor confinement and low concrete strength. Another aspect investigated in this study is the effect of having different aspect ratios on the response of shear walls strengthened with externally bonded FRP sheets. The walls are designed to simulate a wall that would exhibit a brittle shear failure, this is a typical failure mechanism of walls designed using old code provisions. The design resulted in walls with longitudinal and transverse reinforcement ratios of 3.0 and 0.25%, respectively. Two different height-to-length aspect ratio h_w/l_w for the walls were used. Two walls have an aspect ratio 1.20 and thickness of t_w of 0.10 m (Figure 2-13). Another three walls have an aspect ratio of 0.85 and a thickness of t_w of 0.12 m (Figure 2-14). For the purpose of identifying the walls, the walls with aspect ratio of 1.20 will be referred to as the slender walls, whilst the walls with aspect ratio of 0.85 will be referred to as the intermediate walls.

The first slender wall is tested in its unstrengthened as-built condition up to failure and the response of the wall recorded to serve as a baseline to determine the efficiency of the strengthening and repair techniques; this wall will be referred to hereafter as the slender control wall (SLCW). The slender control wall is then repaired using conventional techniques of crack filling and resurfacing and then externally bonded FRP is applied to the surface of the wall; hence the wall will be referred to as slender repaired wall (SLRW). Both vertical and horizontal FRP layers are added to the concrete substrate according to the strengthening scheme in Table 2-3. The wall is then tested cyclically up to total collapse. The second slender wall is strengthened with FRP sheets as noted in Table 2-3 and then tested up to failure to determine the efficiency of using the FRP sheets for strengthening the RC shear wall. This wall is referred to as the strengthened slender wall (SLSW). The anchorage for the FRP sheets in both the repair and strengthening applications for the slender wall was provided by the steel tube anchor system that was discussed earlier and introduced in the second phase of the study by Hiotakis (2004).

Similarly, the first intermediate wall is tested in its unstrengthened as-built condition up to failure and the wall is referred to as the intermediate control wall (ICW). The intermediate control wall is then repaired and then externally bonded FRP is applied to the surface of the wall; with the wall referred to as intermediate repaired wall (IRW). The second and third intermediate walls were both strengthened with the same number of FRP sheets as recorded in Table 2-3 and then tested up to failure. The difference between the first intermediate strengthened wall (ISW-1) and the second intermediate strengthened wall

(ISW-2) is the application and anchorage of the FRP. In the first strengthened wall, the tube anchor was used with layers of FRP applied to both side of the wall. This is the same technique used for the repaired walls as well as the slender walls as described earlier. For the second strengthened wall, Carbon fiber reinforced polymer (CFRP) and Glass fiber reinforced polymer (GFRP) anchors were used to anchor the vertical and horizontal FRP sheets respectively (Figure 2-15). Also, double the number of FRP sheets was applied to one side with the other side having no FRP sheets. This was done to determine the effectiveness of using fan anchors in comparison with the tube anchor system.

When looking at the response of the repaired walls (Figure 2-16 & 2-17) it can be observed that the ductility and energy dissipation capacity of the wall specimens has not increased dramatically when compared with the control walls, however, the retrofitting system is capable of restoring or slightly exceeding the performance level of the walls when compared to their original state (Woods et al., 2015). The strengthened walls on the other hand exhibit significant improvements in ductility when compared to the control walls, achieving displacement ductility ratios ranging from 2.5-4.0 (Figure 2-18 to 2-20). The strengthened wall specimens also exhibit higher energy dissipation capacity, identified by wide loops in the hysteretic response. In strengthening applications, the retrofitting system is shown to be able to increase the flexural strength, ductility, and energy dissipation capacity while preventing premature diagonal tension shear failure (Woods et al., 2015).

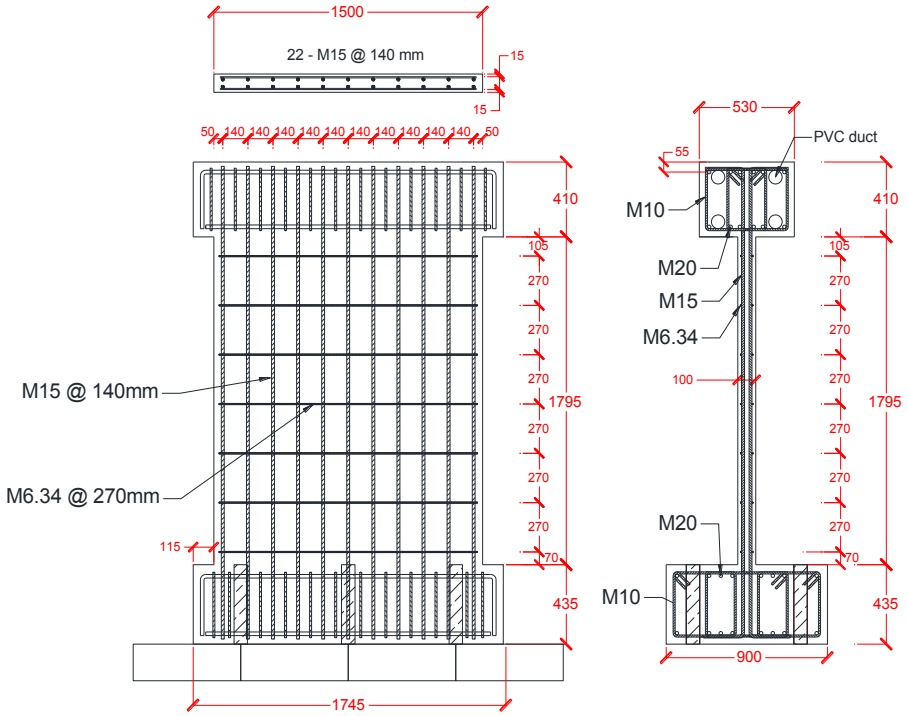

Figure 2-13: Reinforcement details of slender wall specimens in phase 3 (Shaheen et al., 2013)

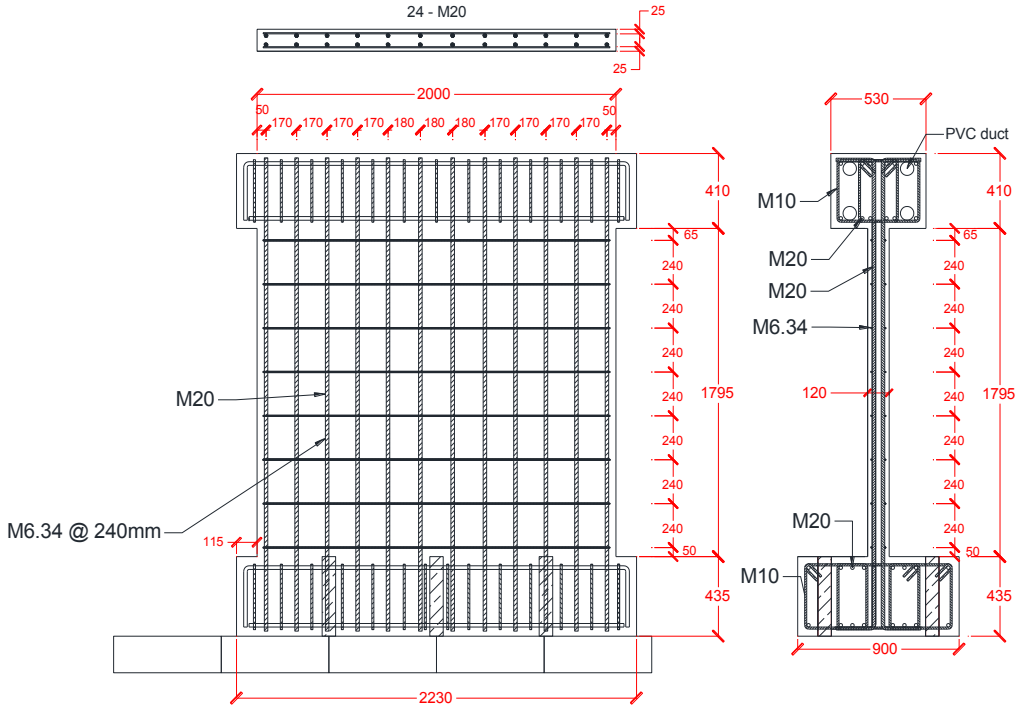

Figure 2-14: Reinforcement details of intermediate wall specimens in phase 3 (Shaheen et al., 2013)

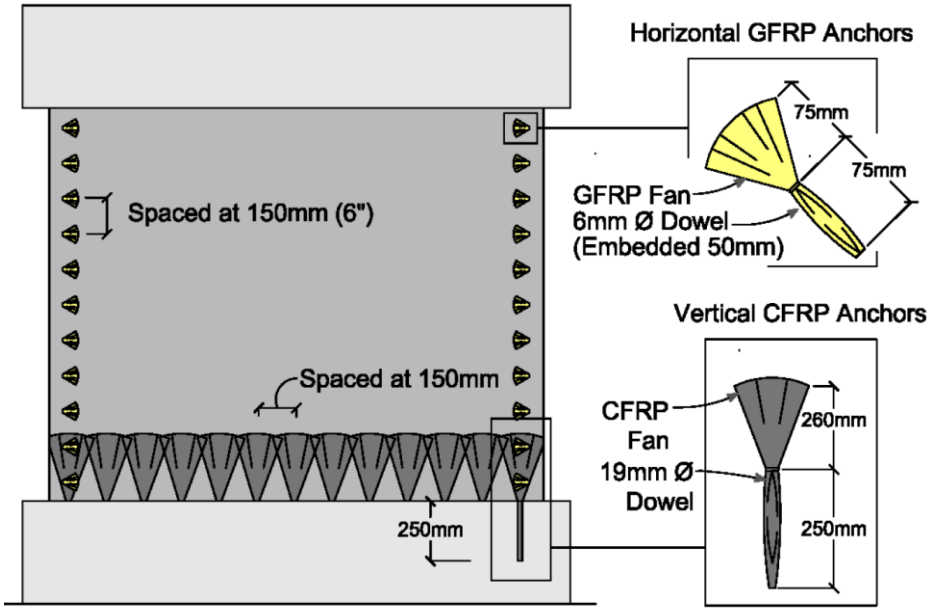

Figure 2-15: Fan FRP anchor system used in ISW-2 (Woods et al., 2015)

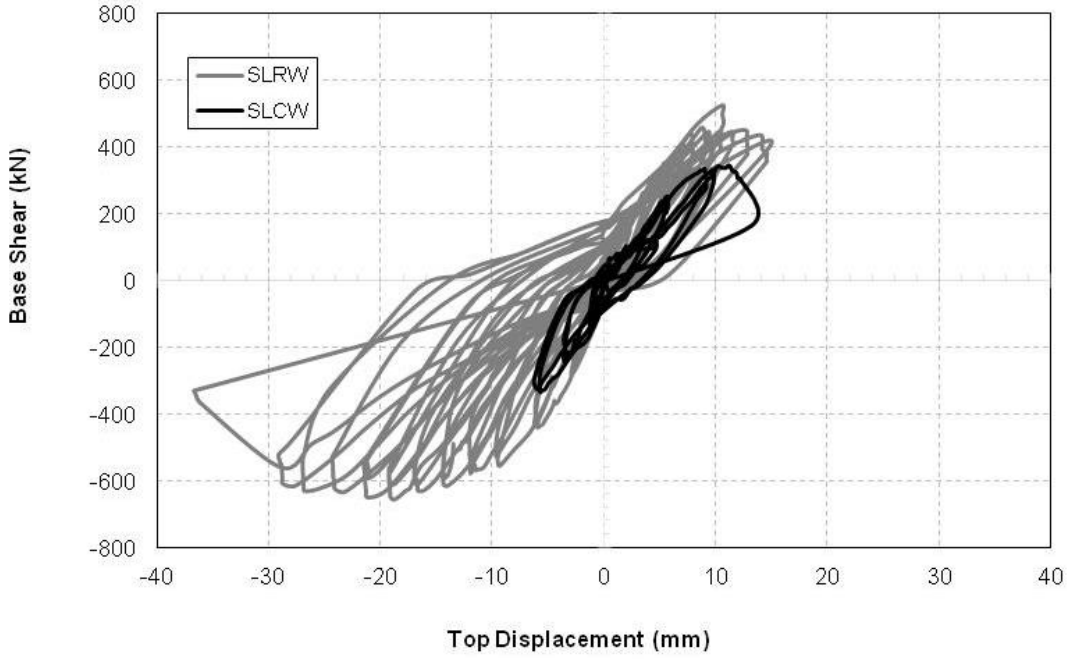

Figure 2-16: Hysteresis response of slender repaired wall (Woods et al., 2015)

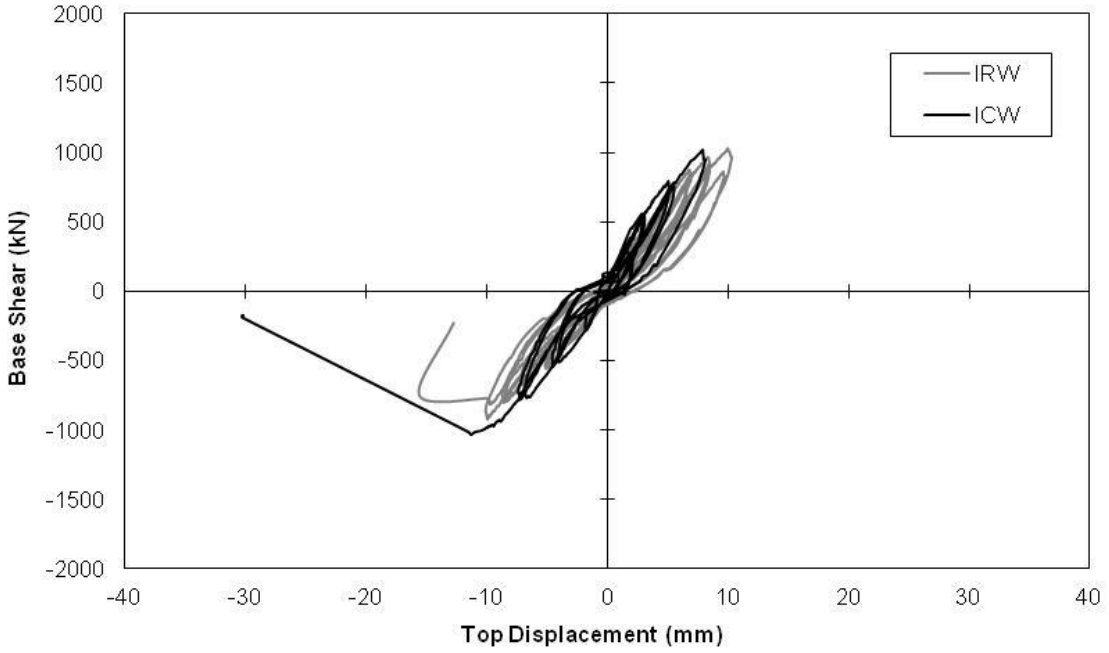

Figure 2-17: Hysteresis response of intermediate repaired wall (Woods et al., 2015)

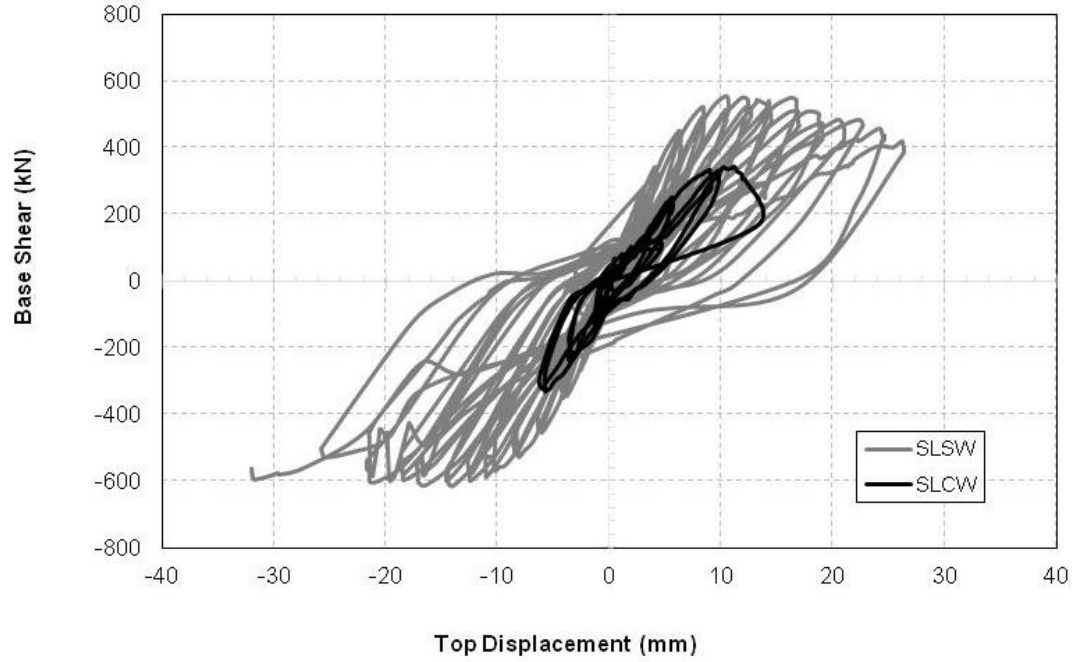

Figure 2-18: Hysteresis response of slender strengthened wall (Woods et al., 2015)

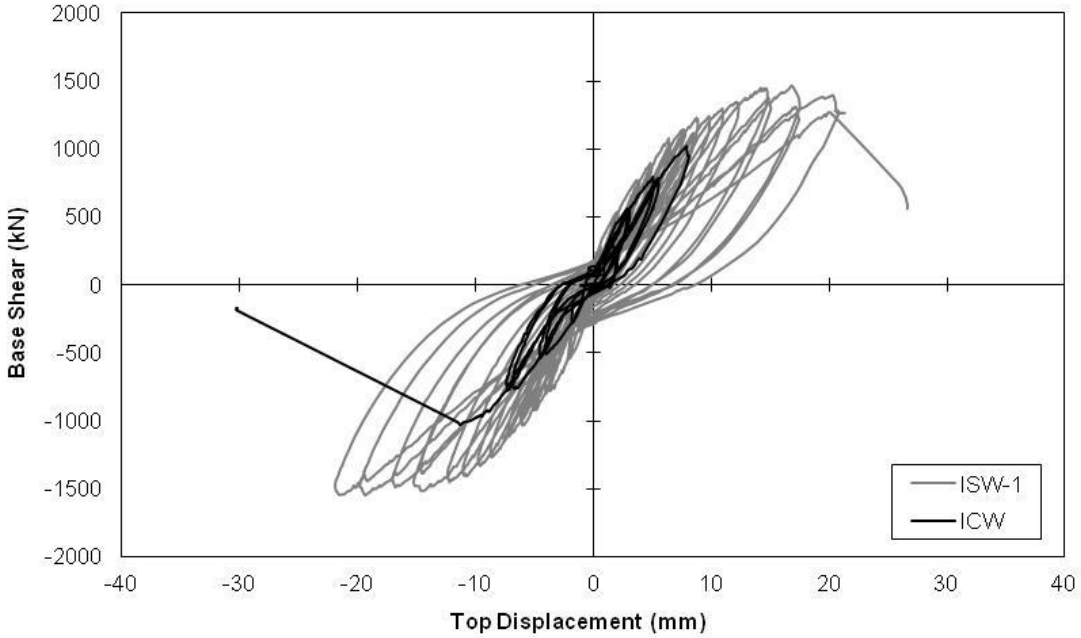

Figure 2-19: Hysteresis response of intermediate strengthened wall 1 (Woods et al., 2015)

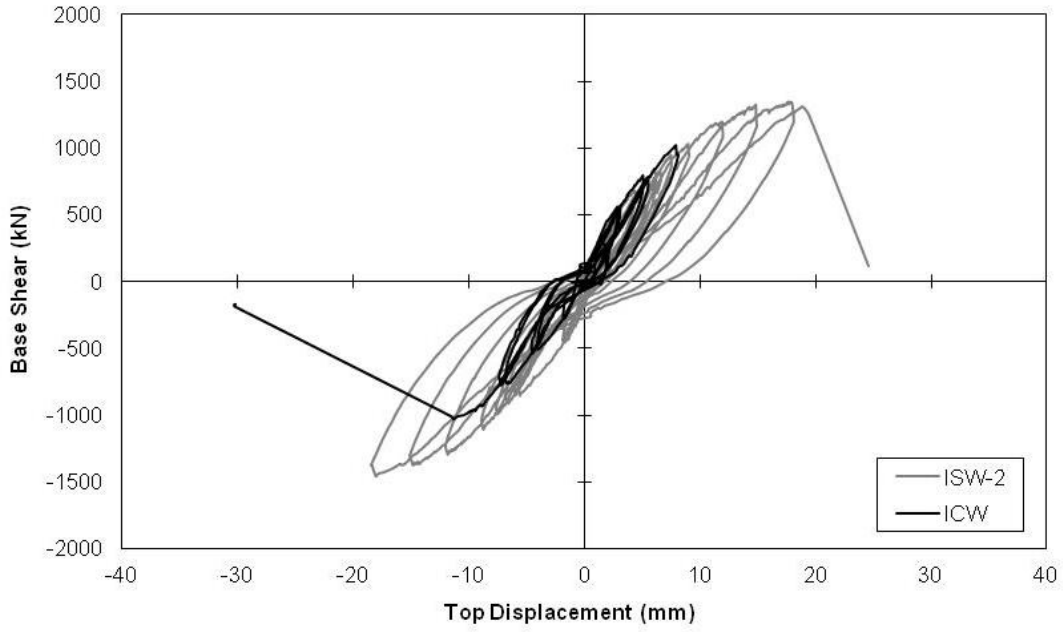

Figure 2-20: Hysteresis response of intermediate strengthened wall 2 (Woods et al., 2015)

Table 2-3: Strengthening and repair schemes used in phase 3 of the experimental program

Phase	Anchor type	Aspect Ratio	Type of Specimen	Repair/Strengthening Scheme*	Code
3	Tube	1.20	Control	---	SLCW
		1.20	Repaired	1V+3H	SLRW
		1.20	Strengthened	1V+3H	SLSW
	Tube	0.85	Control	---	ICW
		0.85	Repaired	1V+3H	IRW
		0.85	Strengthened	1V+3H	ISW-1
	Fan	0.85	Strengthened	1V+3H	ISW-2

*V-Vertically oriented FRP sheets and H-Horizontally oriented FRP sheets

3.0 MODELLING OF REINFORCED CONCRETE SHEAR WALLS

In this chapter, the modelling of the shear wall specimens in their as-built condition is discussed. As discussed in the previous section, these walls are tested without the use of externally bonded FRP sheets and their results are used as a baseline for evaluation of the efficiency of the externally bonded FRP repair and strengthening schemes. The shear walls in their original as-built state are referred to as the control walls.

3.1 Finite Element software

The finite element (FE) program VecTor2 (Wong and Vecchio, 2002) is used for analyzing the cyclic response of the tested walls. The program VecTor2 is based on the Modified Compression Field Theory (MCFT) formulated by Vecchio and Collins (1986), and the Disturbed Stress Field Model (DSFM) proposed by Vecchio (2000). In these formulations, the concrete is modeled as an orthotropic material with smeared, rotating cracks. An attractive feature of this program is that the structural model can be modified at any stage of the analysis by adding (activating) unstressed elements and eliminating (deactivating) previously stressed elements, allowing the simulation of chronological repair/strengthening procedures while keeping track of the previous (damaged) state of existing elements. This feature is used extensively when analyzing the strengthened RC shear walls which will be discussed in details later in the study.

3.2 Geometric modelling

Three different models are used to model the walls tested in the experimental study discussed earlier based on the different dimensions and design of the walls. Two-dimensional, four-node quadrilateral elements are used to model the concrete. In the test setup, a cap beam is used to transfer the load from the actuator to the wall panel. In the analysis, only the wall panel is modeled in the FE simulation. The cyclic lateral load is applied as a uniform distributed load along the top of the wall. During displacement control loading phase of the simulation, nodal displacement equal to the measured top displacement of the wall at each load step of the test is applied to all the nodes along the top edge of the wall panel. Similarly, pinned supports are added to all the nodes along the base of the wall to evenly distribute the reaction forces and thus avoid load concentrations which result in convergence issues. In the analysis a finer mesh than the one adopted for obtaining the reported simulation results has been used to confirm the convergence of the numerical results. For the modelling of the flexural dominant wall (CW-2), a finer mesh is used at the base of the wall in order to capture more accurately the flexural cracking behavior at the wall base. It is worth noting that both the slender shear dominant wall and the flexural dominant wall share the same dimensions with a different structural design as mentioned in the previous section and thus it would be possible to determine the effect of the two discretization schemes.

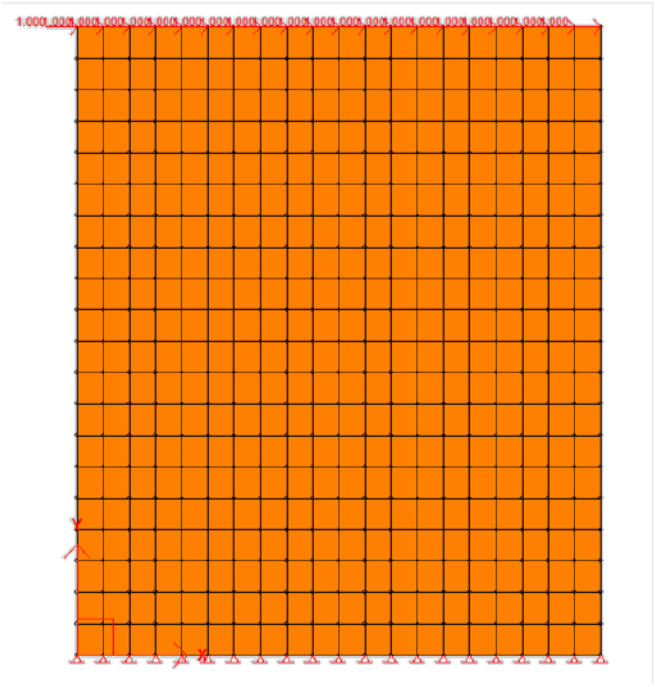

Figure 3-1: The geometric modelling of the control slender shear dominant wall (SLCW)

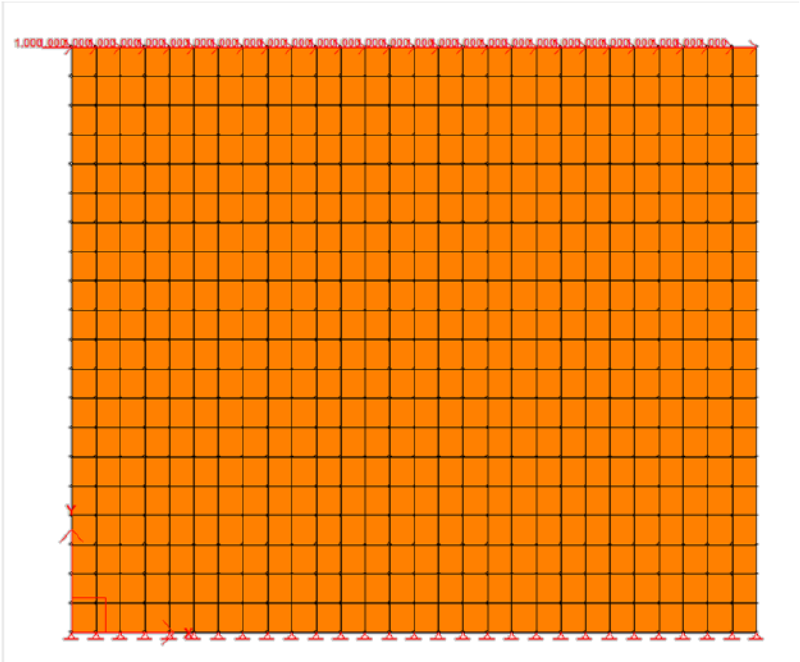

Figure 3-2: The geometric modelling of the control Intermediate shear dominant wall (ICW)

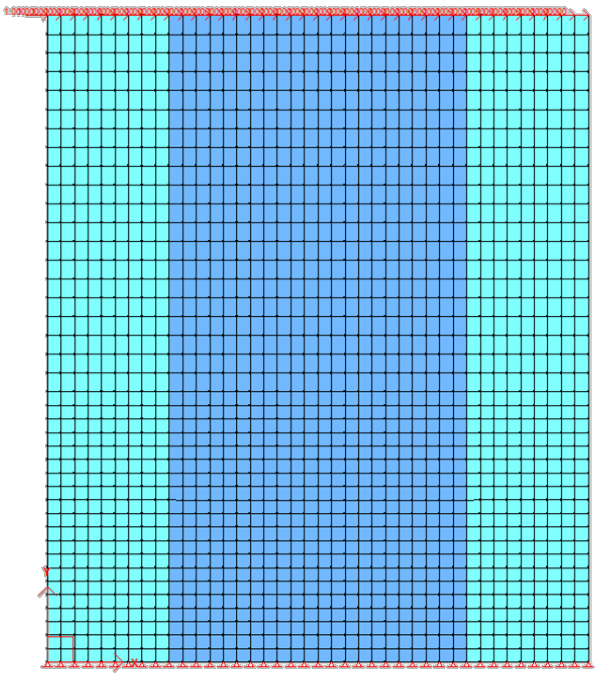

Figure 3-3: The geometric modelling of the control flexural dominant wall (CW-2)

3.3 Concrete material modelling

The constitutive relationships used to model the concrete are selected from the library of models in VecTor2 according to the recommendations of Cortés-Puentes (2009) who has conducted an extensive finite-element study of the nonlinear response of retrofitted shear walls. For the pre-peak response, the model proposed by Popovics (1973) for normal strength concrete is used. For the post-peak response, the modified Park-Kent model (Scott et al., 1982) is chosen. The effect of the strains due to shear slip along the cracks in the concrete is considered by using the Vecchio-Lai model (Vecchio & Lai, 2004) this is a stress-based model that relates the shear slip and the local shear stress along the crack (Vecchio & Lai, 2004). To model concrete damage, the Palermo-Vecchio nonlinear loading/reloading hysteretic model with decay is selected. This model has the ability to

capture the damage that occurs during reloading (Palermo and Vecchio 2002). In the flexural dominant wall (CW-2) two different sets of concrete material properties are used to model the concrete materials at different regions of the wall panel as shown in Figure 3-3. This is necessary for modelling the confined concrete in flexural dominant walls with design detailing of current design standards, i.e. walls with edge elements with confinement reinforcing detailing. The concrete material properties for the walls are obtained from compressive cylinder tests (Hiotakis, 2004 and Woods, 2014). Figure 3-4 summarizes all constitutive models used for modeling the concrete using VecTor2.

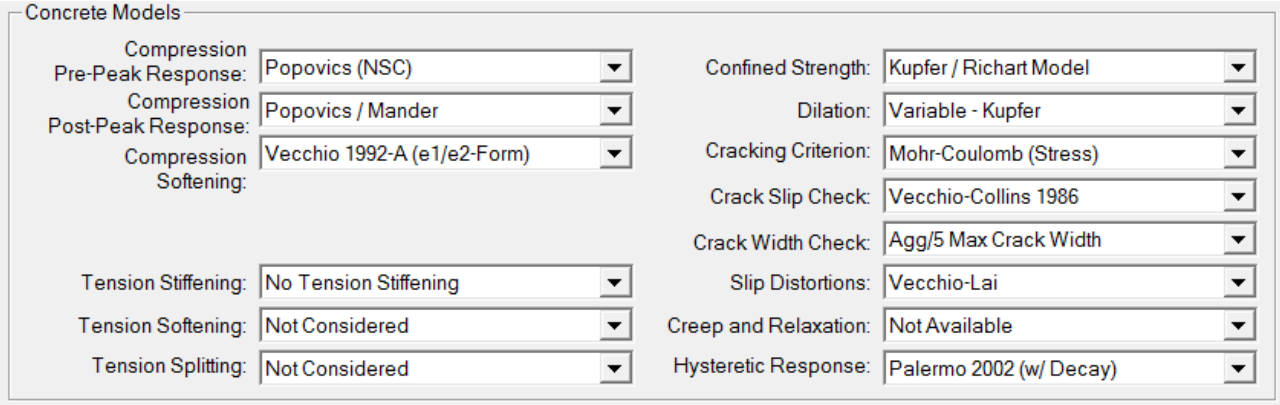

Figure 3-4: A summary of Constitutive models used for modelling of Concrete

3.4 Steel reinforcement modelling

To model the steel rebars and stirrups, the reinforcement ratios at different zones of the wall are assigned as uniformly-distributed ("smeared") reinforcement within the concrete elements. In the case of the shear dominant wall (SLCW and ICW) the reinforcement ratio is uniform over the whole area. The flexural dominant wall is divided into end zone and central zone with the end zone having out of plane reinforcement ratios to model the

confining stirrups at the edges of the wall (Figure 3-3). For modelling of the shear dominant wall, a uniform reinforcement ratio is used throughout the wall area without the differentiation of or central zones (Figures 3-1 & 3-2). The use of smeared reinforcements allows for a more computationally-efficient solution compared to the alternative procedure of defining rebars and stirrups as trusses, while retaining accuracy (Cortés-Puentes, 2009). Although modelling of rebars and stirrups as trusses might sometimes be necessary to model reinforcements that have lap splices; the walls modeled in this study only include continuous longitudinal reinforcements thus modelling of steel reinforcements as trusses is not necessary. It is worth noting that another study is being carried out to investigate the modelling of lap splices in shear deficient walls (Shaheen, 2014). The reinforcing steel is modeled as an elastic-plastic material with strain hardening. The material properties of the steel rebars is determined based on the coupon tests performed by Hiotakis (2004) and Woods (2014).

3.5 FRP reinforcement modelling

The geometric, concrete and steel reinforcement modelling in the strengthened RC shear walls is identical to the modelling discussed earlier for the RC control walls. The distinction between modelling the RC control shear walls and the strengthened walls is the addition of the FRP reinforcement. Two different techniques are originally considered to model the FRP reinforcements, namely the transformed section approach and the FRP truss elements. In the transformed section approach, the FRP tensile strength would be incorporated into the concrete material properties to form transformed concrete elements. The transformed

properties of the concrete element would allow for simulating the wall with the effect of added resistance of the FRP material included in the results. As shown in the previous chapter, all of the strengthened walls experienced FRP debonding prior to the attainment of their ultimate strength and eventual failure. Therefore, it is necessary to consider the debonding of the FRP in the modelling of the strengthened walls. If the transformed section technique is to be used, two different concrete material properties can be defined in the program; one that corresponds to the transformed section properties and the other corresponding to regular untransformed concrete properties. Initially, all of the concrete elements would be assigned transformed properties (since the FRP sheets are applied to the entirety of the wall surface). Once debonding occurs, the elements with debonding will have their transformed material properties deactivated and their untransformed properties activated. This would result in the debonded FRP to no longer contribute to the resistance of the wall. However, this modelling approach is not accurate because it assumes that debonded FRP no longer has any effect on the strength of the wall while in reality the FRP is still attached to the surrounding undebonded FRP and thus it still provides some form of resistance to tensile stresses. Alternatively, truss elements can be used with a cross sectional area equivalent to the cross sectional area of the FRP material bonded to the concrete element. The truss elements would be linked to the concrete substrate using link elements with an appropriate bond strength model. To model debonding two different bond strength models would be used; one that corresponds to bond strength when the FRP is bonded to the concrete substrate and another for the bond strength when the FRP is

debonded. Initially, all the link elements would be assigned bond properties of the bonded FRP. Once debonding in a certain element is detected, the link elements surrounding that element would deactivate the bonded material properties and activate the debonded material properties. The advantage of using this techniques is that the debonded FRP trusses would still contribute to the resistance of the wall which is the true response observed in the experimental testing. Therefore, after reviewing of preliminary results, it is decided that the approach of using FRP trusses and link elements is a better approach for modelling the FRP by being able to capture the debonding mechanism of FRP and the post-debonding FRP resistance to tensile stresses in the wall.

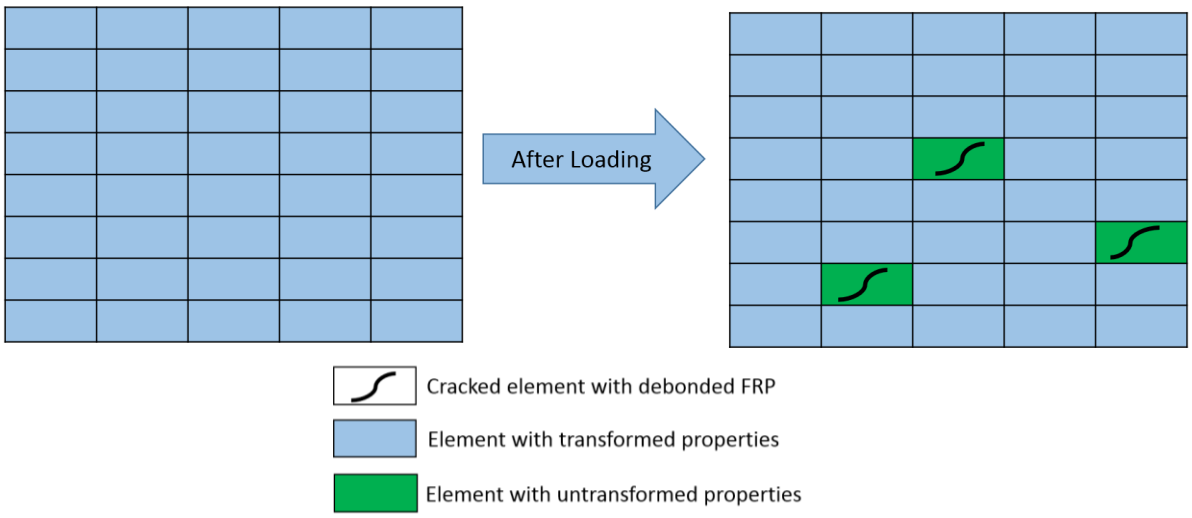

Figure 3-5: Transformed section technique

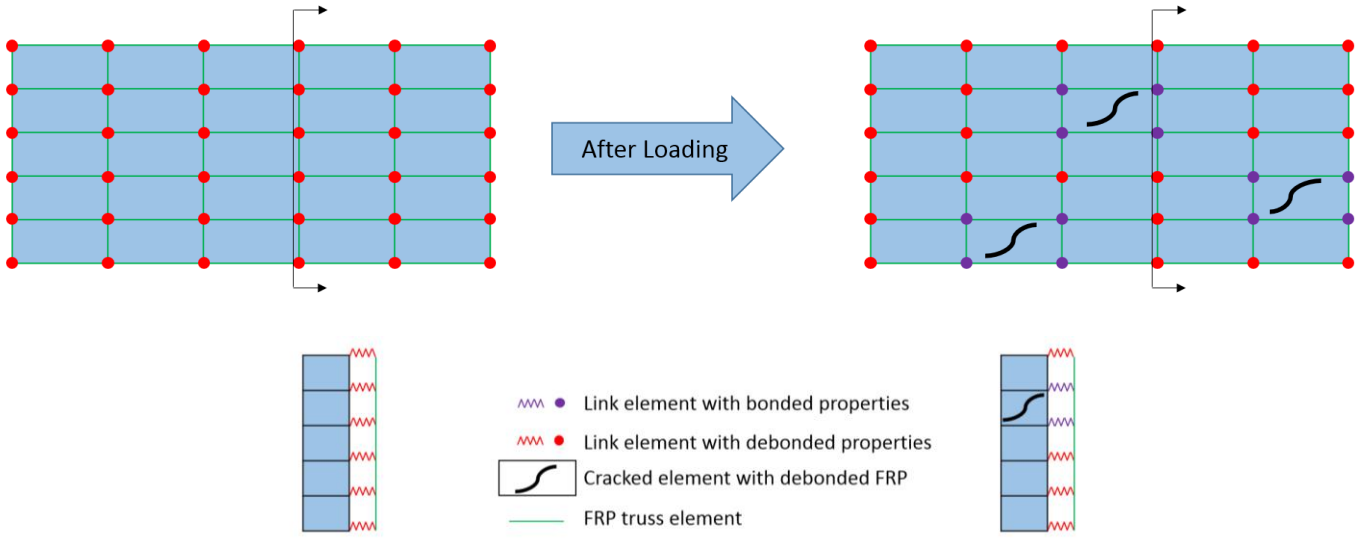

Figure 3-6: FRP trusses and link technique

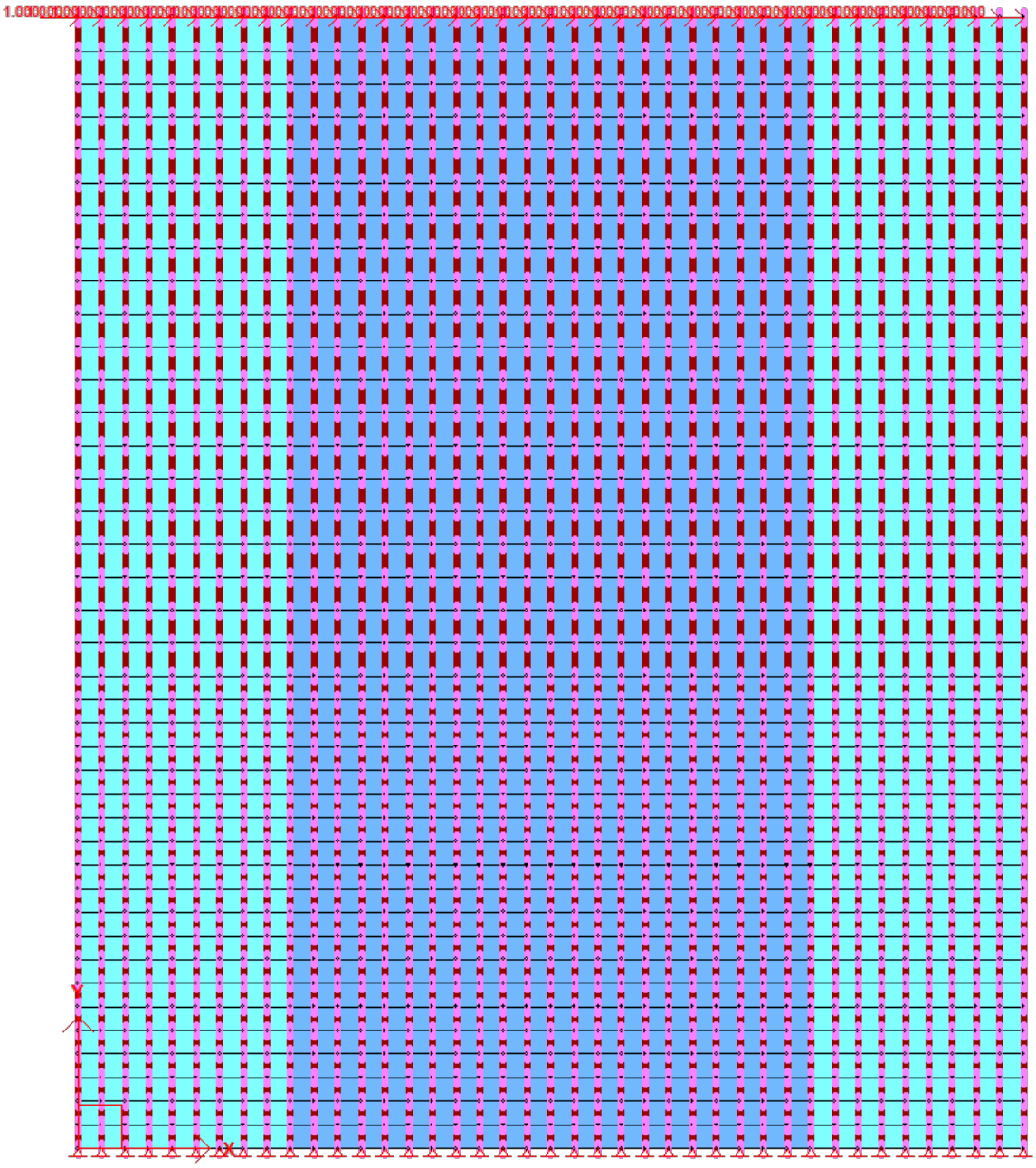

Figure 3-7: Model for SW1-2 & SW 2-2 with added FRP trusses

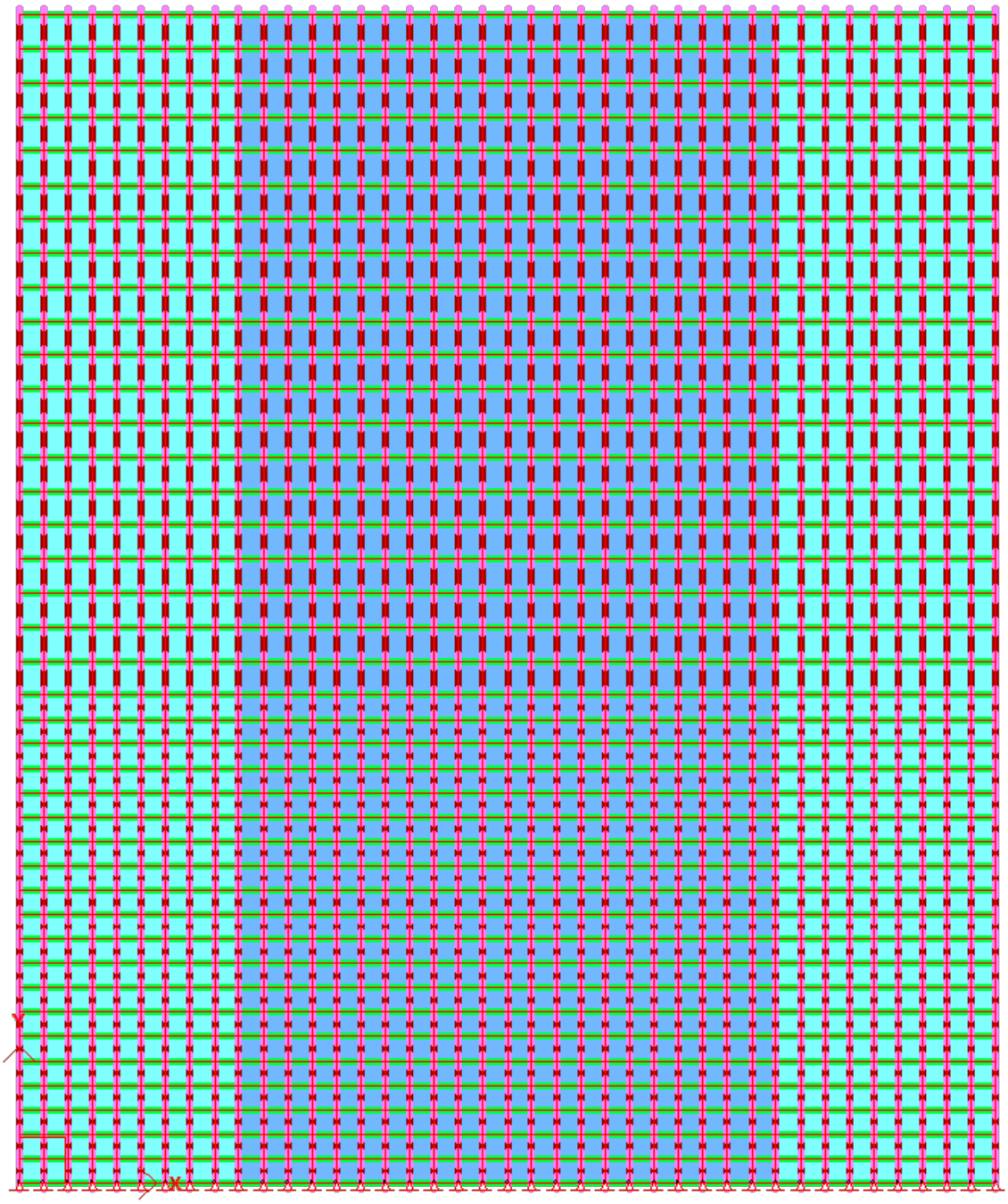

Figure 3-8: Model for SW3-2 with added vertical and horizontal FRP trusses

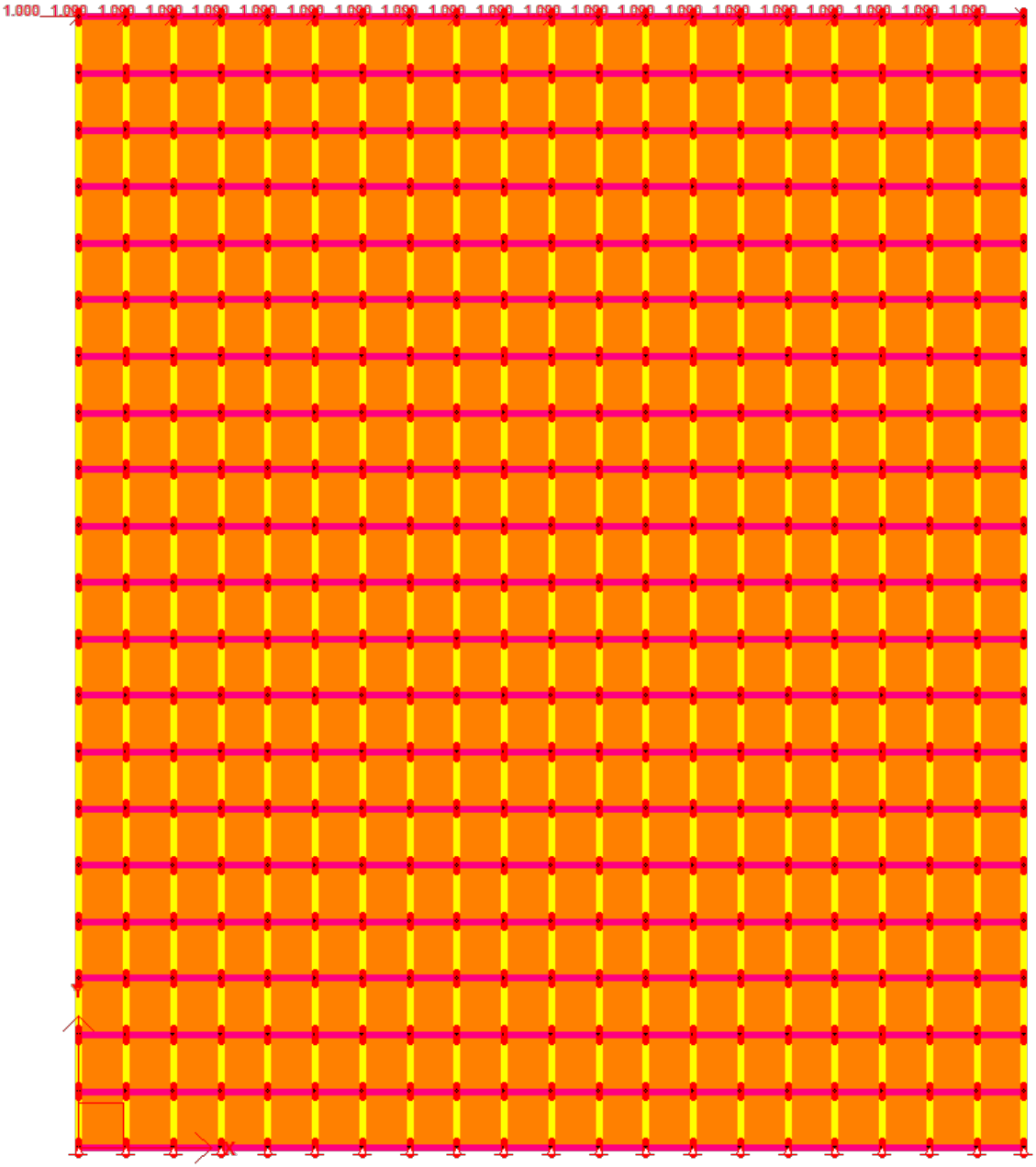

Figure 3-9: Model for SLSW with added vertical and horizontal FRP trusses

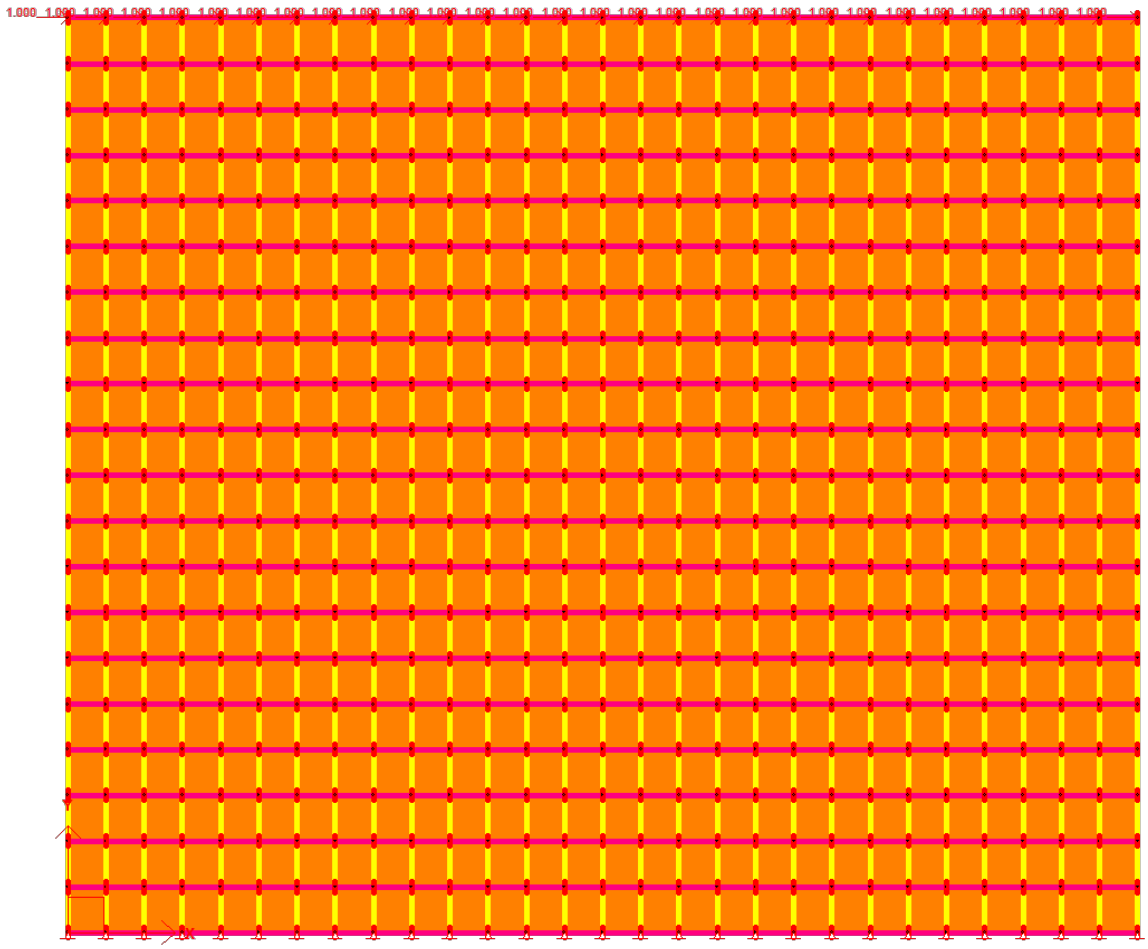

Figure 3-10: Model for ISW with added vertical and horizontal FRP trusses

The dry fibre material properties for the FRP sheets rather than the resin matrix properties is used to determine the material properties of the truss elements. The dry fibre properties is provided by the manufacturer and results in a more consistent reporting of material properties as compared to testing of resin matrix. In the analytical model, the FRP material is assumed to have no compressive strength which is consistent with provisions in current FRP design standards (CSA, 2012 and ACI, 2008). To determine the cross sectional area of the truss elements, the total area of FRP bonded to the concrete wall is divided by the

number of trusses along the width (or height in the case of horizontal FRP trusses). The area of the FRP bonded to the concrete wall is the product of the dimension of the wall perpendicular to the orientation of the FRP sheet, the thickness of the dry fibre sheet and the total number of sheets applied to the wall.

$$A_{truss} = \begin{cases} t_f \times \frac{l_w}{n_{truss}} \times n_{layers}, & for\ vertical\ FRP\ trusses \\ t_f \times \frac{h_w}{n_{truss}} \times n_{layers}, & for\ hotrizontal\ FRP\ trusses \end{cases} \qquad \textit{(Equation 3-1)}$$

Since the purpose of the analysis is to determine the response of the RC shear wall and the effect of using FRP sheets, the anchorage system is not explicitly modelled. This is supported further by looking at the response of the anchorage system in the experimental study. The tube anchor system, which is used in experimental setups, is never the cause of failure in the tests. The tube anchor is proven to be capable of providing support to the FRP sheets and preventing premature debonding. The observed debonding is rather due to a phenomenon referred to as Intermediate crack debonding, which will be discussed in the next chapter.

4.0 MODELLING OF FRP-CONCRETE DEBONDING MECHANISM

It is apparent when looking at the results of the experimental study discussed in chapter 2 that FRP-Concrete debonding is an important component to the response of FRP strengthened RC shear walls subjected to cyclic loading. Although the last chapter discussed in details the techniques used to model the RC control and strengthened walls, accounting for debonding in the analytical study is a complex procedure that shall be discussed further in this chapter. As mentioned earlier, this is not the first study to account for debonding; however, this is the first study to investigate the effect of debonding in shear dominant large scale RC structures such as shear deficient RC shear walls.

4.1 Overview

The failure mechanism of the FRP strengthened wall is not as simple as failure of the material since this only occurs after the FRP debonds from the concrete substrate. Hence, the debonding of FRP from the concrete substrate controls the failure mode and overall response of the shear wall (Teng et al. 2002). If no debonding is allowed to occur, RC elements strengthened with FRP would exclusively fail under either compressive concrete crushing or FRP tensile rupture; however, in most cases the FRP material debonds from the concrete before the ultimate strength of the FRP is achieved.

Reviewing the results of experimental tests of 77 beams and slabs strengthened with FRP, Lu et al. (2007) concluded that one of the most critical debonding mechanisms during the tests is that caused by the opening up of flexural cracks in the concrete, referred as intermediate crack (IC) debonding. In this mechanism, FRP-concrete debonding first occurs at a flexural crack and quickly propagates towards the laminate edges, causing a sudden drop in the load carrying capacity of the structural member, as shown in Figure 4-1. It is important to note here that this is observed in the experiment with small differences that will be highlighted in the following sections. In the RC shear walls strengthened with FRP sheets, there are two main crack patterns observed. The more dominant crack pattern is determined based on the design of the wall. Flexural dominant walls tested in phase 1 and 2 of the experimental studies have major flexural cracks at the base of the wall with a few shear cracks observed near the very end of the test and well beyond the ultimate strength of the wall is reached. This is because in these walls a sufficient amount of steel transverse reinforcement is used to delay shear failure and force the wall to fail in a ductile flexural failure. Shear dominant walls on the other hand have major diagonal shear cracks with a few flexural cracks. This is not because of excessive longitudinal reinforcements but rather due to the limited transverse reinforcements present in the wall. Although both walls have different cracking patterns, the effect of cracking on the debonding stays the same. The main reason behind the debonding of the FRP sheets is the transfer of the tensile stresses released by the crack to the adjacent FRP sheets, a process that is independent of the type of crack. The only reason shear crack is not reported as a source of IC debonding

in previous studies is the fact that other researchers only investigated beams strengthened by an FRP sheet applied to the tension side of the beam. On the tension side of the beam only flexural cracks can be observed, especially for well-designed beams with sufficient shear reinforcements. Had the previous researchers studied FRP sheets applied to the sides of beams designed according to old code detailing requirements with insufficient shear strength, it would have been apparent that shear cracks have the same effect on FRP debonding as flexural cracks, as observed in the shear wall experimental study. It is however worth noting that there are a distinct difference when accounting for debonding due to shear cracks as opposed to flexural cracks as will be discussed later in this study.

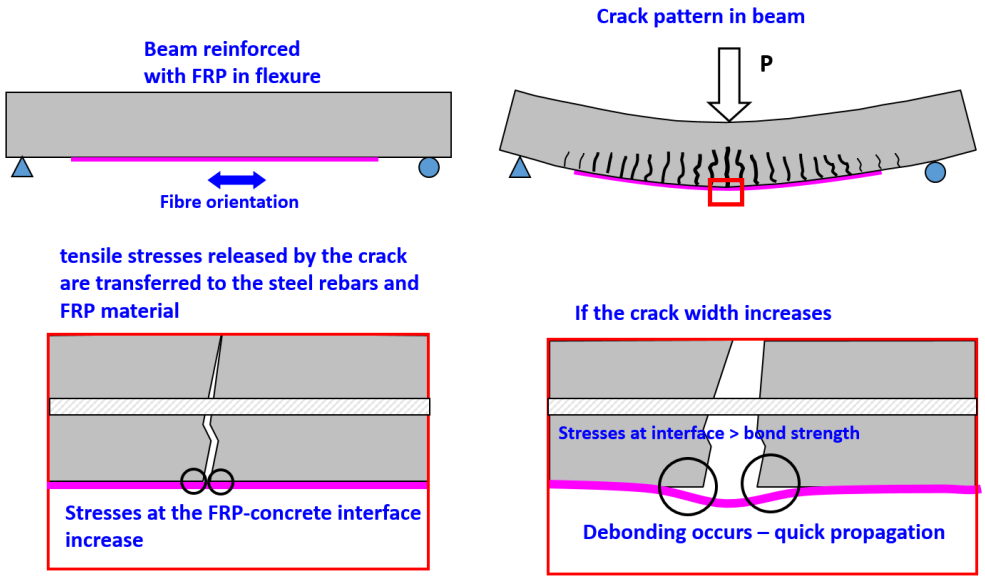

Figure 4-1: IC debonding mechanism in beams (Cruz-Noguez et al., 2012)

4.2 Analytical modelling of concrete cracking

Modelling of concrete cracking is very critical for modelling of FRP-Concrete interaction because it is the bases for the FRP-Concrete debonding. Two different approaches have

been developed using the finite-element method (FEM) for modelling concrete cracking: the discrete crack approach and the smeared crack approach. In the discrete crack approach (Yang et al. 2003; Niu and Wu, 2006), the propagation of predefined, dominant cracks is captured by remeshing the model at each load step to follow crack development, with the disadvantage that this can be an expensive process when a large number of cracks need to be studied. Although this approach yields very accurate results, it is computationally demanding especially if large structures such as walls are to be modeled. A more computationally-efficient method, in which remeshing is not required, is the smeared crack approach (Wong and Vecchio, 2003; Pham and Al-Mahaidi, 2007). In this model, the concrete is effectively treated as a continuum: cracking is represented as tensile straining over the concrete element, and crack propagation is simulated by reducing the stiffness and strength of the concrete with a suitable constitutive model. Due to its simplicity, the smeared crack approach is used in most FEM studies of plain and FRP-reinforced concrete structures (Wong and Vecchio, 2003; Lu et al. 2007), and is therefore the approach adopted in this study.

4.3 Modelling of FRP-Concrete debonding

As discussed in the literature review, modelling of FRP-Concrete debonding can be done in two different approaches depending on the approach used to model the concrete cracking. If the discrete crack approach is used to model concrete cracking, meso-scale technique can be used in which a very fine mesh is to be used. Excellent correspondence

between measured and calculated results (in terms of load deflection curves, crack patterns and debonding progression) has been reported by Lu et al. (2007) using the meso-scale method to predict the response of two FRP-strengthened beams tested by Wu and Yin (2003). The meso-scale technique is not applicable to the modelling technique adopted in this study. The models developed for the strengthened walls include mesh sizes ranging from 35 to 90 mm in size which is much larger than the upper limit of the mesh size required for meso-scale testing. The element number limit in VecTor2 makes it impossible to apply the meso-scale technique for modelling of large scale RC shear walls.

As an alternative, interface elements (also referred to as link elements) can be used with bond-slip constitutive laws that simulate the mechanics of the debonding caused by the tensile fracture in the concrete layer (Wong and Vecchio, 2003; Wu and Yin, 2003; Ebead and Neale, 2007; Lu et al. 2007). These interface element would eliminate the need for small mesh size since the interface element would account for the FRP-concrete interaction. Results from meso-scale studies that rigorously account for IC debonding effects are used to generate appropriate bond-slip models in structures where flexural cracking is present. Using the meso-scale FE analyses of the beams of Wu and Yin (2003), Lu et al. (2007) obtained representative bond-slip relationships obtained for FRP-concrete interfaces with and without major flexural cracks and commonly used adhesives. For parts of the FRP-concrete interface outside the major flexural crack zone, the bilinear bond-slip model developed by Lu et al. (2005) is used (will be called bond-slip model I). The Bond

slip model with regions outside major flexural crack zones (Bond-Slip model I) is described below:

$$\tau = \begin{cases} \frac{\tau_{max} s}{s_o} \; if \; s \leq s_o \\ \frac{\tau_{max}(s_f - s)}{(s_f - s_o)} \; if \; s_o < s \leq s_f \\ 0 \; if \; s > s_f \end{cases} \qquad (Equation\ 4-1a)$$

where

$$s_f = \frac{2G_f}{\tau_{max}} \qquad (Equation\ 4-1b)$$

$$\tau_{max} = 1.5\beta_w f_t \qquad (Equation\ 4-1c)$$

where f_t is the tensile strength of Cocnrete

$$s_o = 0.0195\beta_w f_t \qquad (Equation\ 4-1d)$$

$$G_f = 0.308{\beta_w}^2\sqrt{f_t} \qquad (Equation\ 4-1e)$$

$$\beta_w = \sqrt{\left(2.25 - {b_f}/{b_c}\right)/\left(1.25 + {b_f}/{b_c}\right)} \qquad (Equation\ 4-1f)$$

In the above equations, τ = shear bond stress (MPa); s= interfacial slip (mm); G_f=interfacial fracture energy (MPa); b_f= width of the strip of FRP laminate (mm); b_c=Width of the concrete member (mm) where the FRP strip is located and β_w= FRP to concrete width ratio.

For parts of the FRP-concrete interface inside the major flexural crack zone, the bond-slip response is averaged over lengths of 15 and 20 mm. The resulting curves indicated a brittle drop in the shear stress after the peak bond stress is achieved. To account for this drop another model is developed for the interface between the concrete and FRP in regions of major flexural cracking. This model (which will be called Bond-Slip Model II) follows the

same response as bond-slip model I up to the peak stress but is modified to account for the drop as shown:

$$\tau = \begin{cases} \frac{\tau_{max} s}{s_o} \; if \; s \leq s_o \\ 0 \; if \; s > s_o \end{cases} \qquad (Equation\ 4-2)$$

In this study, the externally-bonded carbon fibre tow sheets are modeled as discrete reinforcing units attached to the concrete through link elements that follow Bond-Slip Model I if the concrete does not have major flexural cracks, and Bond-Slip Model II if major flexural cracks are present. A "major flexural crack" is defined here as a crack that produces a total slip in the FRP-concrete interface greater than the limit given by Equation 2. Thus, a careful monitoring of the crack widths in all concrete elements during each load step is required. In any given concrete element with a flexural crack of width *w*, the interfacial FRP-concrete slips *s* that appear at both sides of the flexural crack can be approximated as *w*/2 (Lu et al. 2007). Since IC debonding is considered to take place if $s>s_o$, the crack width in a concrete element that causes FRP-concrete debonding should be therefore equal or larger than $2s_o$. However, if the crack width in a concrete element is smaller than $2s_o$, the bond-slip relationships from Equations 1 still apply. Therefore, two bond models are defined in the VecTor2 model, one corresponding to bond-slip model I and the other corresponding to bond-slip model II. Initially all the link elements are assigned bond-slip model I. Once a concrete element is found to have cracks large enough to initiate cracking, the link elements surrounding that concrete element would have bond-

slip model I deactivates and Bond-slip model II activated. Note that once a link element follows Bond-Slip Model II, it effectively acts as a spring with zero stiffness since no stresses are transmitted from the FRP to the concrete.

4.4 Modifying simplified bond-slip to account for shear cracks

Although the technique discussed above proved to be effective in providing satisfactory results when modelling flexural walls, it is not appropriate to use for modelling shear deficient walls for a number of reasons. The major cracks are no longer flexural cracks but rather shear cracks, which result in a completely different FRP-Concrete interaction. The slip due to the diagonal crack is no longer 1 dimensional but rather 2 dimensional, identifying the component of the slip in each direction is important to determine the crack width corresponding to debonding initiation. In the experiment, the vertical FRP is applied to the concrete surface with horizontal FRP layers applied on top of each other with a layer of adhesive in between each layer (Figure 4-2). This indicates that in reality the horizontal FRP is never directly connected to the concrete substrate but rather they are connected to the vertical FRP. However, linking FRP to FRP in the finite element model caused a number of computational problems that could be avoided if the FRP is directly connected to concrete substrate. Therefore, the horizontal FRP trusses are connected to the Concrete mesh nodes with link elements having the same Bond-slip models described earlier i.e. Bond-Slip model I in regions with no major cracking and Bond-Slip model II in regions with major cracking. Since the FRP layers (whether vertical or horizontal) never debonded

from each other in any of the experiments, it indicates that the horizontal and vertical FRP debonded simultaneously; thus, the debonding criteria for the vertical and horizontal FRP will be identical. In order to develop the debonding criteria discussed previously a few points had to be considered.

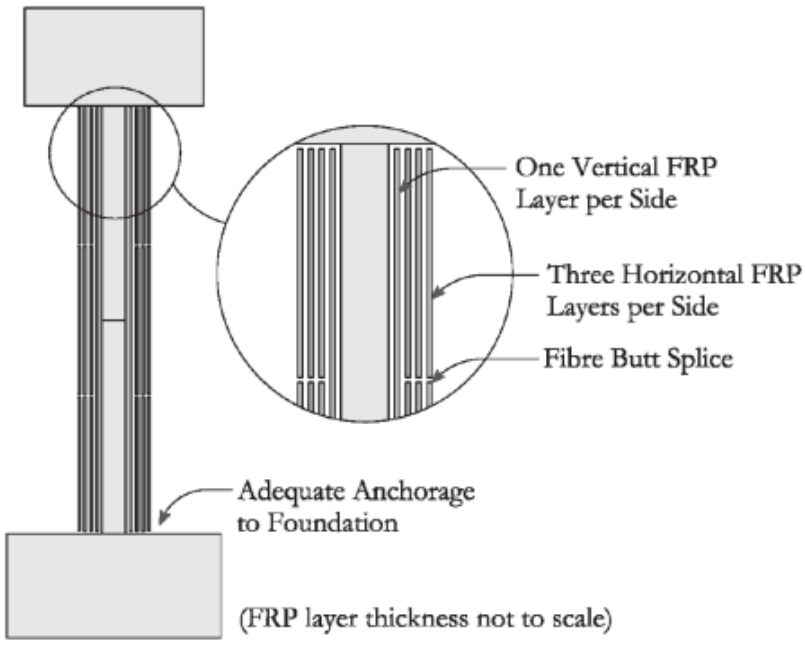

Figure 4-2: FRP reinforcing scheme (Woods, 2014)

Major cracks in the shear dominant walls are expected to be diagonal shear cracks. This is verified when looking at the results of experimental testing of the control walls mentioned earlier. The orientation of the shear cracks is different from that of the flexural cracks as shown in Figure 4-3, thus the interfacial FRP-Concrete slip s has to be calculated differently. As discussed earlier, both horizontal and vertical FRP trusses debond at the same time, however, once the crack is at an angle there will be both a horizontal and vertical slip associated with cracking (Figure 4-3). Since the vertical FRP layer is the layer

connected directly to the concrete the vertical slip would control the debonding criteria. That would mean that if a slip s_o is required for debonding, a crack width has to be $w \geq 2 \times s_o/_{cos\theta}$ for a link element to follow Bond-Slip model II.

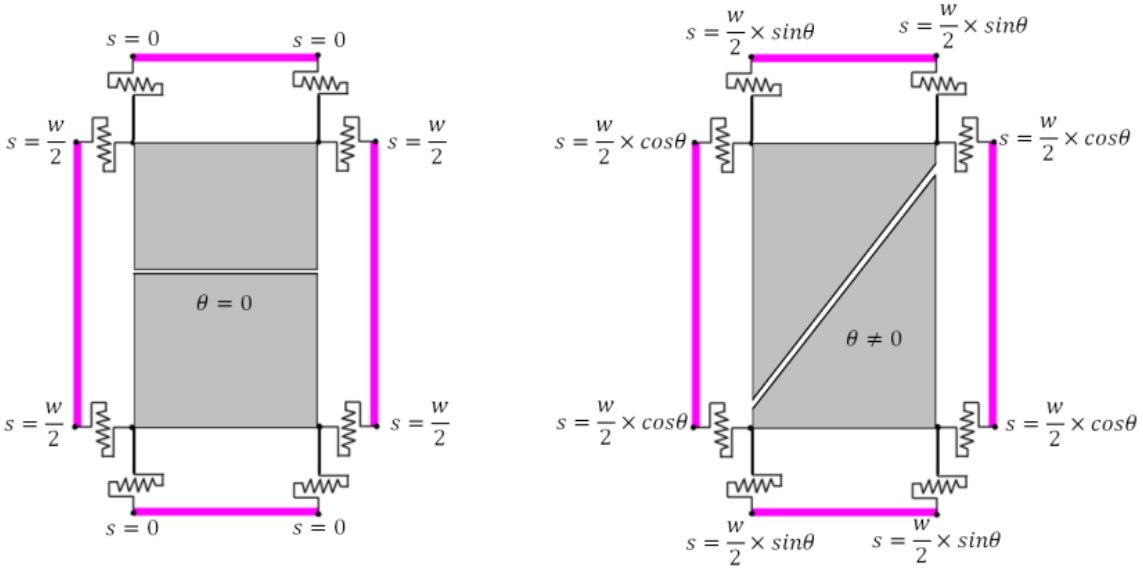

Figure 4-3: Calculating the slip based on different crack orientations

In the case of flexural dominant walls, most of the cracks will be oriented horizontally with very small crack angle. Therefore, this modification will have very limited effect on the flexural dominant walls unlike the shear dominant walls in which this consideration is critical.

4.5 Modification to account for element size effect

The model developed by Lu et al. (2007) accounted for mesh elements sized between 30 mm and 40 mm. The reason behind choosing this mesh size is referring to this mesh size being the "typical" mesh size used in most FE analyses. This is however not necessarily

accurate because mesh sizes are highly dependent on the size of the specimen to be modeled. When analyzing large-scale walls, using a coarser mesh with larger mesh sizes might be required. This can be due to the large computational demands of a fine mesh or due to limitations of the program or both. The bond-slip models described earlier are determined empirically by investigating a number of experimental studies as well as FE meso-scale models. The stress and thickness of the FRP are measured and divided by the averaging length to determine the bond stress as follows:

$$\tau = \frac{t_f \times f_{frp}}{L} \qquad (Equation\ 4-3)$$

Where L is the averaging length which is set to 15 and 20 mms or half the mesh size. The slip is measured along the averaging length. The mesh size of the elements used in this model are almost three times that of the "typical" mesh size mentioned in Lu's work. The maximum bond stress can therefore be modified according to the mesh size as follows:

$$\tau_{max} = 1.5\beta_w f_t \times {}^{1}\Big/_{\frac{L_{actual}}{L_{standard}}} \qquad (Equation\ 4-4)$$

where L_{actual} is half the mesh size in the direction parallel to the FRP orientation for the modeled structure. Also, assuming that the rate of FRP slip is constant per unit length, the slip at the maximum bond stress can be calculated as follows:

$$s_o = 0.0195\beta_w f_t \times \frac{L_{actual}}{L_{standard}} \qquad (Equation\ 4-5)$$

Analytical results of modelling the RC shear walls with or without accounting for the FRP debonding mechanisms are compared. The results considering debonding correctly capture the response of the wall from initial failure to final collapse throughout its entire response history in terms of stiffness, strength, and ductility, as shown in Figure 4-4.

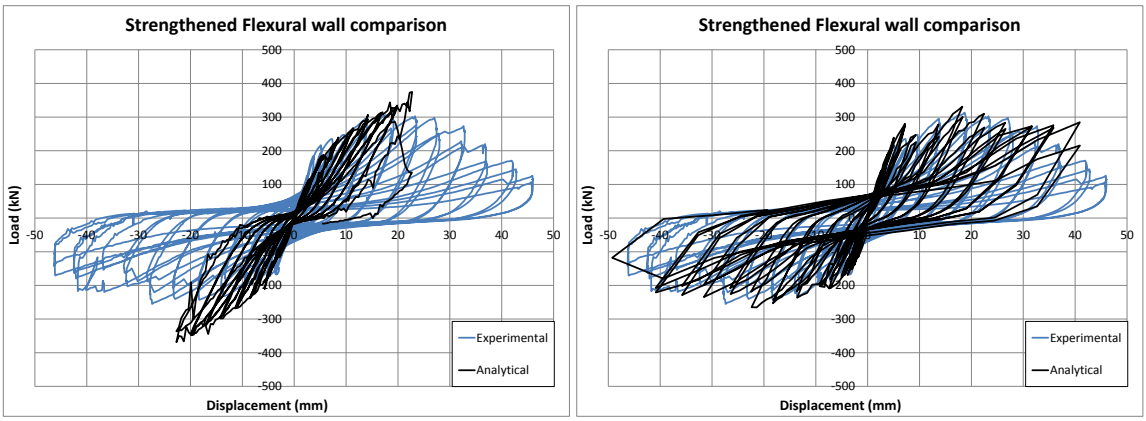

Figure 4-4: Analytical result of modelled strengthened wall with debonding not considered (left) and result for the modelled wall with debonding considered (right)

5.0 ANALYTICAL RESULTS AND DISCUSSIONS

In this chapter the analytical results of eight shear walls are be presented. Both the global and local response of the walls are investigated and correlate with experimental results.

5.1 Flexural control wall

A number of model verifications are investigated for the flexural control wall (CW-2). First, the hysteresis force-displacement response at the top of the wall obtained from modelling is compared with the response recorded by a load cell and LVDT in the experiment. This capability of the numerical model in predicting the initial stiffness, strength, ductility and energy dissipation capacity of the wall under cyclic loading is investigated. As shown in Figure 5-1, the model is capable of providing good correlation with the measured initial stiffness and ductility. The strength is also satisfactorily predicted with a slight underestimation which could be attributed to the variation in the concrete strength in the wall specimen. The energy dissipation capacity is also predicted accurately with the pinching effect predicted very accurately.

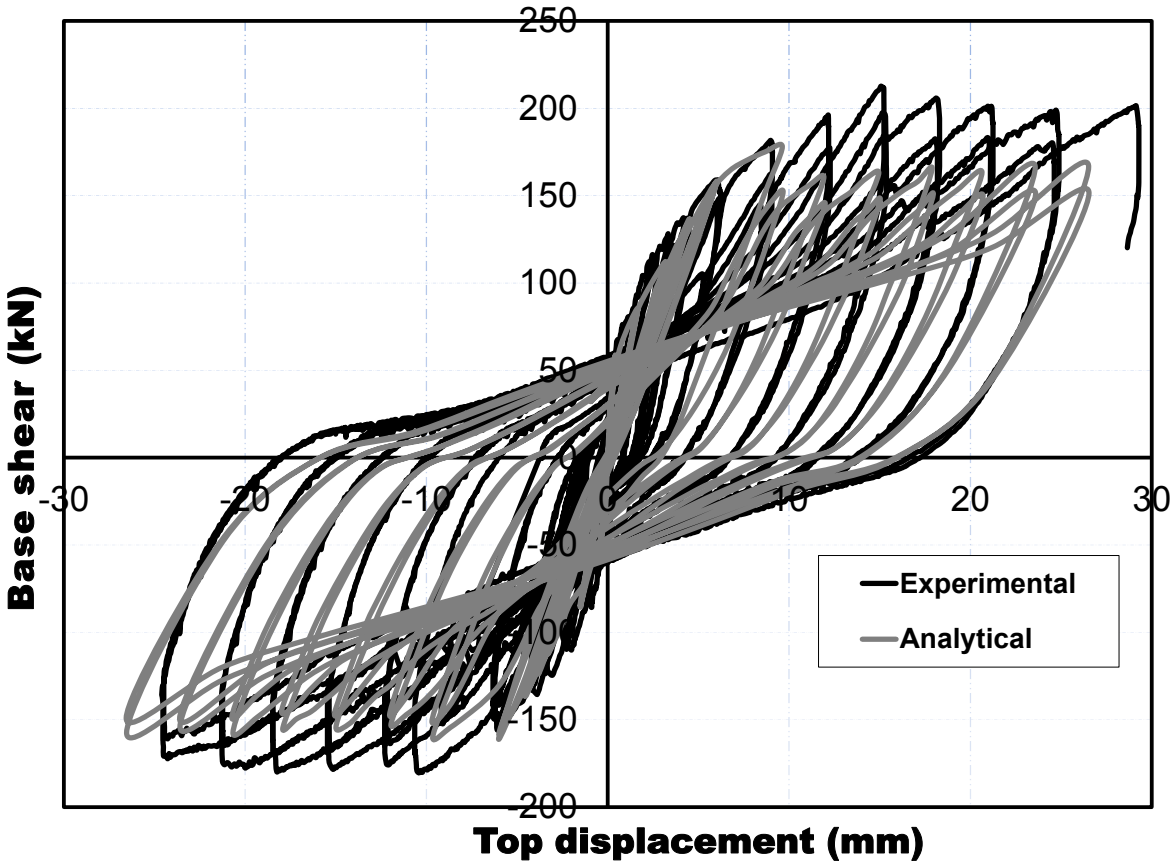

Figure 5-1: Force-displacement response of the modeled flexural control wall (CW-2)

The next verification conducted on the model aims to determine the ability of the model to predict the local response at the element level. The theoretical applied moment at the base of the wall is calculated by multiplying the applied shear force at the top of the wall by the moment arm, which in this case is equivalent to the height of the wall. The stresses within each concrete element at the base of the wall is then multiplied by the area of the concrete and steel in each element to determine the force in each element. The forces in the elements at the base of the wall are then multiplied by their distance from the centroid of the wall to determine the calculated moment from the local response of the wall. As can be seen in

Figure 5-3, the theoretical and calculated moments at the base of the wall correlate with each other very well with an average error around 2%. This provided a meaningful insight on the ability of the model to predict the local response of the wall.

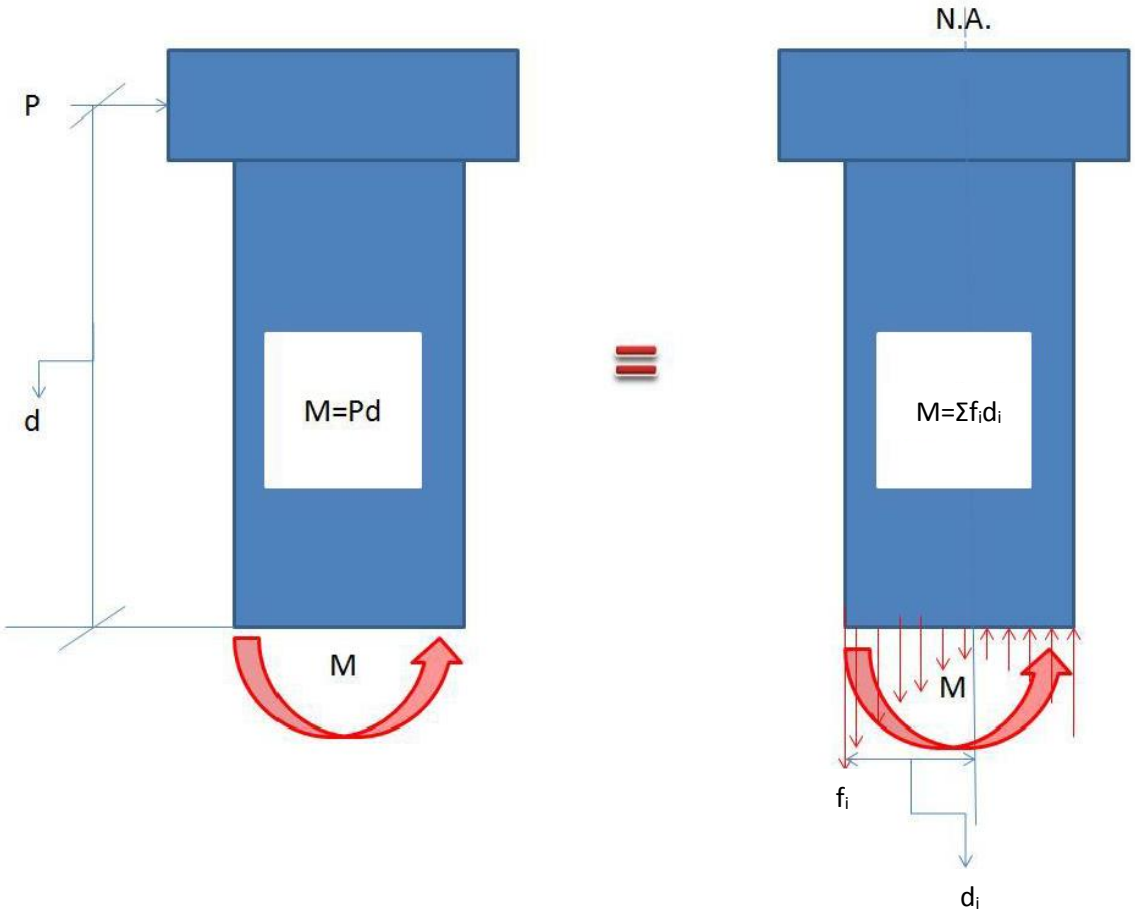

Theoretical moment at the base of the wall

Calculated moment at the base of the wall

Figure 5-2: The theoretical and calculated moments at the base of the wall

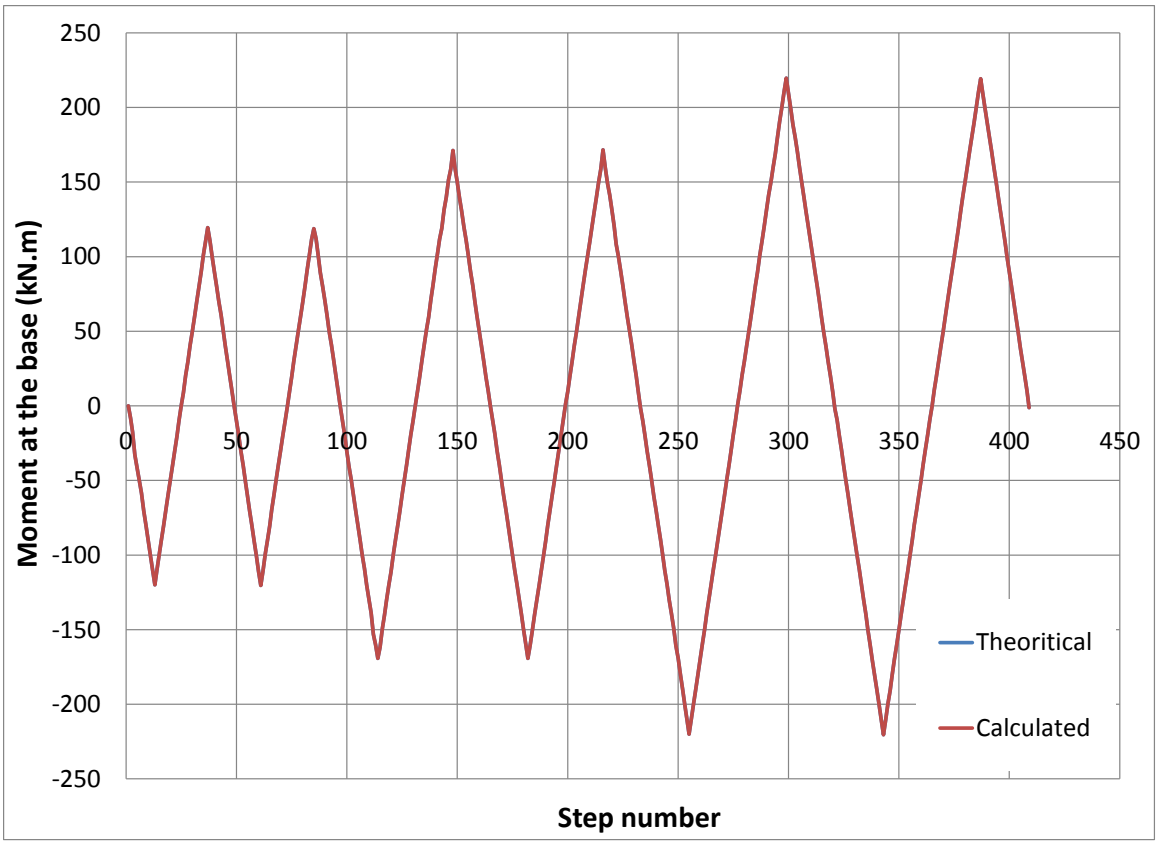

Figure 5-3: Theoretical vs calculated moment at the base of the wall

The final verification performed on this model is investigating the failure mechanism of the analytical model and comparing it to the failure mechanism in the experimental study. In the experimental study, a large number of large flexural cracks are observed at the base of the wall (where the flexural forces are at their peak). Along the height of the wall, smaller diagonal shear cracks are observed in locations where the moment is relatively low, such as the top of the wall. Compared to the flexural cracks that initiate spalling of the concrete, the shear cracks are much smaller and do not damage the wall extensively as shown in Figure 5-4. The model can accurately predict the crack pattern, shear response mechanisms of the wall under cyclic loading as shown in (Figure 5-5) by accurately capturing of the

stress distribution in the wall. Overall the response of the flexural control wall is predicted accurately by the numerical model.

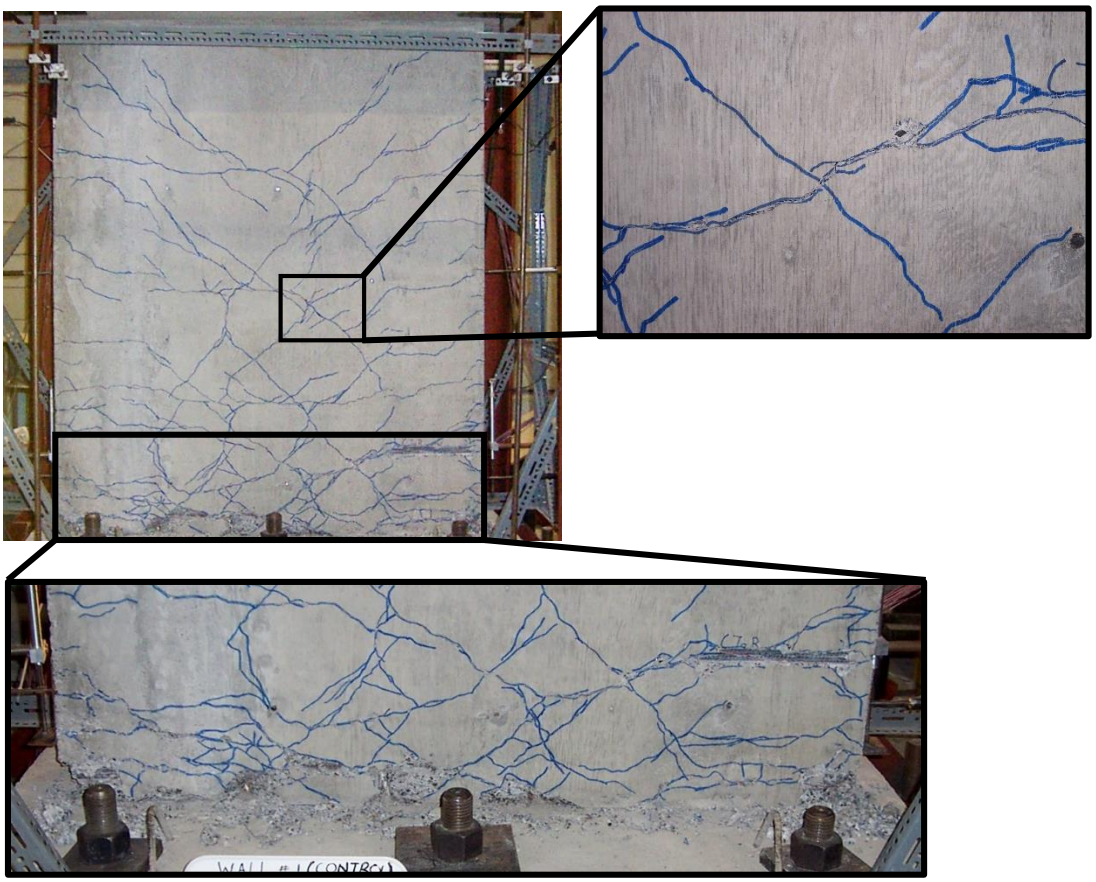

Figure 5-4: Extensive damage observed at the base of the wall due to flexural cracks as compared to the smaller diagonal cracks at the center and top of the wall (Hiotakis, 2004)

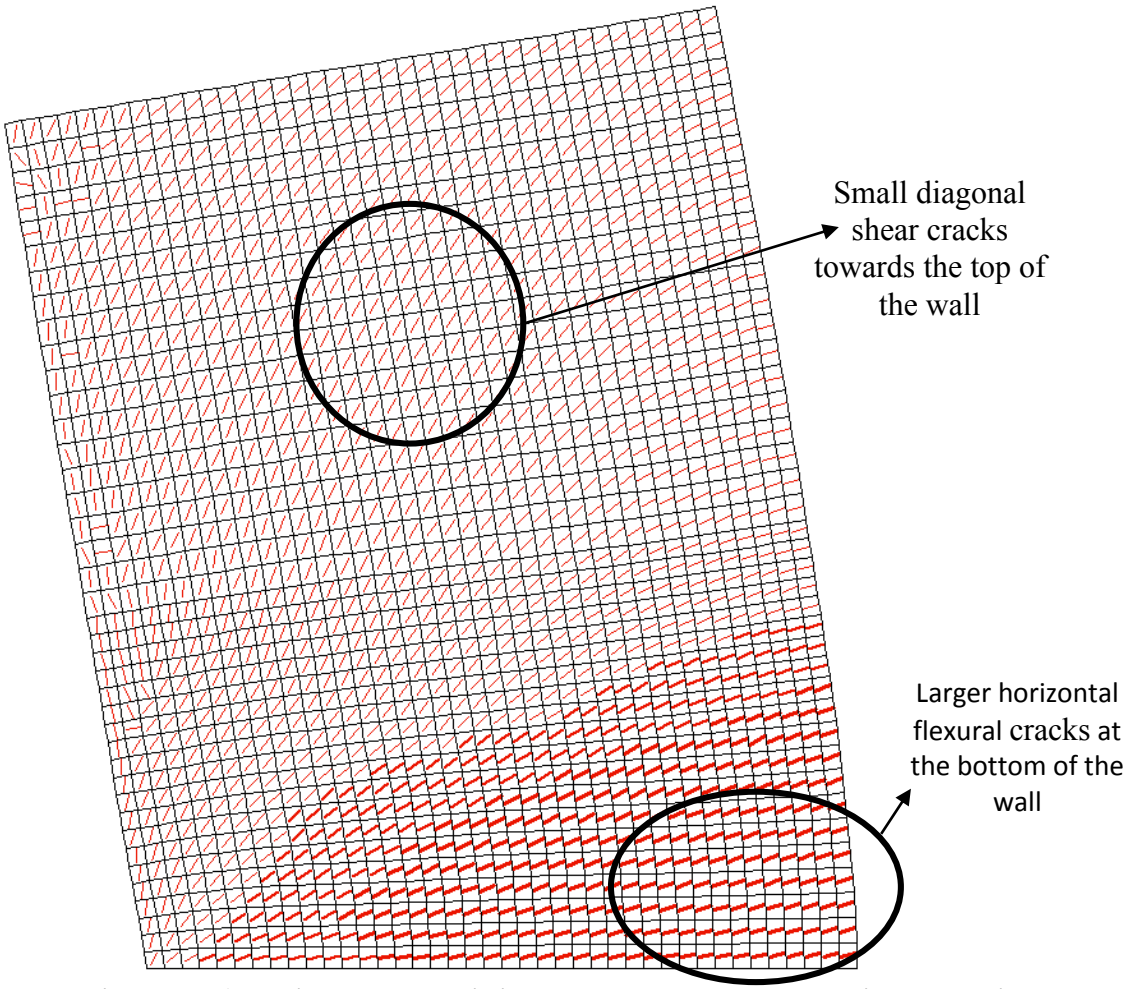

Figure 5-5: Analytical model predicting the same response observed in the experiment

5.2 Shear dominant control walls

The hysteresis load-displacement response of the shear dominant control walls is plotted against the measured response to determine the accuracy of the model. First the response of the slender control wall (SLCW) is investigated. The initial stiffness of the wall is predicted quite well when compared to the measured initial stiffness. The analytical model however overestimates both the ductility and the ultimate strength of the wall (Figure 5-6).

This discrepancy in the results can be attributed to a number of events that occurred in the experimental setup. During the experiment, the testing had to be stopped twice without the wall being brought back to its original position. This results in a significant amount of residual load and strains in the wall specimen which significantly weakens the wall. The correlation of the numerical simulation results of the intermediate control wall (ICW) with the test results shows much better agreement as shown in Figure 5-7. The analytical initial stiffness, strength and ductility correlated well with the measured values in the experiment. It is worth noting however that although the analytical results are relatively very symmetric with both loops of the same shape, the experimental response is not as symmetric with one of the cycles stronger than the other. This is a typical response observed in walls tested under cyclic loading because of slight shift from the centreline position of the placement of the wall reinforcements.

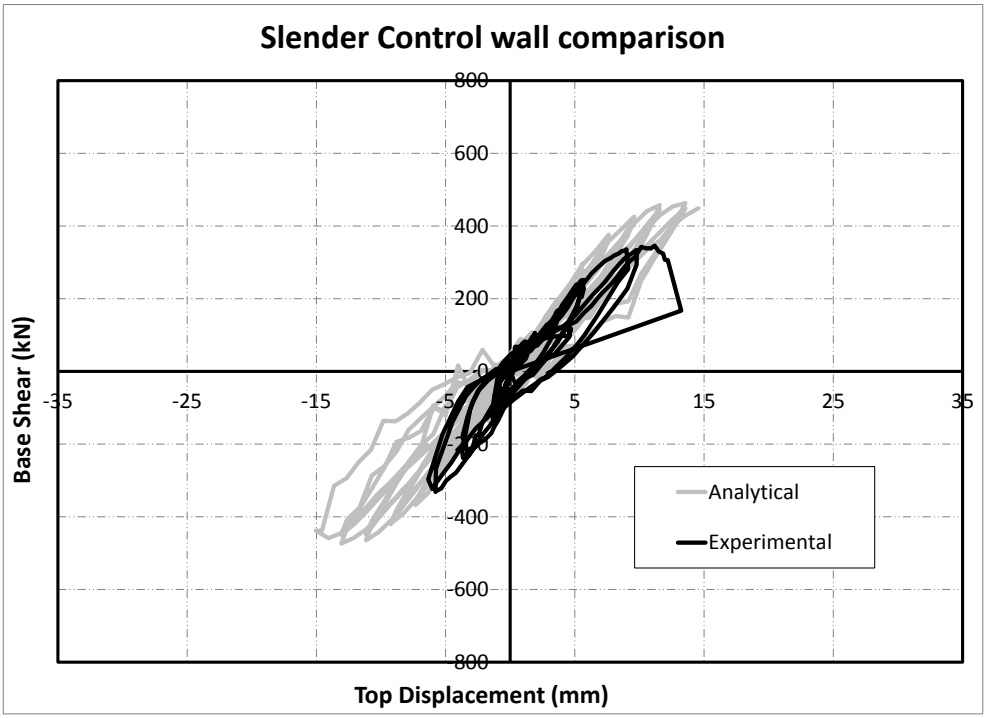

Figure 5-6: Comparison of Slender Control wall (SLCW) hysteresis response

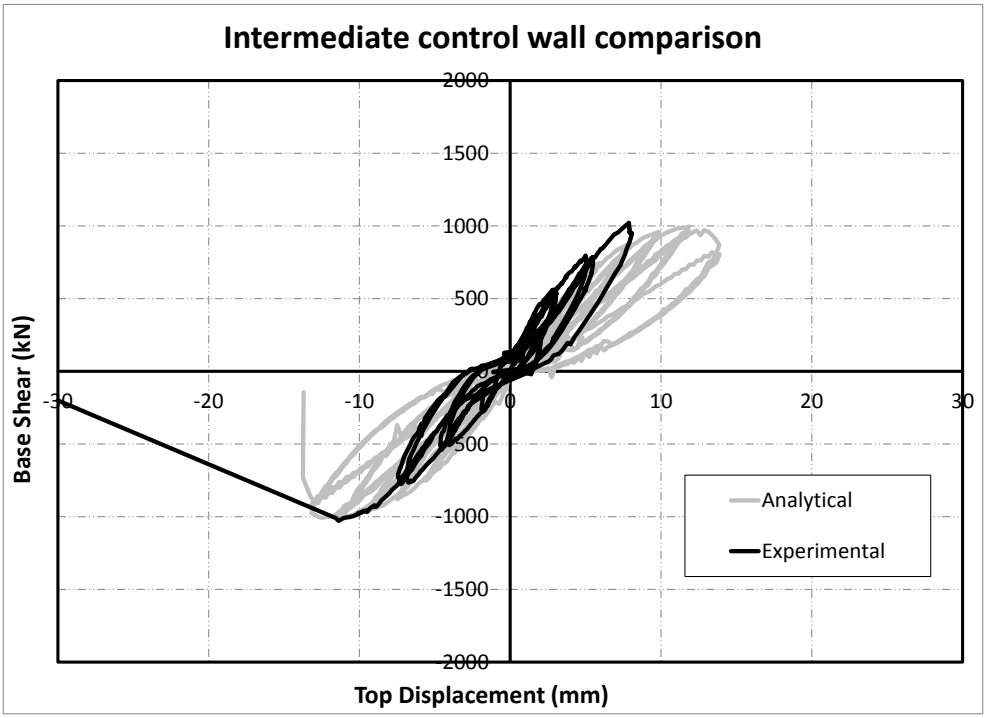

Figure 5-7: Comparison of Intermediate Control wall (ICW-1) hysteresis response

The next step is to determine the accuracy of the analytical model in predicting the local response of the walls. In the walls tested more recently, strain gauges are mounted on the longitudinal steel reinforcement near the wall base to measure the strain at each of the longitudinal reinforcements. Then the strain profile at the base of the wall measured using the strain gauges and the calculated strain profile predicted using the analytical model are compared. The strain profile measured in the experiment for the slender control wall had yielding at both ends of the wall almost simultaneously, the neutral axis is closer to the compressive end of the wall with a steep slope up to a certain inflection point after which the slope decreases (Figure 5-8). The reason the strain profile is investigated at onset of longitudinal steel yield is because beyond yield the strain gauges start to get damaged due to excessive deformations in the yield and opening up of the cracks. A very similar response is observed when investigating the strain profile produced by the analytical model, both ends of the wall yield simultaneously with a bilinear strain profile with a clear inflection point as shown in Figure 5-9. The measured and the analytical strain profiles for the intermediate wall has the same response as the slender shear deficient wall (Figures 5-10 and 5-11). In order to understand the reason behind the occurrence of this inflection point, it is necessary to understand the wall response at ultimate strength. As the load is applied to the cap beam of the wall, flexural cracks start forming at the base of the wall. The flexural cracks start increasing in width as the load increases in magnitude. Post-yielding the cracks on the tension side of the wall increase in size (Figure 5-12). Once the cracks are large enough, the portion of the wall that is above the crack will start acting as a rigid body

causing less strain demand on the steel compared to the steel that is still firmly attached to the walls. This decrease in demand causes the drop in slope observed explaining the inflection point observation.

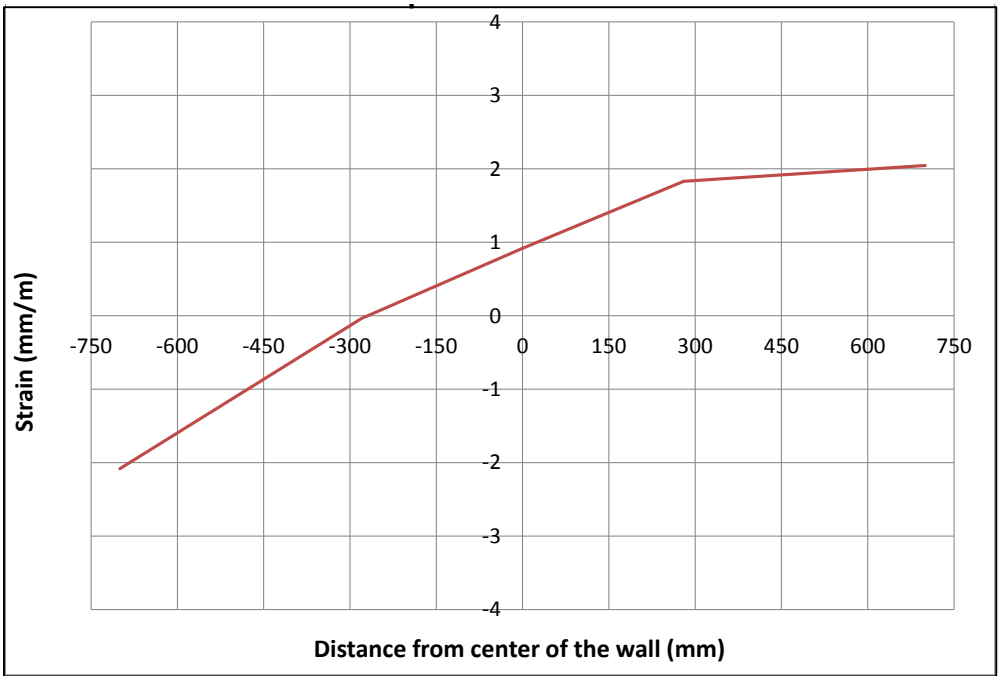

Figure 5-8: Measured strain profile at the base of the slender wall at yield

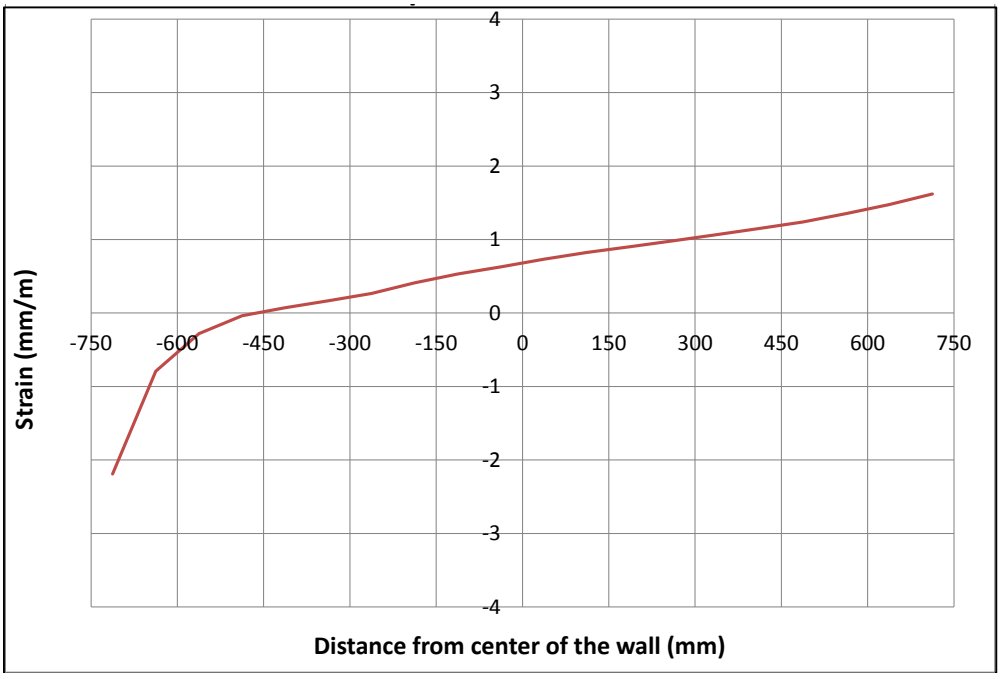

Figure 5-9: Calculated strain profile at the base of the slender wall at yield

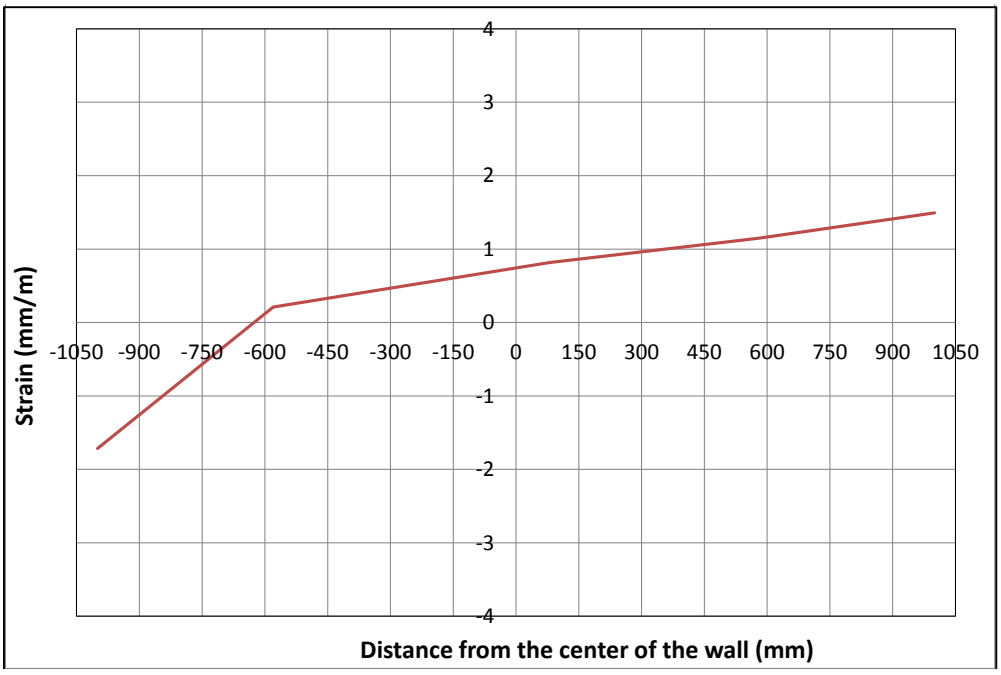

Figure 5-10: Measured strain profile at the base of the intermediate wall at yield

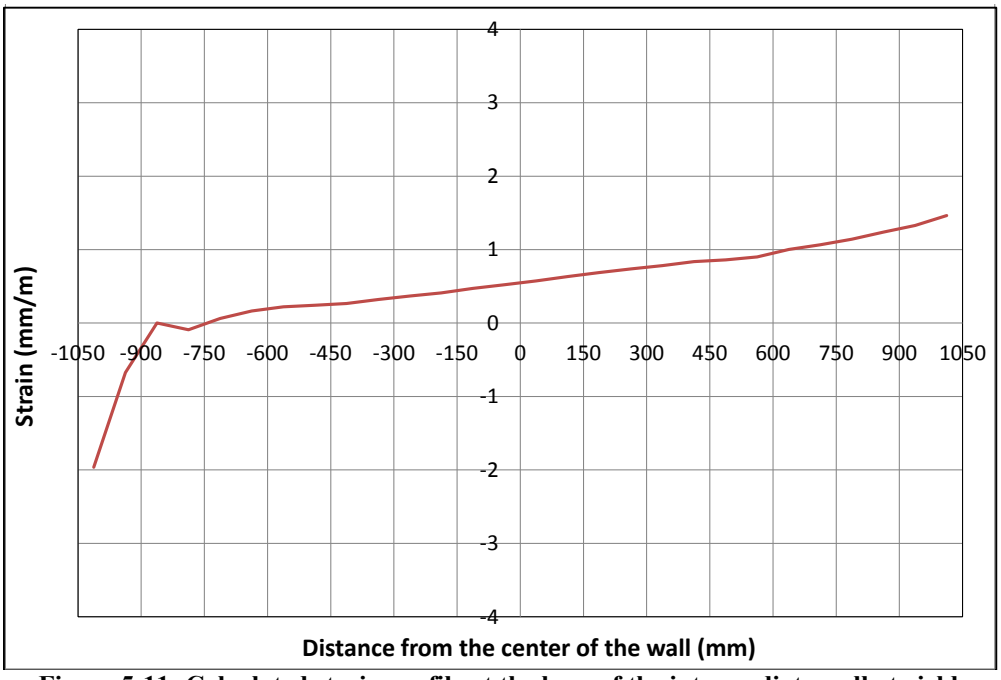

Figure 5-11: Calculated strain profile at the base of the intermediate wall at yield

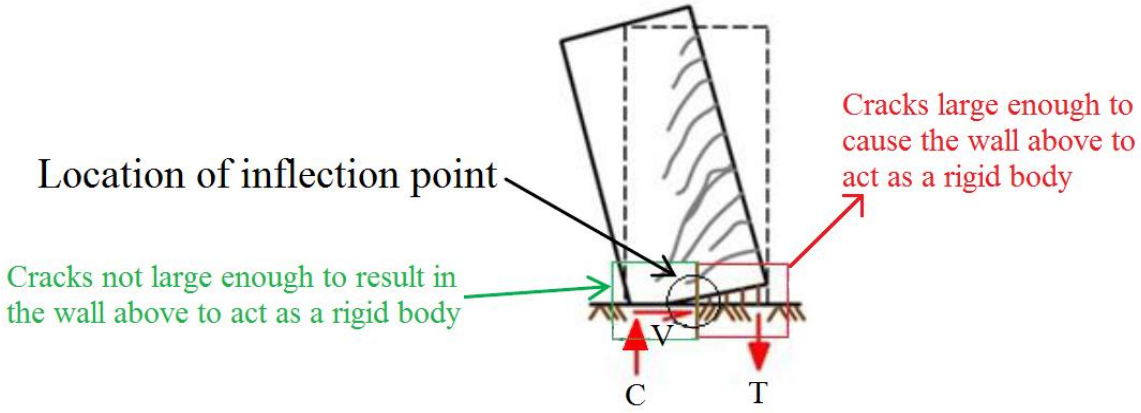

Figure 5-12 Explanation of the bilinear sectional response in shear dominant walls

Due to a limited number of shear reinforcements and lack of confinement at the edges of the wall, the failure mechanism is defined by a formation of a large diagonal crack. This was observed in the laboratory for both the slender and intermediate walls as shown in Figures 5-14 and 5-16. The analytical model had the same response at the onset of failure. A large band of elements along the diagonal of both the slender and the intermediate shear dominant walls had large diagonal cracks that ultimately resulted in the failure of the wall as shown in Figures 5-13 to 5-15.

Another point to be considered is the effect of changing the mesh size between modelling the slender flexural dominant wall and the slender shear dominant wall. Although the flexural dominant wall had a much finer mesh, both models provide a satisfactory prediction of the initial stiffness and the ultimate strength. Therefore it can be concluded that the accuracy of the control wall analytical modelling is relatively independent of the mesh size.

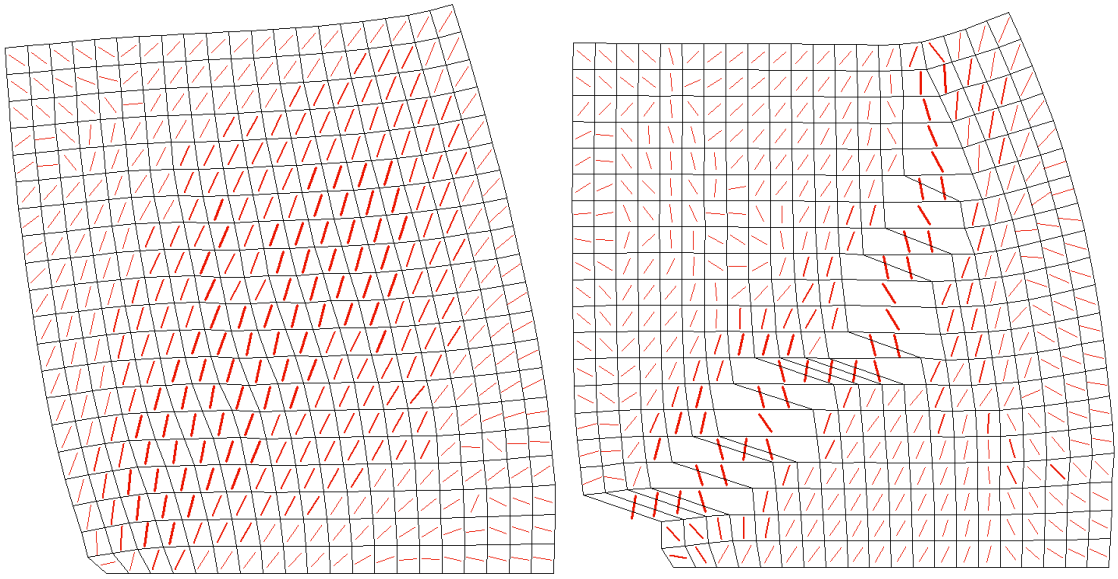

Figure 5-13: Analytical prediction of the failure mechanism in the slender wall

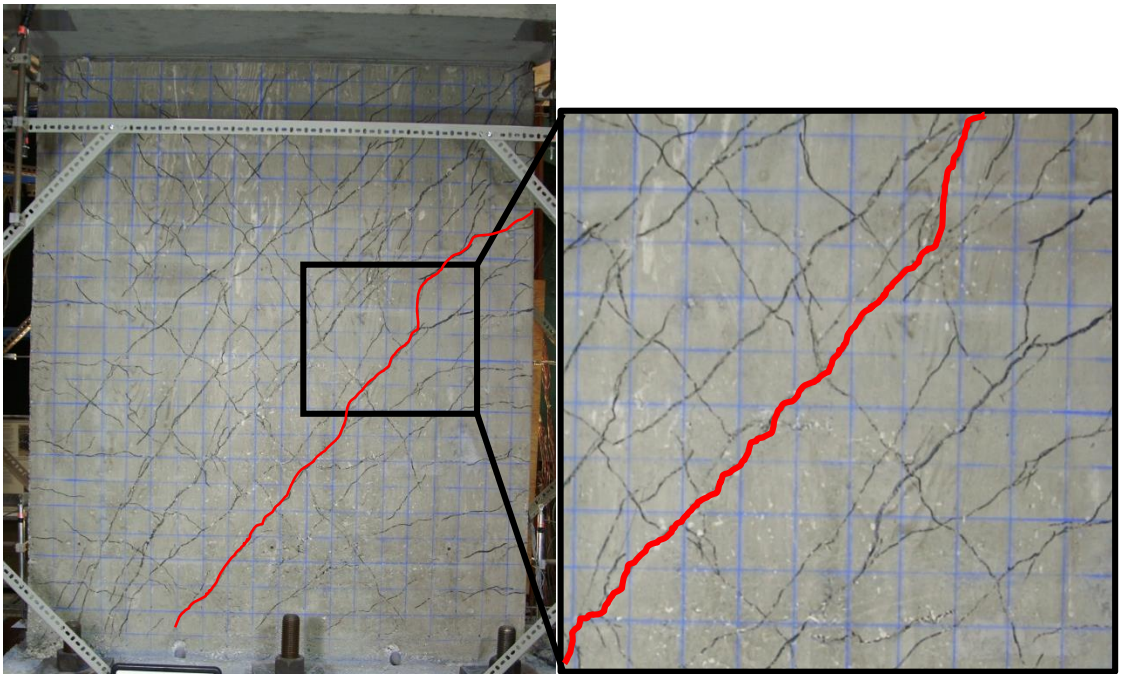

Figure 5-14: Observed failure mechanism in the slender wall

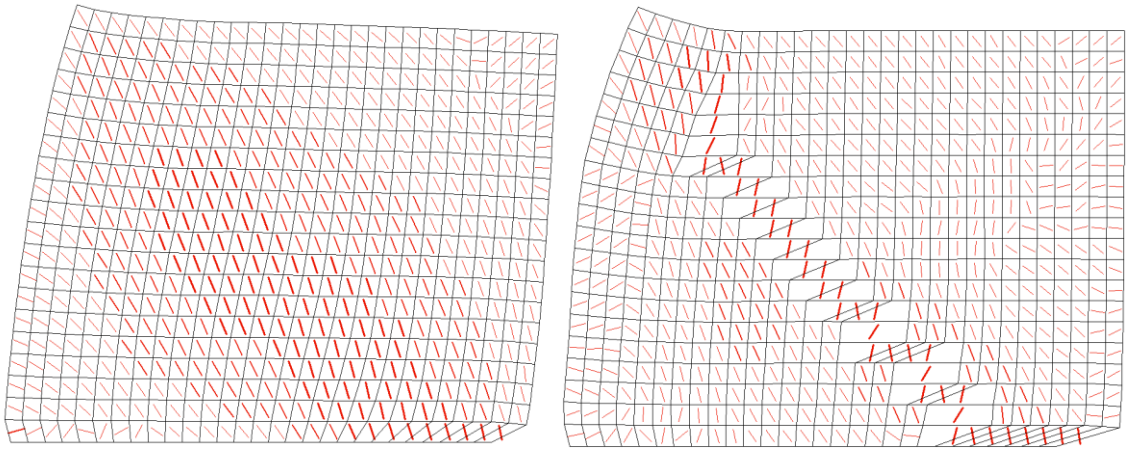

Figure 5-15: Analytical prediction of the failure mechanism in the intermediate wall

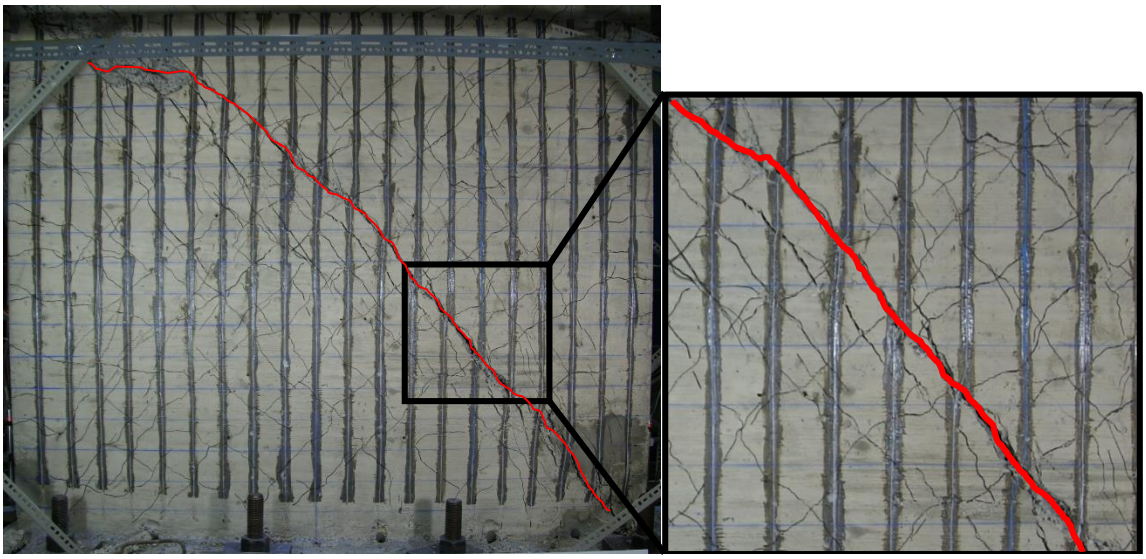

Figure 5-16: Observed failure mechanism in the slender wall

5.3 Flexural strengthened walls

Three strengthened flexural walls tested during the second phase of the experimental study are modeled using the techniques discussed earlier. The hysteresis response for the wall strengthened with 1 layer of FRP (SW1-2) for the analytical model shows very good correlation with the experimental initial stiffness, strength and ductility as well as the energy dissipation capacity (Figure 5-17). When investigating the wall strengthened with 2 layers of vertical FRP sheets (SW2-2) the analytical model slightly overestimates the strength and the initial stiffness but is capable of predicting ductility with a good degree of accuracy (Figure 5-18). When the wall with 3 vertical layers and 1 horizontal layer is analyzed it overestimates the strength and stiffness (Figure 5-19). The reason for this difference can be attributed to the effect of having more than 1 layer of FRP. FRP sheets do not have any compressive strength, however when more than 1 layer of FRP is added it starts being capable of providing some compressive resistance. The analytical model is incapable of accounting for the compressive resistance of the multiple layers of FRP. Therefore it can be concluded that the overestimation of the stiffness and strength is dependent on the number of layers of FRP used in strengthening. This will also be noticed when analyzing the strengthened shear dominant walls, which will be discussed in the following section. Another observation is the divergence between the results obtained experimentally and analytically as the loading increases. Initially, the correlation between the analytical and experimental results is very good, however as the loading increases and the wall exceeds its ultimate capacity ductility, the correlation between the analytical and

experimental results losses accuracy. Initially, both the experimental and analytical walls have fully bonded FRP sheets. The post peak response shows a decrease in strength mainly due to the initiation of the FRP sheets debonding. Once debonding of FRP initiates, the modelling of the debonding in FRP sheets, although satisfactory for the overall response, is not as accurate as modelling of walls with undebonded FRP; therefore some of the accuracy of the analytical model is lost beyond ultimate strength and after major debonding.

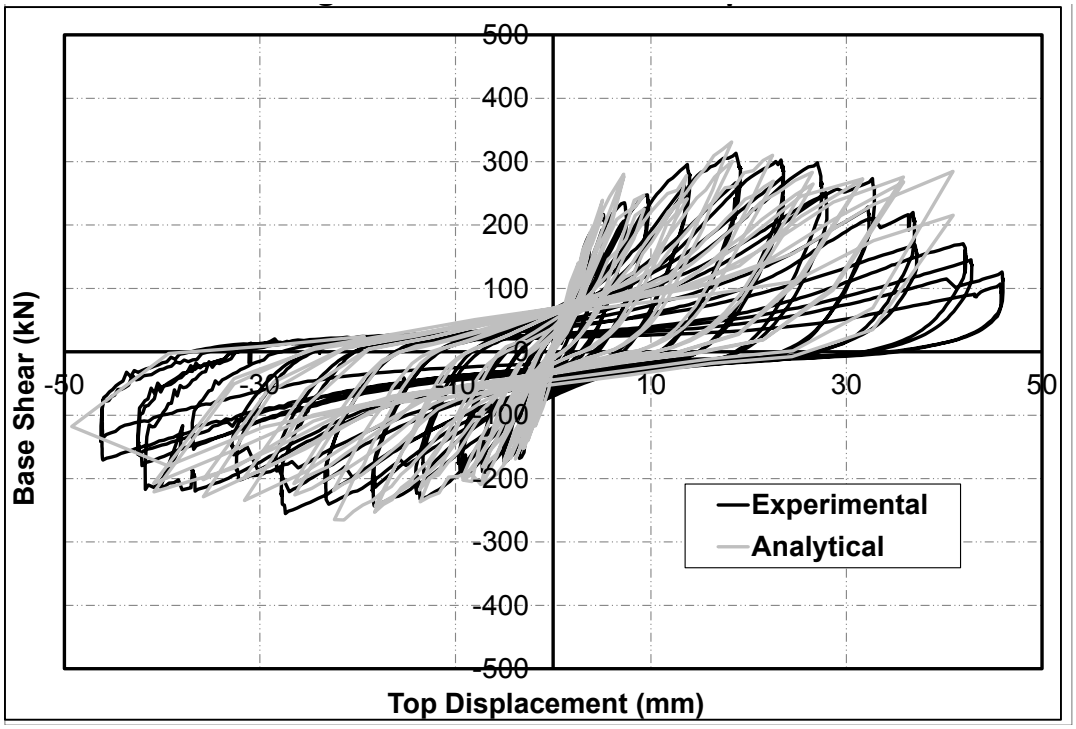

Figure 5-17: Hysteresis response of the strengthened wall 1 in phase 2 (SW1-2)

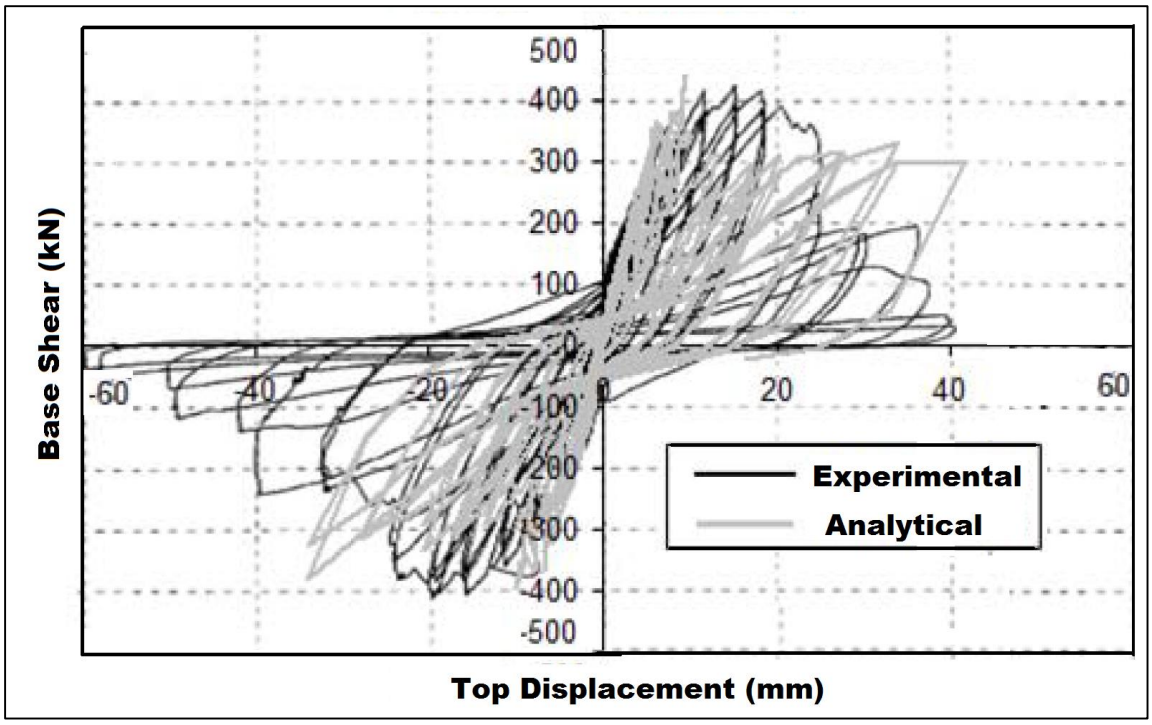

Figure 5-18: Hysteresis response of the strengthened wall 2 in phase 2 (SW2-2)

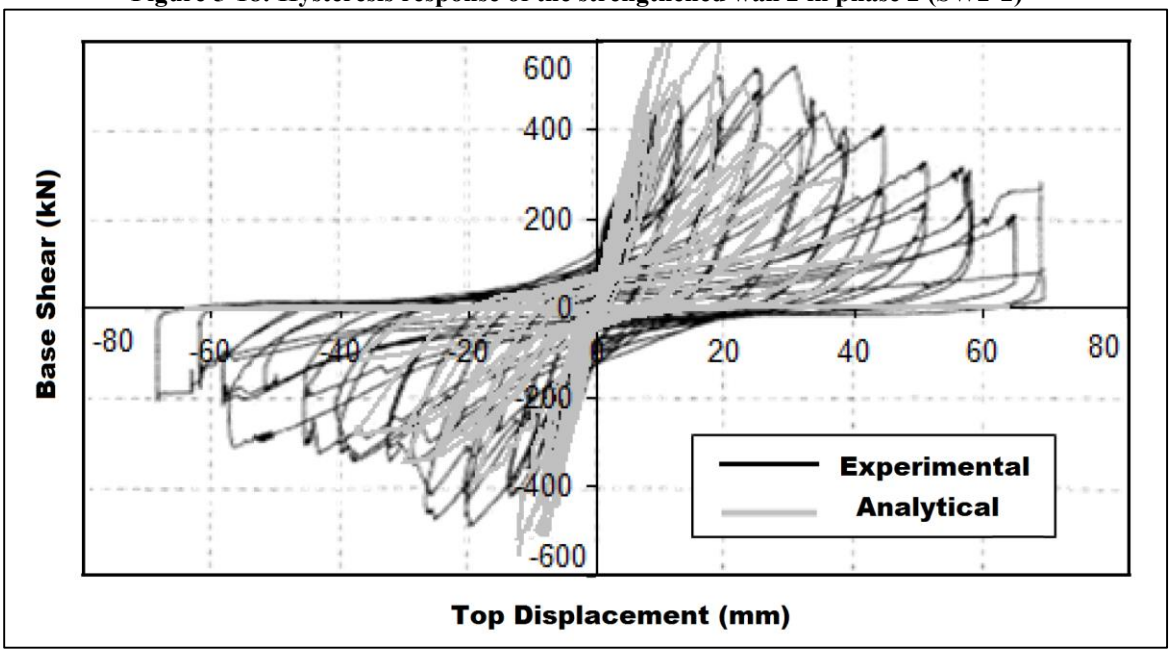

Figure 5-19: Hysteresis response of the strengthened wall 3 in phase 2 (SW3-2)

Since the strengthened walls in phase 2 of the experimental test did not have strain gauges mounted on the steel rebars, the theoretical and calculated base moment verification discussed in section 4.1 has to be used again. The calculated and theoretical moments at the base of the wall are collected and plotted against each other for the slender wall strengthened with 1 layer of FRP (SW1-2). Overall, the theoretical and calculated moment correlate very well with a maximum error of only 5% (Figure 5-20). This provides a good indication of convergence since the local response on the element level matches the global response of the wall. Similar to the hysteresis response, the correlation between theoretical and calculated moment at the base of the wall loses accuracy as the loading increases.

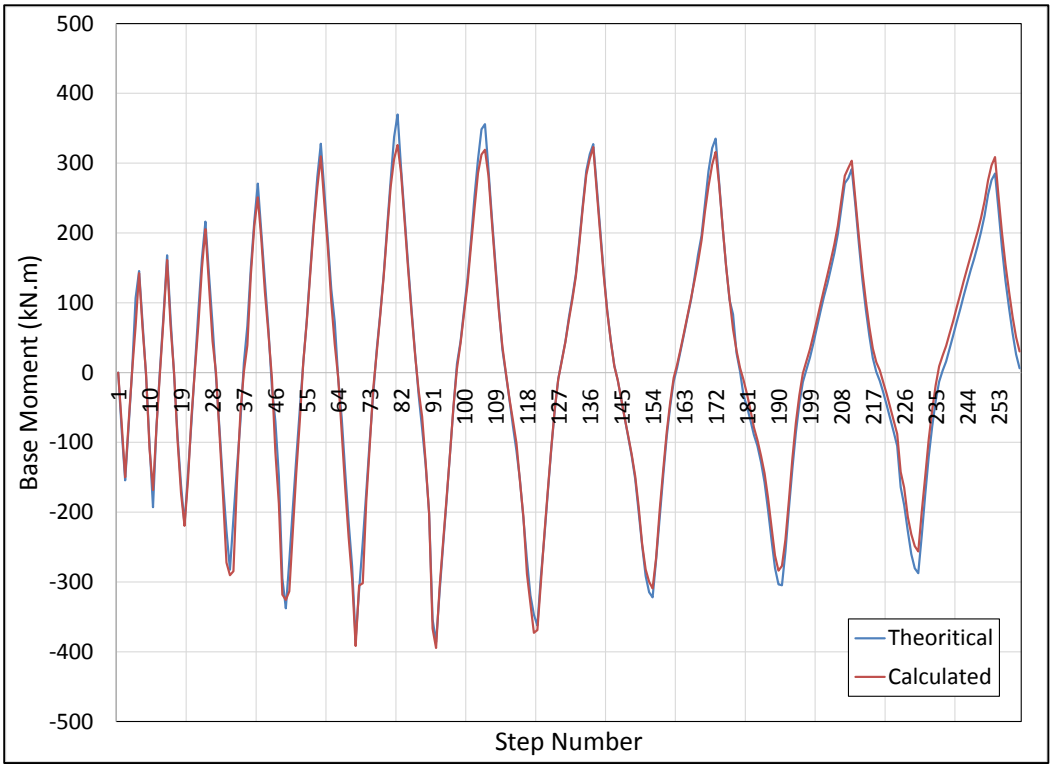

Figure 5-20: The theoretical and calculated moment at the base for the analytical model

The failure mechanism for the flexural walls strengthened with FRP are the same regardless of the number of FRP layers used. The FRP sheets start debonding once the flexural cracks are large enough to cause excessive strains in the FRP sheets as shown in Figure 5-21. After the FRP sheets debond, the flexural cracks start widening causing concrete to spall and the flexural strength to deteriorate as shown in Figure 5-22. The analytical model is also capable of predicting the same failure mechanism observed in the laboratory. The analytical model is capable of predicting the FRP debonding from the FRP substrate (Figure 5-23). The model also predicted the formation of large horizontal flexural cracks at the bottom of the wall near the complete collapse of the wall shown in Figure 5-24. Results presented below correspond to SW1-2; however, the responses for SW2-2 and SW3-2 are almost identical both experimentally and analytically and therefore will not be presented.

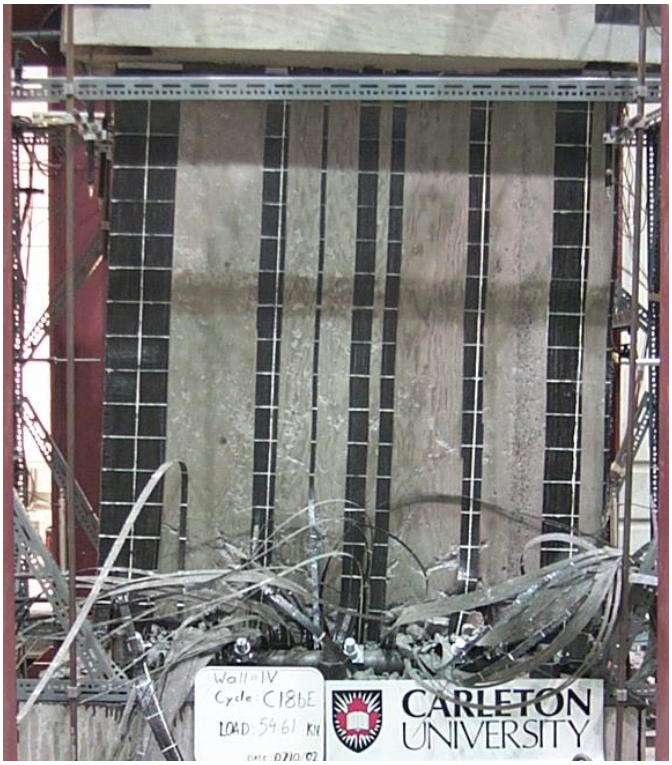

Figure 5-21: Debonding of FRP sheets observed in testing SW1-2

Figure 5-22: Large flexural cracks visible after debonding of FRP sheets in SW1-2

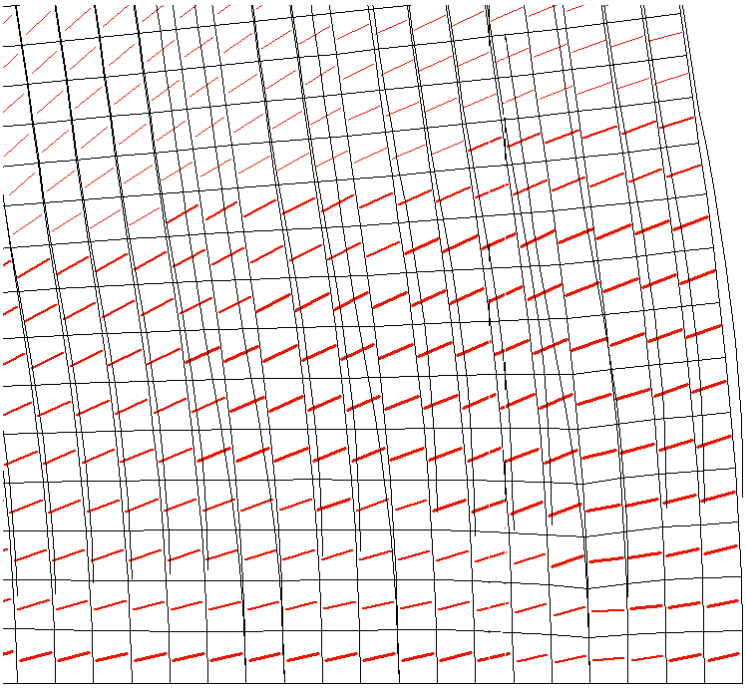

Figure 5-23: Debonding of FRP sheets predicted by the analytical model for SW1-2

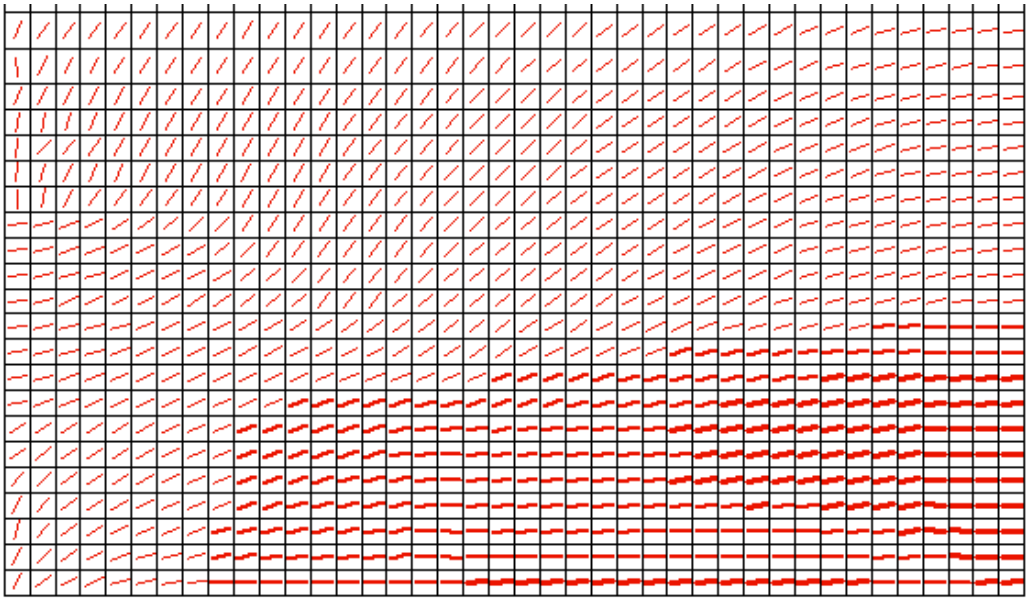

Figure 5-24: Large flexural cracks predicted by the analytical model for SW1-2

5.4 Shear dominant strengthened walls

The force-displacement response of the slender strengthened wall showed very good correlation with the ultimate strength and ductility observed in the experimental test as shown in Figure 5-25. The model underestimates the initial stiffness of shear dominant strengthened walls. This underestimation of the initial stiffness can be attributed to the inability of the model to account for confining effects added by the large number of horizontal FRP sheets. Although the horizontal FRP sheets is not wrapped around the wall, it is still capable of providing some confinement effect preventing or delaying the debonding of the vertical FRP layer from the concrete substrate and thus has some confinement effect on the wall panel concrete material. In the flexural walls the debonding of the FRP sheets causes some of the sheets to tear vertically parallel to the fibre orientation. In the shear deficient walls, the fibres cross each other and the horizontal FRP sheets add confinement effect to the sheets preventing debonding of small FRP strips along the fibre orientation as shown in Figure 5-26. Debonding is delayed significantly and large areas of FRP debond at a time unlike what occurs in the flexural dominant walls. The horizontal trusses used to model the horizontal FRP sheets are incapable of modelling the confinement effect applied to the wall due to presence of FRP.

The force-displacement hysteresis response of the intermediate wall shows a satisfactory correlation with the ultimate strength of the wall, but an underestimation of the stiffness and ductility seen in Figure 5-27. As discussed earlier, the underestimation of the stiffness can be due to the model being incapable of accounting for the compressive resistance of

multiple layers of FRP as well as the confining effects added due to the presence of the horizontal FRP. The underestimation of the ductility is caused by a modelling limitation. At high levels of ductility, major crushing of the concrete at the ends of the wall is observed as shown in Figure 5-28. In the reverse cycle, the concrete that undergoes crushing spalls off and is held in position solely due to the presence of the horizontal FRP sheets. In modelling, when the concrete crushes and spalls off, this is presented using large cracks. When the cracks get larger than the size of the concrete element the model stops running due to errors in the stiffness matrix. Therefore, although the wall is capable of resisting loads up to high levels of ductility, an analytical model would not be able to simulate that resistance since it is solely dependent on mechanical interlock of the aggregates rather than structural resistance.

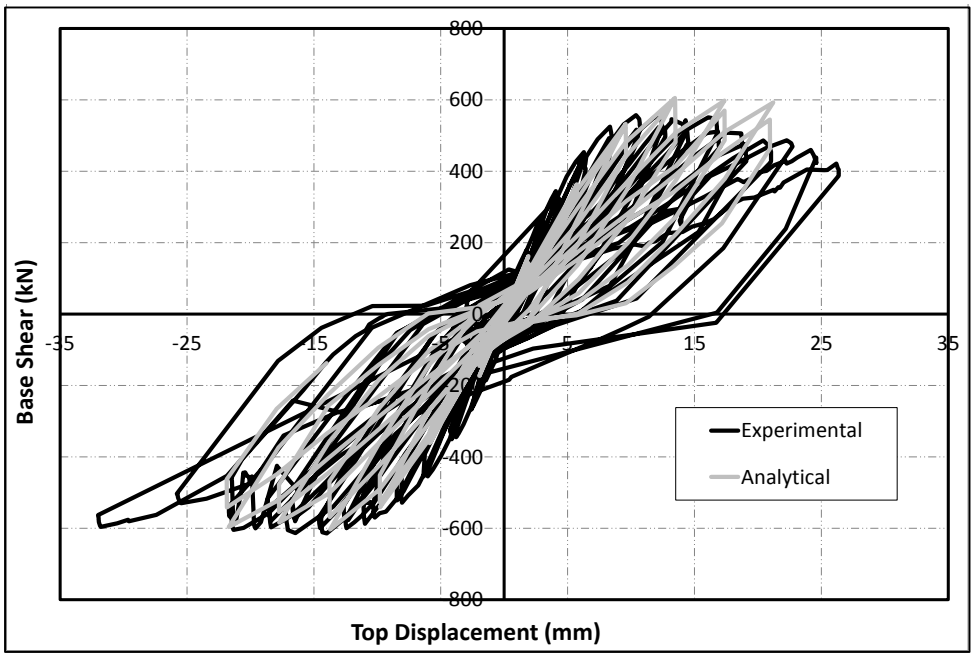

Figure 5-25: Load-displacement hysteresis of the slender strengthened wall (SLSW)

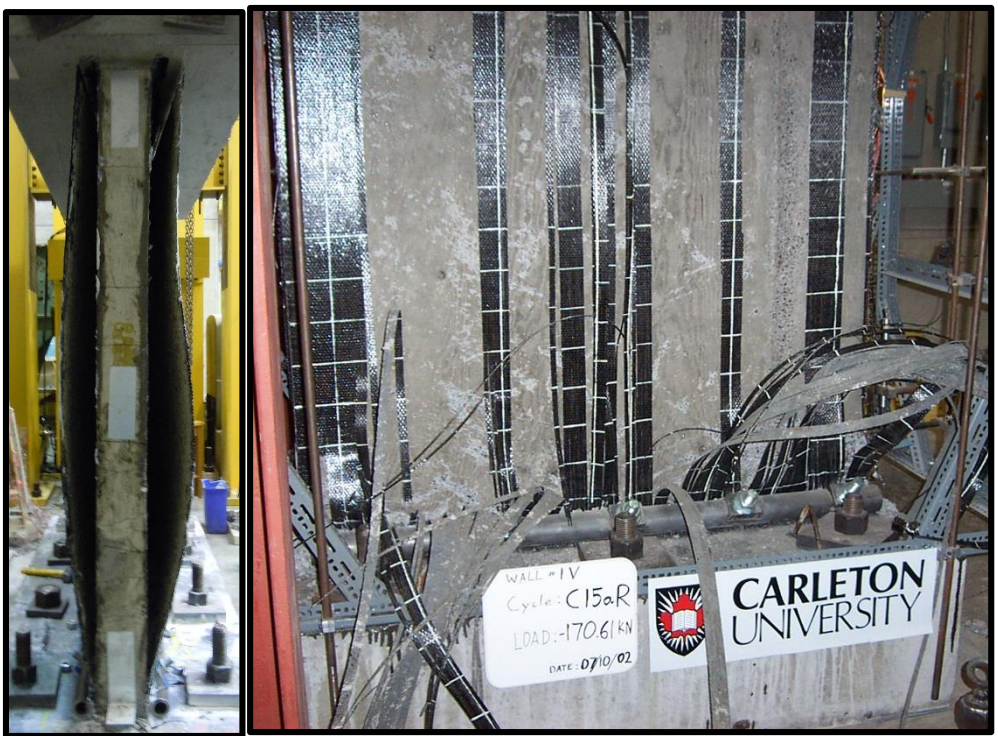

Figure 5-26: Debonding in the shear dominant walls with large areas debonding as 1 sheet (left) vs. debonding in the flexural dominant wall with tears along the FRP fibre (right)

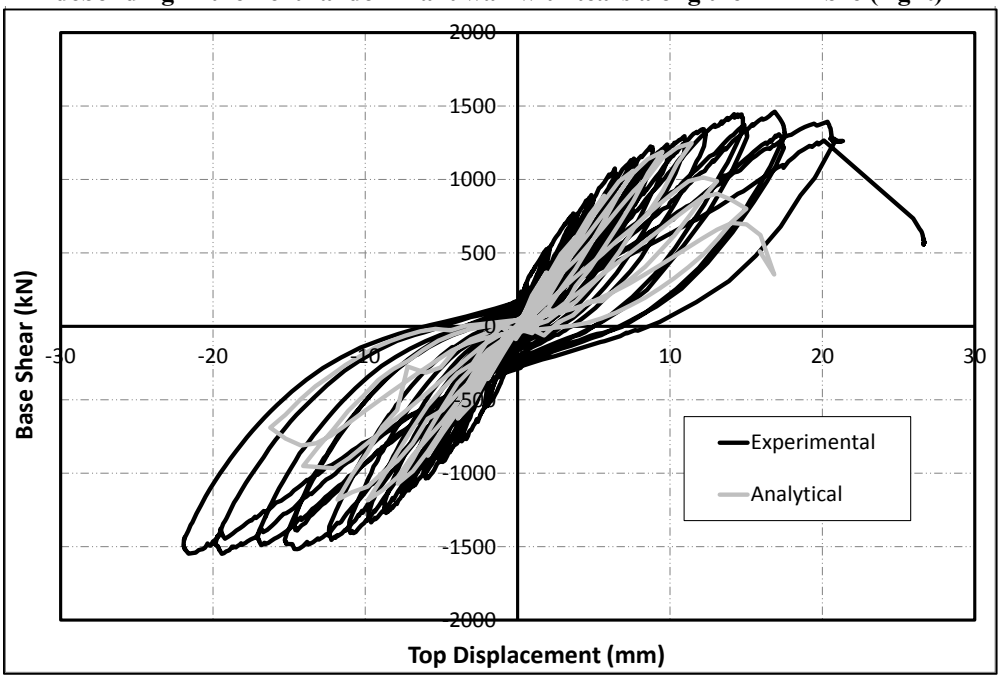

Figure 5-27: Load-displacement hysteresis of the intermediate strengthened wall (ISW)

Figure 5-28: Crushed concrete at the ends of the wall staying intact due to presence of FRP

Unlike the flexural dominant walls tested in phase 2 of the project, the shear dominant walls had strain gauges mounted on the steel reinforcements. Also, a new fiber optics system is applied to the surface of the FRP sheets to measure the strain in the FRP sheets. The strain profiles obtained from the analytical models are compared with the measured values of the FRP strain as well as the steel strain to verify the accuracy of the local response prediction of the wall. Similar to the control shear dominant walls, the strain profiles are obtained at the onset of the steel reinforcement yielding since the strain gauges usually get damaged due to large deformations that occur post yielding. As expected the measured strain profile of the FRP sheets and steel reinforcements followed a very similar pattern with the neutral axis closer to the compressive end of the wall and the strain profile

following a bilinear pattern due to the reasons discussed in section 4.2 above. The calculated strain profile obtained from the analytical model also showed a strain profile where the steel on both ends of the wall yield at the same loading stage. The calculated strain profile showed that the strain in steel and FRP are equivalent which indicates that the FRP sheets are still perfectly bonded. In the experimental test the FRP did not debond prior to the yield of the steel reinforcement confirming the findings of the analytical study. Both the intermediate and slender walls had similar strain profile patterns as shown in Figures 5-29 to 5-32.

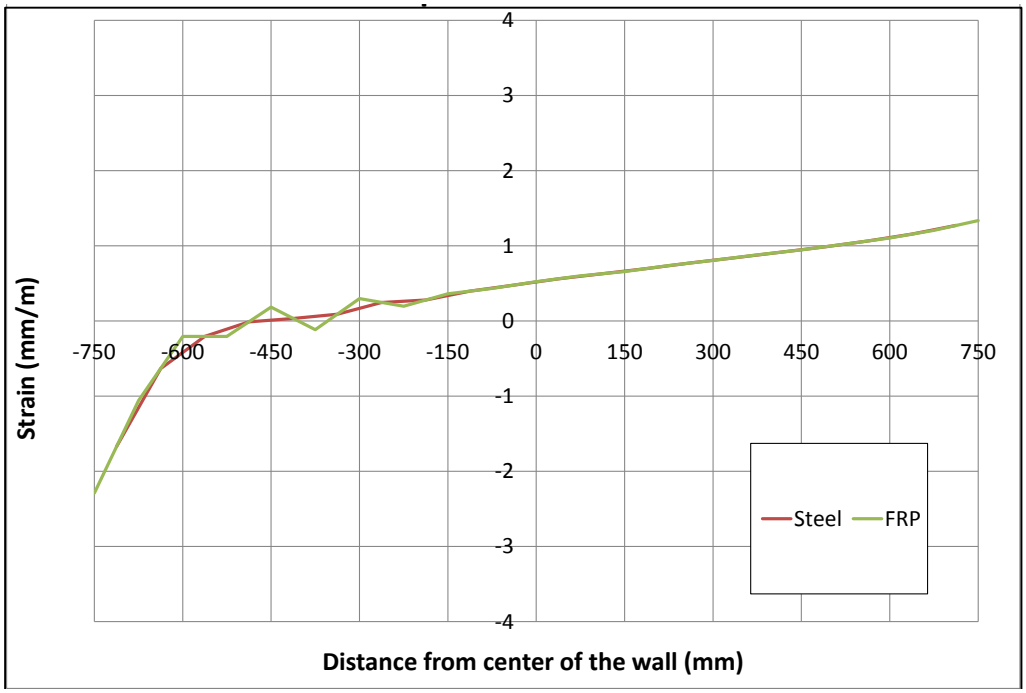

Figure 5-29: Calculated strain profile at yield for the slender strengthened wall (SLSW)

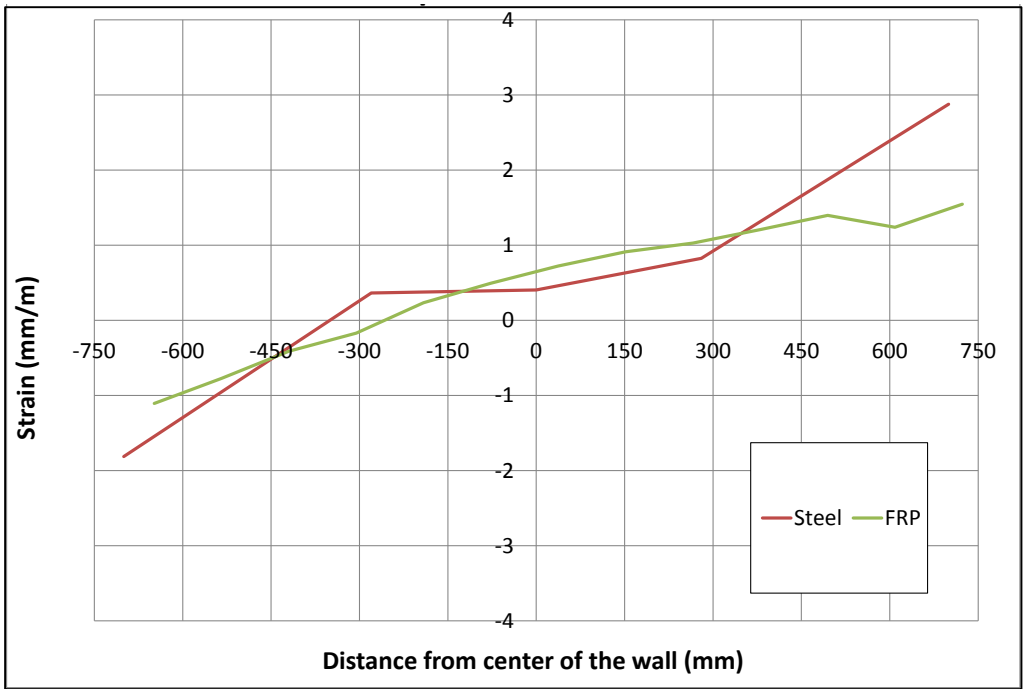

Figure 5-30: Measured strain profile at yield for the slender strengthened wall (SLSW)

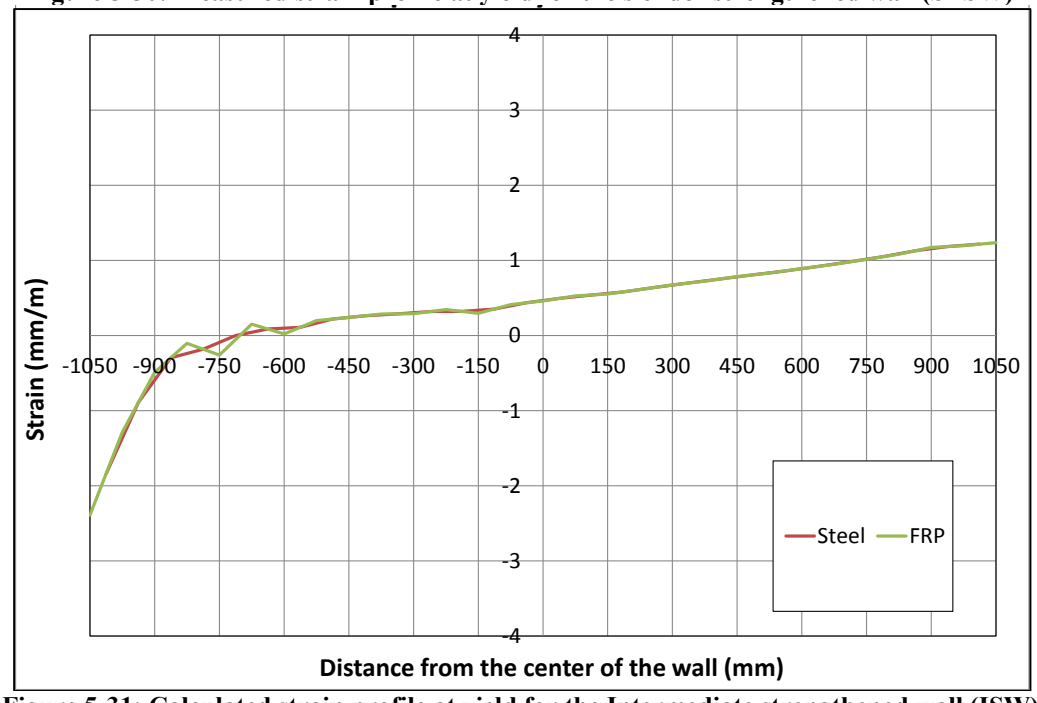

Figure 5-31: Calculated strain profile at yield for the Intermediate strengthened wall (ISW)

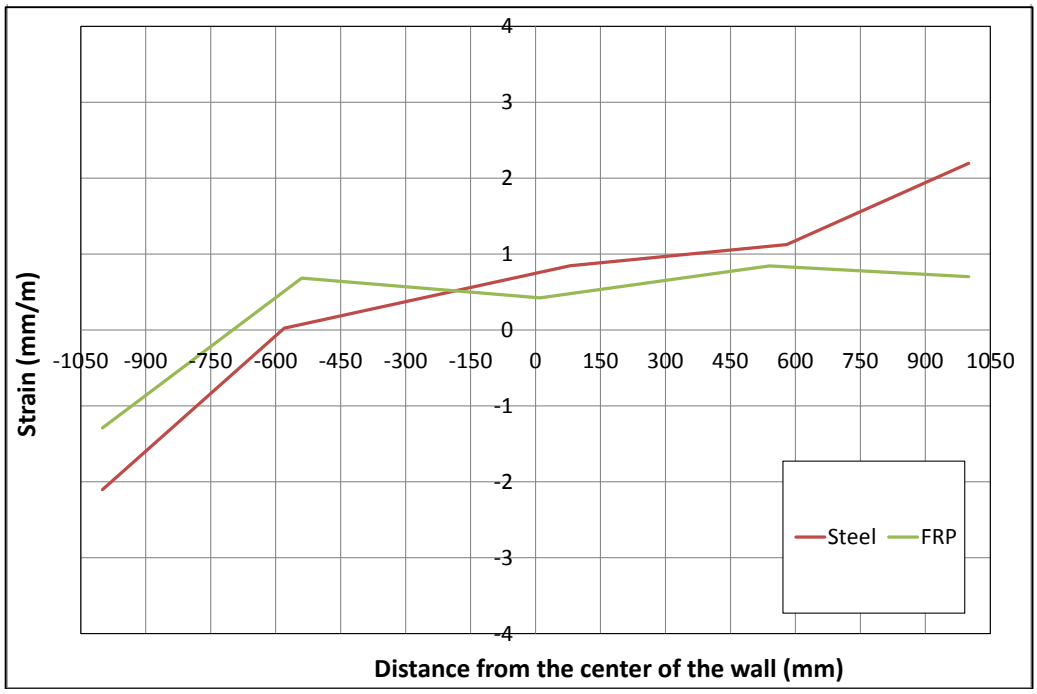

Figure 5-32: Calculated strain profile at yield for the Intermediate strengthened wall (ISW)

The analytical model predicted the debonding of the vertical and horizontal FRP sheets prior to the failure of the wall as shown in Figure 5-33. The wall collapse is predicted to have been caused by a large diagonal crack along the face of the wall with concrete crushing at the toe of the wall seen in Figure 5-34. In the experimental study, the vertical and horizontal FRP sheets also debonded prior to failure. Once the wall completely collapsed, the FRP sheets were removed and a large diagonal crack which caused the failure of the wall was visible. Also, the failure of the wall is very brittle indicating that after the FRP sheets debonded, the RC shear wall independently resisted the shear force resulting in the observed diagonal shear failure (Figure 5-35).

In the intermediate wall, the analytical model predicted debonding of the FRP at very late stages of loading and just prior to complete failure (Figure 5-36). The wall is predicted to

have large diagonal cracks that link with flexural cracks at the bottom of the wall to cause the failure of the wall. This occurs because the FRP is still bonded at the center of the very wide substrate of the wall, therefore, it is easier for the cracks to propagate downwards toward the flexural cracks and cause the failure mechanism seen in Figure 5-37. In the experimental study, only the side of the FRP sheet is debonded with the large crack causing failure occurring behind that area of the FRP sheets. The pattern of debonding and crack of the wall is very similar to that predicted by the analytical model as shown in Figure 5-38. Overall the analytical model is capable of accurately predicting the failure mechanism of both the intermediate (ISW) and slender (SLSW) strengthened shear dominant walls.

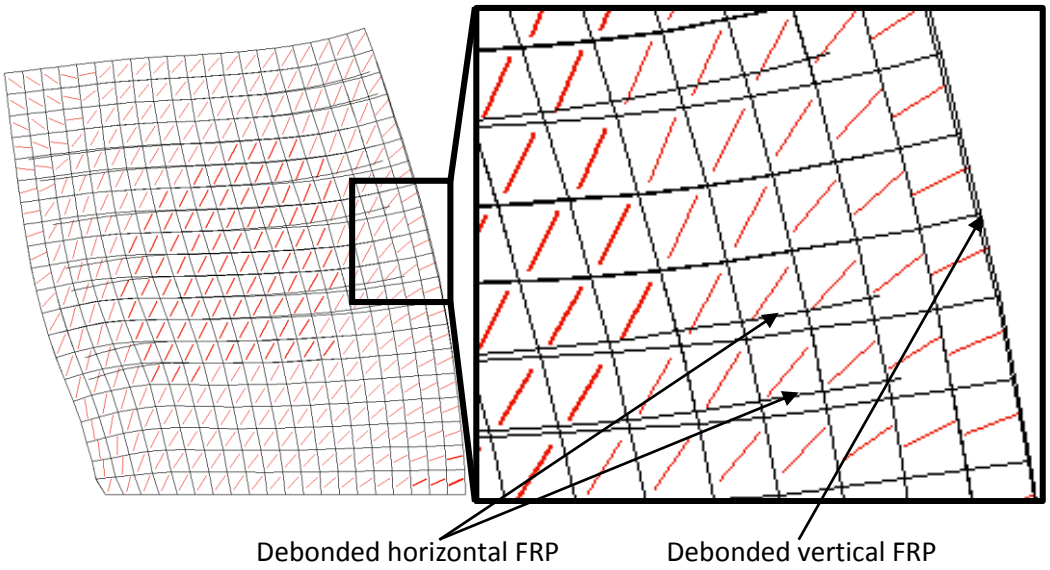

Figure 5-33: Analytical model predicting vertical and horizontal FRP debonding

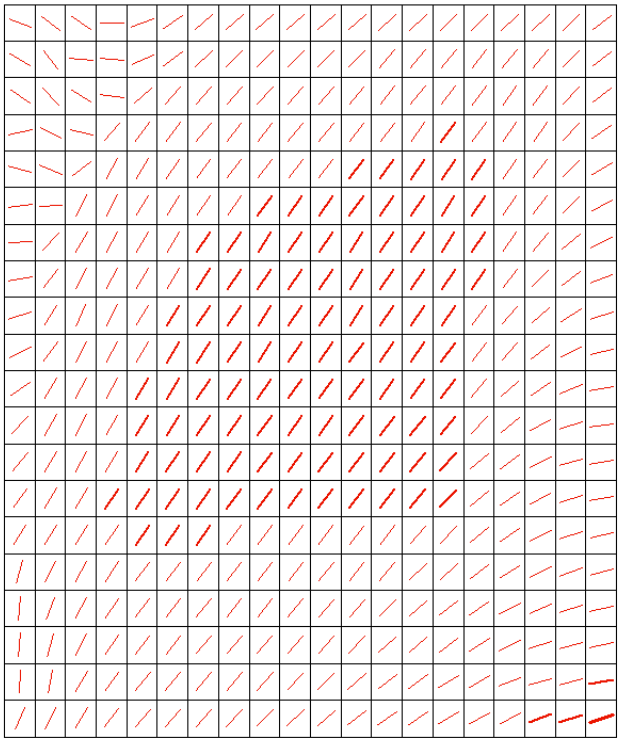

Figure 5-34: Large diagonal crack and crushing at the tow of the concrete predicted

Figure 5-35: Large diagonal crack observed post failure of the wall

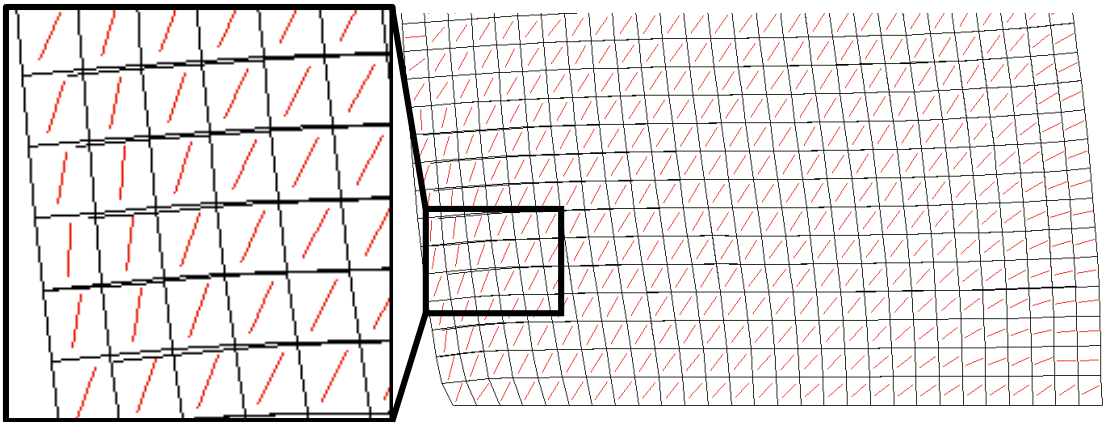

Figure 5-36: Observed horizontal FRP on one side of the wall

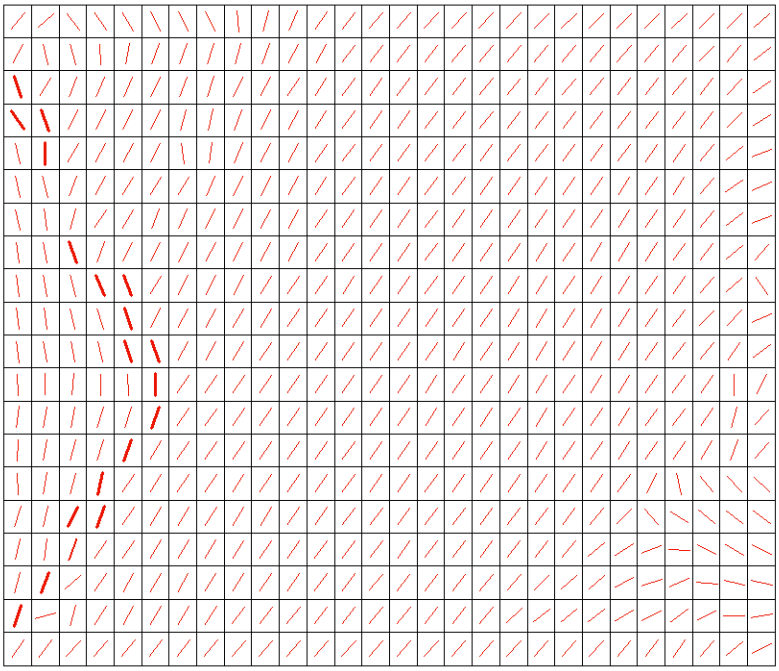

Figure 5-37: Large cracks on the side of the wall causing sudden failure of the wall

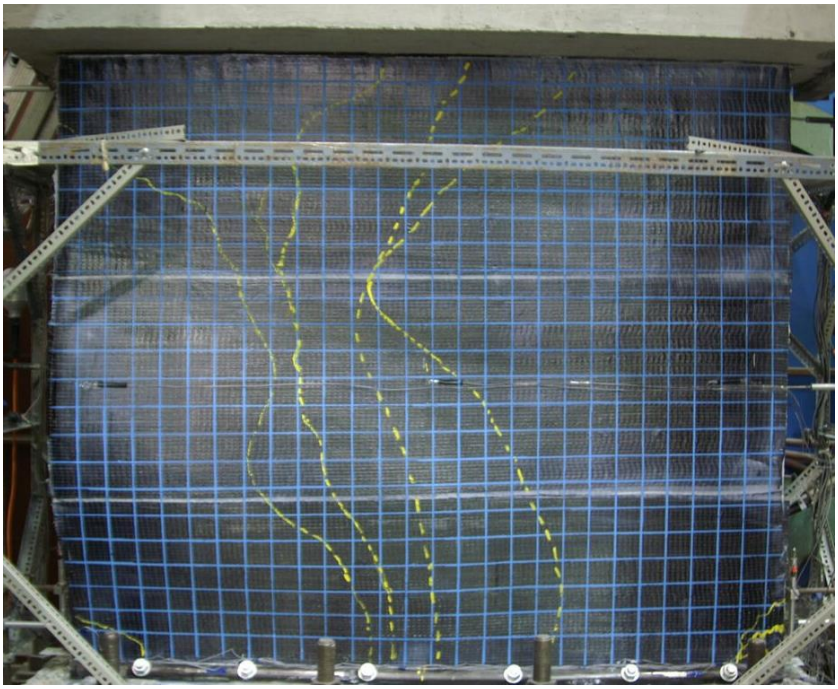

Figure 5-38: The debonded FRP follows the same cracking pattern predicted by the analytical mode

6.0 CONCLUSIONS AND RECOMMENDATIONS

Although the use of FRP sheets for strengthening of RC shear walls has gained major interest and its application has been widely accepted for a number of years, very limited efforts have focused on understanding the response of the walls. A number of experimental studies have proven the efficiency of the FRP application to RC shear walls but there is still a lack of analysis tools for these walls. This thesis focuses on developing analytical models capable of predicting the overall response of the walls, the local response of the walls as well as the failure mechanism of the walls. The analytical models are developed using the FE program vecTor2. The process of developing the analytical models includes being able to model the as built walls geometrically, incorporating the FRP sheets into the model and accounting for the IC debonding of the FRP sheets that occur due to widening of concrete cracks. The thesis also introduces modifications to previous modelling techniques to be capable of accounting for debonding due to shear cracks present in shear deficient walls. The effect of using different mesh sizes has also been considered. The modelling techniques are used to model walls with different aspect ratios as well as different design details, with some walls flexural dominant and some being shear dominant. The analytical model results is then verified by comparing it to the experimental study results measured in the laboratory.

6.1 Conclusions

A simple computationally efficient algorithm is developed to account for the debonding of FRP sheets in the RC strengthened shear walls. The algorithm is used with the RC strengthened shear walls both shear dominant and flexural dominant. The results showed very good correlation for the control walls both the flexural and the shear deficient. The hysteresis response, local distribution of forces and failure mechanism were predicted accurately using the models. The flexural strengthened wall model results also showed very good correlation with the experimental results. It is concluded that the accuracy of the model is lost as the number of FRP layers is increased due to the compressive resistance of the FRP when multiple layers are used. The models for the shear deficient strengthened walls provided satisfactory results for the hysteresis and very good prediction of the failure mechanism and the strain profile at the base of the wall. Overall the models for all the walls provide very satisfactory prediction of the walls both on the global and local levels.

6.2 Recommendations

A number of improvements can be done to improve on the results of any future modelling:
1-The bond-slip models used to determine the concrete-FRP interaction is based on meso-scale testing of flexural beams with flexural cracks. This bond-slip model is modified and used for both the debonding of shear and flexural crack induced debonding. A meso-scale model for shear walls will provide a much more relevant bond-slip relations for the modelling of strengthened shear walls.

2- The bond-slip model adapted paid very little attention to the effect of using different mesh sizes for modelling of the RC element and its bonded FRP sheets. An assumption had to be made to account for the mesh size effect. If a new meso-scale model is developed to form new bond-slip models, a wide range of averaging lengths has to be used to account for all different mesh sizes.

3-VecTor2 FE program used has an upper limit on the number of elements that can be included in the analysis. If another FE program with no upper limit on the number of elements is used, a much finer mesh can be used with smaller trusses allowing for a more accurate prediction of the debonding of the FRP sheets.

4- An experimental program can investigate the compressive resistance of multiple layers of FRP sheets to be able to estimate the effect of the FRP sheets on the stiffness and ultimate strength of the strengthened shear walls.

5-An experimental program can investigate the confining effect of the horizontal FRP sheets. A number of RC shear wall panels can be subjected to compressive loads and closely monitor the strains in the transverse and longitudinal directions to develop a confinement model. It is worth noting that confinement models for FRP wrapped concrete elements exist however there are no present model that account for confinement due to unwrapped horizontal FRP sheets.

REFERENCES

ACI. (2008). *Guide for the design and construction of externally bonded FRP systems for strengthening concrete structures.* Farmington Hills, MI: American Concrete Institute.

ACI 318. (1968). *Building requirements for structural concrete.* Detroit, Michigan, USA: American concrete institute.

ACI Committee 318. (2005). *Building Code Requirements for Structural Concrete (ACI 318-05) and Commentary (318R-05).* Farmington Mills, MI: American Concrete Institute.

Antoniades, K., Salonikios, T., & Kappos, A. (2003). Cyclic Tests on Seismically Damaged Reinforced Concrete Walls Strengthened Using Fiber-Reinforced Polymer Reinforcement. *ACI Structural Journal, 100*, 510-518.

Canadian Standards Association. (1994). *Design of Concrete Structures.* Ottawa, ON: CAN/CSA A23.3-94.

Chen, J., & Teng, J. (2001). Anchorage strength models for FRP and steel plates bonded to concrete. *Journal of Structural Engineering*(127), 784-791.

Cortés-Puentes, W. L. (2009). *Nonlinear Modelling and Analysis of Repaired and Retrofitted Shear Walls.* M.A.Sc. (Civil Engineering) Thesis, Ottawa.

Cruz-Noguez, C. A., Lau, D. T., Sherwood, E. G., Lombard, J., & Hiotakis, S. (2012). *Seismic Behaviour of RC shear walls with externally bonded FRP sheets- Part I: Experimental studies.* Experimental paper, Carleton University, Department of Civil and Envirnomental Engineering, Ottawa.

CSA. (1977). *Code for the Design of Concrete structures for buildings.* Rexdale, Ontario, Canada: CAN3-A23.3-M77, Canadian Standard Association.

CSA. (2012). *Design and Construction of Building components with Fibre-Reinforced Polymers.* Mississauga, Ontario: Canadian Standards Association.

CSA A23.3. (2004). *Design of Concrete Structures.* Rexdale, Ontario, Canada, Ontario, Canada: Canadian Standards Association.

Elnady, M. (2008). *Seismic Rehabilitation of RC Structural Walls.* PhD Thesis, McMaster University Department of Civil and Environmental Engineering.

El-Sokkary, H., Galal, K., Ghorbanirenani, I., Leger, P., & Tremblay, R. (2013). Shake Table Tests on FRP-Rehabilitated RC Shear Walls. *Journal of Composites for Construction*, 79-90.

FEMA. (1997). *NHERP Guidlines for the seismic rehabilitation of buildings.* Federal Emergency Management Agency, FEMA 273 (and Commentary FEMA 274).

Hassan, A., Cruz-Noguez, C. A., & Lau, D. T. (2013). Influence of FRP-Concrete Debonding Mechanisms on the seismic response of FRP-reinforced shear walls. *CSCE 2013 General Conference* (pp. GC-235-1-11). Montreal: CSCE.

Hiotakis, S. (2004). *Repair and Strengthening of Reinforced Concrete Shear Walls for Earthquake Resistance Using Externally Bonded Carbon Fibre Sheets and a Novel Anchor System.* Master's Thesis, Carleton University, Department of Civil and Envirnomental Engineering.

Homam, S., Sheikh, S., Perica, G., & Mukherjee, P. (2000). *Durability of Fibre einforced Polymers (FRP) Used in Concrete Structures.* Toronto, Canada: Department of Civil Engineering, University of Toronto.

Khalil, A., & Gobarah, A. (2005). Behaviour of Rehabilitated Structural Walls. *Journal of Earthquake Engineering 9:3*, 371-391.

Lombard, J. (1999). *Seismic strengthening and repair of reinforced concrete shear walls using externally-bonded carbon fibre tow sheets.* Master's Thesis, Carleton University, Department of Civil and Envirnomental Engineering, Ottawa.

Lombard, J., Lau, D., Humar, J., Foo, S., & Cheung, M. (2000). Seismic strengthening and repair of reinforced concrete shear walls. *Proceedings of 12th World Conference on Earthquake Eng.*

Lu, X. Z., Teng, J. G., Ye, L. P., & Jiang, J. J. (2007). Intermediate crack debonding in FRP-strengthened RC beams: FE analysis and strength model. *Journal of Composites for Construction, 11*(2), 161-174.

Lu, X., Teng, J., Ye, L., & Jiang, J. (2004). Bond-Slip models for FRP sheet/plate-to-Concrete interfaces. *2nd international Conference of advanced polymer composites for structural applications in construction* (pp. 152-161). Cambridge, England: Woodhead Publishing Limited.

Lu, X., Ye, L., Teng, J., & Jiang, J. (2005). Meso-scale finite element model for FRP sheets/plates bonded to concrete. *Engineering structures*(27), 564-575.

Moehle, J. (2014). *Seismic Design of Reinforced Concrete Buildings.* McGraw-Hill Education.

Oehlers, D., Park, S., & Mohamed Ali, M. (2003). A structural engineering approach to adhesive bonding longitudinal plates to RC beams and slabs. *Composites-Part A: Applied Science and Manufacturing*, 887-897.

Paterson, J., & Mitchell, D. (2003). Seismic Retrofit of Shear Walls with Headed Bars and Carbon Fiber Wrap. *Journal of Structural Engineering, 129*, 606-614.

Pham, H., & Al-Mahaidi, R. (2007). Modelling of CFRP–concrete shear–lap tests. *International Journal of Construction and Building Materials, 21*, 727-735.

Seible, F., Priestley, M., & Innamorato, D. (1995). Earthquake retrofit of bridge columns with continuous carbon fibre jackets-Volume II, Design guidelines. *Advanced Composites Technology Transfer Consortium* (pp. Rep. No, ACTT-95/08). San Diego, CA: University of California.

Shaheen, I. (2014). *Seismic Retrofit and Strengthening of Deficient Reinforced Concrete Shear Walls Using Externally Bonded Fibre Reinforced Polymer Sheets.* Ottawa, Ontario: Department of Civil and Environmental Engineering, Carleton University.

Shaheen, I., Cruz-Noguez, C. A., & Lau, D. (2013). Seismic Retrofit of R.C. Shear Walls with Externally Bonded FRP Tow-Sheets. *3rd Speciality Conference on Disasted Prevention and Mitigation.* Montreal, Quebec: CSCE.

Smith, S. T., & Teng, J. G. (2002). FRP-strengthened RC beams. I: Assessment of debonding strength models. *Engineering structures*(24), 397-417.

Smith, S. T., & Teng, J. G. (2002). FRP-Strengthened RC beams. I: Review of debonding strength models. *Engineering Structures*(24), 385-395.

Teng, J., Smith, S., Yao, J., & Chen, J. (2003). Intermediate crack-induced debonding in RC beams and slabs. *Construction and Building Materials Journal*(17), 447-462.

Triantafillou, T. (1998). Shear Strengthening of Reinforced COncrete beams using epoxy-bonded FRP composites. *ACI Structural Journal, 95*(2), 107-115.

Vecchio, F. (2000). Disturbed Stress Field Model for Reinforced Concrete: Formulation. *Journal of Structural Engineering, 126*(9), 1070-1077.

Vecchio, F. J., & Lai, D. (2004). Crack Shear-Slip in Reinforced Concrete Elements. *Journal of Advanced Concrete Technology*, 289-300.

Vecchio, F., & Collins, M. (1986). The Modified Compression Field Theory for Reinforced Concrete Elements Subject to Shear. *ACI Structural Journal, 83*(2), 219-231.

Vecchio, F., & Lai, D. (2004). Crack Shear-Slip in Reinforced Concrete Elements. *Journal of Advanced Concrete Technology, 2*(3), 289-300.

Wong, S. Y., & Vecchio, F. J. (2003). Towards modeling of reinforced concrete members with externally bonded fiber-reinforced polymer composites. *ACI Structural Journal*, 47-55.

Woods, J. E. (2014). *Seismic Retrofit of Deficient Reinforced Concrete Shear Walls using Fibre-reinforced Polymer Sheets: Experimental Study and Anchor Design.* Ottawa, ON, Canada: Department of Civil and Environmental Engineering, Carleton University.

Woods, J., Cruz-Noguez, C., Lau, D., & Khabra, J. (2015). CYCLIC BEHAVIOUR OF NON-DUCTILE REINFORCED CONCRETE SHEAR WALLS RETROFITTED WITH CFRP SHEETS. *11th Canadian Conference on Earthquake Engineering.* Victoria, BC, Canada: Canadian Association for Earthquake Engineering.

Yang, Z., Chen, J., & Proverbs, D. (2003). Finite-element modeling of concrete cover separation failure in FRP plated RC beams. *Construction Building Materials, 17*(1), 3-13.